SYNTHESIS AND STRUCTURES OF MAIN GROUP ORGANOMETALLIC COMPLEXES WITH STERICALLY BULKY ALLYL LIGANDS

By

Cameron Karl Gren

Dissertation

Submitted to the Faculty of the

Graduate School of Vanderbilt University

in partial fulfillment of the requirements

for the degree of

DOCTOR OF PHILOSOPHY

in

Chemistry

August, 2009

Nashville, Tennessee

Approved:

Professor Timothy P. Hanusa

Professor Charles M. Lukehart

Professor David W. Wright

Professor Eva Harth

Professor Bridget R. Rogers

To my wife and children for putting up with me through too many years of graduate school.

ACKNOWLEDGEMENTS

There are many people and organizations that contributed to the successful completion of my graduate studies. I would first like to thank my high school chemistry teacher, Kim McAbee for sparking my interest in the subject. This spark was fanned into a flame by the wonderful chemistry faculty at Middle Tennessee State University, where I received my bachelor's degree. I would especially like to thank my advisor and undergraduate research mentor Andrienne Friedli for urging me to attend graduate school, and for her guidance on a research project that did not always produce the best results.

When I first arrived at Vanderbilt University, I had not decided what discipline to pursue. It only took a brief rotation through Prof. Timothy Hanusa's research lab, though, to convince me that inorganic chemists truly are the guardians of the periodic table! I will be forever grateful to Prof. Hanusa for welcoming me into his group and guiding, supporting, and occasionally feeding me for six years!

I would also like to thank the other chemistry faculty at Vanderbilt from whom I took a class or with whom I simply had meaningful conversation. Special thanks go to my other committee members—Profs. Lukehart, Wright, Harth, and Rogers.

Faculty aside, it really is the other students that make the everyday grind of graduate school enjoyable, even in the toughest of times. I would never be able to list all of my fellow students that have made a positive impact on my experience at Vanderbilt, but I am grateful to all of you. I must thank all past and present members of the Hanusa research group—especially Rose White, Jeff Crisp, and Steve Chmely—you have made the work day, at times, far more fun than it should have been!

While it often fun and exciting, it was also very hard work, and the work would not have been possible without funding. Thanks go to the Chemistry Department for funding me through teaching assistantships and fellowships for many semesters. When research funds were available to pay my way, they came from either an ACS-PRF or NSF grant.

Finally, I would like to thank my parents, who always encouraged me to expand my education as far as I could and supported me every step of the way. My wife, Lori, who has been by my side through my entire graduate school career and put up with the long hours and stress I have had to endure. My children, Izzie and Sammy, who are relatively new additions to our family have been a true blessing. Nothing relieves a stressful day at work like coming home to smiling children! I would not have made it through graduate school if not for the love and support of my family.

TABLE OF CONTENTS

Page

LIST OF TABLES

LIST OF FIGURES

CHAPTER I

CHEMISTRY OF THE ALLYL LIGAND: DEVELOPMENT OF STABLE COMPLEXES EXHIBITING UNIQUE BONDING AND REACTIVITY

Since the discovery of ferrocene by Kealy and Paulson in 1951,[1] and the description of its bonding by Woodward and Wilkinson a year later,[2] much of the effort of organometallic chemists has been dedicated to studying transition metal complexes of conjugated π-ligand systems. These complexes are varied not only in their structure and bonding, but also in their subsequent reactions and uses. An early player in this field was G. Wilke, who in 1961 reported the first bis(allyl) metal complex, $(C_3H_5)_5Ni$.[3] The allyl ligand is the smallest π-delocalized hydrocarbon anion, and is formally a four-electron donor to metals. However, as the ligand is so compact, the metal in a homoleptic allyl complex (i.e., $M(C_3H_5)_n$) is often coordinatively unsaturated, leaving the complex prone to decomposition. Table 1 provides a sampling of homoleptic allyl complexes prepared by Wilke and notes their thermal instability.

Table 1. Properties of selected homoleptic transition metal-allyl complexes.[4]

Compound	Valence Electrons	Decomposition Temp
$(C_3H_5)_3V$	14	Explodes above −30 °C
$(C_3H_5)_4Zr$	16	Decomp above 0 °C
$(C_3H_5)_3Co$	18	Decomp above −40 °C
$(C_3H_5)_2Ni$	18	Decomp above 20 °C

Allyl complexes are of interest because of their use as initiators for the polymerization of ethylene[5] and vinylpyridine[6] and as reagents in organic and materials chemistry, such as initiators for hydrosilylation reactions,[7,8] coupling reagents,[9,10] and volatile sources for metal deposition.[11,12] However, these complexes must be made more stable if they are to see extensive use.

In allyl complexes, improvements in stability are tied to increasing the occupancy of the metal's coordination sphere. Such increases can often be achieved by the addition of other, more coordinatively saturating ligands to the metal. This does not necessarily improve the thermal stability, however, as seen in the work of Jolly with the synthesis of $(C_3H_5)_2Cr\cdot(PR_3)_2$ (PR_3 = PMe_3, PMe_2Ph, $PMePh_2$) and $(C_3H_5)_2Fe\cdot(PR_3)_2$ (PR_3 = PMe_3, PMe_2Ph, $P(OMe)_3$), which decompose above −10 °C and 0 °C, respectively.[13,14] Another approach to increasing the coordinative saturation of allyl complexes is the addition of sterically bulky substituents to the allyl ligands. This is a common technique in the chemistry of the related cyclopentadienyl and indenyl

ligands. The addition of steric bulk by substituting a proton—even for simply a methyl group—is often used to alter the properties of the resulting organometallic complex of those ligands. The effectiveness of this approach on allyl complexes was demonstrated by Grosselin *et al.* in the synthesis of an iron allyl complexes analogous to Jolly's.[15] With simply the addition of a methyl group on the second carbon of the allyl ligand, $Fe(\eta^3\text{-}2\text{-}Me\text{-}C_3H_5)_2(PR_3)$ (PR_3 = PMe_3, PMe_2Ph, and $P(OMe_3)$) is now stable at room temperature.

Silyl groups have also been used to add bulk to the allyl moiety, as shown by Fraenkel *et al.* in 1990 with the synthesis of 1,3-(trimethylsilyl)allyl.[16] With a straightforward, three-step synthesis, Fraenkel constructed a ligand with approximately four times the spatial volume as the unsubstituted allyl ligand. With such increased bulk, the 1,3-(trimethylsilyl)allyl ligand has been successfully used to synthesize complexes of main group,[16-20] transition,[21-27] and f-block[28-33] metals with greatly increased stability over that of their unsubstituted allyl congeners. The nickel compound $[\eta^3\text{-}1,3\text{-}(SiMe_3)_2C_3H_3]_2Ni$, for example, is stable in water for several hours and in air for several days, unlike $(C_3H_5)_2Ni$, which inflames on contact with air.[25] Similarly, in contrast to $(C_3H_5)_4Th$, which decomposes at 0 °C, the trimethylsilylated derivatives $[(SiMe_3)_nC_3H_{5-n}]_4Th$ (n = 1, 2) are stable up to 90 °C.[31] Despite the kinetic stabilization provided by the bulky ligands, the geometries of the compounds are sometimes similar to their parent

counterparts (e.g., the Ni–C bond lengths in $[1,3\text{-}(SiMe_3)_2C_3H_3]_2Ni$ and $(C_3H_5)_2Ni$ differ by an average of only 0.02 Å).

(a) (b)

Figure 1. (a) σ-bonded and (b) π-bonded allyl ligands

A characteristic feature of the allyl ligand, with bulky substituents or not, is its ability to adopt σ- or π-coordination modes in metal complexes (Figure 1).[34] Whether in the σ-bound (η^1) or in the more symmetrical, π-bound (η^3) form, the preference for a specific allyl arrangement has a strongly metal-driven component. Complexes of the alkali metals[20,33,35-41] and f-block elements, for example, almost always possess π-bonded allyls,[30,33] but the post-transition p-block metals typically display σ-bound allyl ligands.[19,42,43] The alkaline earth elements display a variety of bonding types; allyl complexes of the heavy alkaline earth metals calcium, strontium, and barium are expected to be π-bound (e.g., the complex $Ca[C_3(SiMe_3)_2H_3]_2(thf)_2$ has π-bound ligands),[17] but allyls in beryllium and magnesium complexes have consistently been found to be σ-bonded in the solid state.[44,45]

The metal-influenced preferences on allyl bonding modes are not absolute, however. f-Block complexes occasionally display σ-bonded allyl groups as a consequence of steric crowding,[46,47] and it has recently been shown that π-type bonding is in fact energetically feasible in magnesium allyl compounds in the absence of coordinated solvents.[48-51] Coordinated bases are also expected to shift bonding modes in allyllithium complexes,[52] with consequent effects on their reactivity.[53] Thus even though many Group 1 and 2 complexes are prepared in coordinating (usually ethereal) solvents, the unsolvated complexes may reveal substantially different chemistry.

A major goal of this work is to study and classify the variety of bonding modes in main group organometallic complexes with bulky allyl ligands. In order to do this, criteria will be set to distinguish between a σ- and π-bond. The complexes discussed herein will then be evaluated based on these criteria. This information can then be used to explore the variation of bonding among organometallic allyl complexes as well as to further the general study of bonding in all organometallic complexes.

The following criteria will be used for the purpose of evaluating the bonding of complexes described in this work. An "ideally" π-bonded complex has equal C–C bond lengths, indicating completely delocalized π electrons, and the metal is centered over the delocalized region. An "ideally" σ-bonded complex has a large difference (approximately 0.1 Å) between the C–C single

and double bonds, indicating localized π electrons, and the metal is in close contact with only one carbon atom.

As it is quite difficult to set absolute definitions when discussing electrostatic interactions, the criteria itself will also be evaluated through this work and modified if necessary. Consequences of the bonding mode can also be studied, such as whether different reactivity is seen between σ- and π-bonded complexes.

The second chapter of this work will discuss the synthesis and structures of alkali metal complexes of bis- and tris-(trimethylsilyl)allyl ligands as well as introduce some even more sterically bulky ligands having triisopropylsilyl constituents. The focus will be on the structural variety of these complexes and both experimental and calculated results will be discussed.

The most common synthetic route to a metal-allyl complex is a simple metathesis between a halide or triflate of the desired metal and an alkali metal salt or Grignard reagent of the allyl ligand of interest (eq 1).[4,19,25,33,42]

$$MX_n + n\,(\text{allyl}')M' \rightarrow M(\text{allyl}')_n + n\,M'X \downarrow$$

$$(X = Cl, Br, I, OTf;\ M' = Li, Na, K, MgCl, MgBr) \qquad (1)$$

The alkali metal allyl complexes are quite common, but traditionally, the interest in them has been almost exclusively as precursors to allyl complexes with d-, p-, or f-block metals. For instance, the use of allyl complexes as

initiators to polymerization or organic transformation has been explored since their inception.[4-10] However, recently, in the study of complexes of the bis(trimethylsilyl)allyl ligand as initiators for the polymerization of methyl methacrylate (MMA), it was found that the potassium salt of the ligand led to a more rapid polymerization of MMA than any of the lanthanide metal allyl complexes studied.[33]

The third chapter will explore the synthesis and properties of zinc and cadmium complexes of the bis(trimethylsilyl)allyl ligand. Simple metathesis reactions were carried out between an alkali metal salt of the allyl′ ligand and the appropriate group 12 metal salt ($Zn(OTf)_2$ or CdI_2) (eq 2).

$$MX_2 + 2\,A(allyl') \rightarrow M(allyl')_2 + 2\,AX\downarrow$$

$$(MX_2 = Zn(OTf)_2, CdI_2;\ A = Li, Na, K, Cs) \qquad (2)$$

However, instead of the desired homoleptic allyl complex ($M[1,3\text{-}(SiMe_3)_2C_3H_3]_2$, where M = Zn, Cd), the reactions resulted in the heterometallic complexes $A[M(1,3\text{-}(SiMe_3)_2C_3H_3)_3]$. This general type of complex is not new, as there are a number of trialkylzincates in the literature. However, the complexes in this work demonstrate a bonding mode rarely seen in allyl complexes. Each allyl in $K[Zn(1,3\text{-}(SiMe_3)_2C_3H_3)_3]$, for example, is σ-bonded to the zinc, and interacts in a cation-π fashion to the potassium ion.

Cation-π interactions involve the largely noncovalent attraction of a cation (usually an alkali metal or NR_4^+; R = H, Me) with a ligand's π-electrons, which are commonly (although not necessarily) those in an aromatic ring (Figure 2).[54,55] Several factors are thought to contribute to cation-π interactions, including electrostatic and dispersion forces and charge transfer/inductive effects.[56] Complexes of the d^{10} Ag^+ ion with π-bound ligands are sometimes classified as displaying cation-π interactions.[57] However, structural and theoretical characterizations of species such as the $[Ag(C_2H_4)_3]^+$ ion[58] and Ag^+[2.2.2]cyclophane prismands[59] indicate that covalent d-orbital backbonding is also an important component of the silver-ligand interaction.

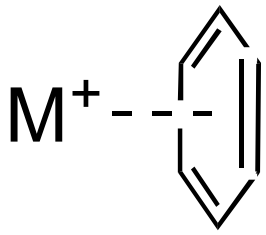

Figure 2. Cation-π bonding to an aromatic ring

The cation-π interaction energy can be substantial: that of K^+ with benzene in the gas phase (ca. 17.7±1.0 kcal mol^{-1}),[60] for example, is about the same as to water (17.9 kcal mol^{-1}).[61] Cation-π interactions with aromatic rings appear in numerous supramolecular and biological contexts, including

cyclophanes,[62,63] calixarenes,[64-67] collarenes,[68] polyaromatics,[69] and amino acids such as tryptophan.[70-73] Even when weak, multiple cation-π (arene) interactions can critically influence ligand conformations and substrate binding.[74]

The final chapter of this work examines the preparations of bulky allyl complexes of p-block metals. The synthesis of allyl complexes of these elements can be very problematic, and few were successfully isolated. One such complex, tris(1,3-bis(trimethylsilyl)allyl)gallium(III), undergoes a 1,3-sigmatropic shift in solution. This phenomenon, as seen in the related compound triallylboron,[75] occurs when the carbon-metal bond of one allyl ligands breaks and is reformed at a different carbon—C-1 to C-3, in this case. This chapter will discuss the synthesis and properties of some stable, heretofore unknown allyl complexes, with an emphasis on explaining their dynamic solution behavior.

CHAPTER II

SOLID-STATE AND SOLUTION PROPERTIES OF SILYLATED ALLYL COMPLEXES OF LITHIUM, SODIUM, AND POTASSIUM

Introduction

There has been a great deal of interest recently in the synthesis, structures, and reactions of compounds containing sterically bulky allyl ligands, especially the (1,3-trimethysilyl)allyl anion.[76] The first structurally authenticated alkali metal complex of this ligand, the *N,N,N′,N′*-tetramethylethylenediamine (TMEDA) solvate of Li[1,3-$(SiMe_3)_2C_3H_3$], was prepared by Gideon Fraenkel in 1990.[16] The potassium salt, K[1,3-$(SiMe_3)_2C_3H_3$], is often mentioned as a starting material for d-, p-, and f-block metal complexes of the bis(trimethylsilyl)allyl ligand.[19,21,23,25,30,31] However, neither it nor the analogous cesium complex were structurally authenticated until 2005 and 2007, respectively,[33,41] and there has yet to be a published structure of a sodium or rubidium complex of this ligand.

The s-block complexes of 1,3-bis(trimethysilyl)allyl are typically isolated as ether (THF, DME) solvates, and in fact it can be difficult to grow crystals of unsolvated compounds for structural authentication. Among the alkali metals, the cesium and potassium solvates $\{Cs[1,3\text{-}(SiMe_3)_2C_3H_3](thf)\}_\infty$,[41] $\{K[1,3\text{-}(SiMe_3)_2C_3H_3](dme)\}_\infty$[33] and $\{K[1,3\text{-}(SiMe_3)_2C_3H_3](thf)_{3/2}\}_\infty$,[41] have been isolated as coordination polymers with π-bound allyl ligands. In

contrast, the lithium solvate Li[1,3-$(SiMe_3)_2C_3H_3$](tmeda) is a monomer, but the allyl ligand remains π-bound.[20]

This work will describe the structures of the solvated bis(trimethylsilylated) complexes {K[1,3-$(SiMe_3)_2C_3H_3$](thf)$_{3/2}$}$_\infty$ and {Na[1,3-$(SiMe_3)_2C_3H_3$](thf)}$_4$, as well as the unsolvated K[1,3-$(SiMe_3)_2C_3H_3$] and tris(trimethylsilylated) complex Li[1,1′,3-$(SiMe_3)_3C_3H_2$]. The lithium complex was initially prepared, although not structurally authenticated, by Fraenkel,[16] who determined that the unique TMS group at C_3 was *exo* in solution, and that the barrier to rotation of the allyl groups in THF was 16.8 kcal mol^{-1}.

The results described here indicate that—with respect to their bonding motif—the alkali metal complexes of the bis- and tris(trimethylsilyl)allyl ligand show a remarkable indifference toward coordinated solvent. This is seen both in the preference for π- vs. σ-bonding in the allyl ligands, and in the retention of the nuclearity between solvated and unsolvated complexes with the same metal.

Experimental

General Considerations. All manipulations were performed with the rigorous exclusion of air and moisture using high vacuum, Schlenk, or dry box techniques. Proton (^{1}H), carbon (^{13}C), and sodium (^{23}Na) NMR experiments were obtained on a Bruker DPX-400 at 400 MHz, 100 MHz, and

106 MHz, respectively. Proton and carbon NMR experiments were referenced to residual resonances of THF-d_8 (δ 3.58 and 67.4, respectively). Sodium NMR experiments were referenced to external 1.0 M NaCl in D_2O at 298 K.

Materials. Hexanes were distilled under nitrogen from potassium benzophenone ketyl. Anhydrous tetrahydrofuran (THF) was purchased from Aldrich and used as received. Anhydrous metal salts were purchased from Strem Chemicals and used as received. Silylated organic compounds were purchased from Gelest, Inc. and used as received. *n*-Butyllithium (2.5 M in hexane) was purchased from Sigma-Aldrich and used as received. D_2O was purchased from Cambridge Isotopic Laboratories, Inc. and used as received. THF-d_8 was vacuum-distilled from Na/K (22/78) alloy and stored over type 4A molecular sieves prior to use. Li[1,1′,3-$(SiMe_3)_3C_3H_2$][16] and K[1,3-$(SiMe_3)_2C_3H_3$][33] were prepared according to literature procedures, and crystals of each were grown from hexanes.

Synthesis of Na[1,3-$(SiMe_3)_2C_3H_3$]. A 250 mL Schlenk flask equipped with a magnetic stir bar was charged with 1,3-bis(trimethylsilyl)propene (3.20 g, 17.2 mmol). The liquid was degassed, and hexane (75 mL) was added. The solution was cooled to 0 °C and *n*-butyllithium (6.8 mL, 17 mmol) was added dropwise over the course of 15 min. The reaction was allowed to warm to room temperature while being stirred overnight. The mixture was then treated with sodium *t*-butoxide (1.65 g, 17.2 mmol) and stirred at room temperature overnight. The mixture was filtered over a medium porosity

fritted-glass filter, rinsed with fresh hexane, and dried under vacuum, resulting in an off-white powder (3.21 g, 91 %), m.p. 128 °C. Anal. Calcd. for $C_9H_{21}NaSi_2$ (wt%): C, 51.85; H, 10.16; Na, 11.03. Found: C, 49.22; H, 9.36; Na, 10.88. ^{1}H NMR (THF-d_8, 298 K): δ 6.76 (t, J = 15.6 Hz, 1 H, C_2-H), 2.84 (d, J = 15.6 Hz, 2 H, $C_{1,3}$-H), −0.14 (s, 18 H, $SiMe_3$). ^{13}C (THF-d_8, 298 K): δ 156.75 (C_2), 65.32 ($C_{1,3}$), 2.50 ($SiMe_3$). ^{23}Na (THF-d_8, 298 K): δ −3.30 (s).

Synthesis of 1-(Si(*i*-Pr)$_3$)-3-(SiMe$_3$)C$_3$H$_4$. A 250 mL Schlenk flask equipped with a magnetic stir bar was charged with allyl trimethylsilane (7.76 g, 67.9 mmol) and TMEDA (7.89 g, 67.9 mmol). The mixture was degassed and hexanes (75 mL) was added. The solution was cooled to 0 °C and *n*-butyllithium (27.2 mL, 67.9 mmol) was added dropwise over the course of 15 min. The reaction was allowed to warm to room temperature while being stirred overnight. The reaction mixture was again cooled to 0 °C, and triisopropylchlorosilane (14.5 mL, 67.9 mmol) was added dropwise over the course of 10 min. The reaction was allowed to warm to room temperature while being stirred for 4 h. The reaction was hydrolyzed with excess water, and the product was extracted with diethyl ether and dried with magnesium sulfate. Removal of solvent by rotary evaporation afforded the title compound. ^{1}H NMR ($CDCl_3$, 298 K): δ 6.09 (dt, J = 18.3, 7.8 Hz, 1H, C_2-H), 5.50 (d, J = 18.3 Hz, 1H, C_1-H), 1.74 (d, J = 7.8 Hz, 2H, C_3-H), 1.03 (m, 21H, Si(*i*-Pr)-H), 0.01 (s, 9H, $SiMe_3$-H).

Synthesis of K[1-(Si(*i*-Pr)$_3$)-3-(SiMe$_3$)C$_3$H$_3$]. A 250 mL Schlenk flask equipped with a magnetic stir bar was charged with 1-triisopropylsilyl-3-trimethylsilylpropene. The liquid was degassed, and hexane (75 mL) was added. The solution was cooled to 0 °C and one equivalent of *n*-butyllithium was added dropwise over the course of 15 min. The reaction was allowed to warm to room temperature while being stirred overnight. The mixture was then treated with one equivalent of potassium *t*-butoxide and stirred at room temperature for 6 h. The mixture was then filtered over a medium porosity fritted-glass filter, rinsed with fresh hexane, and dried under vacuum, resulting in a tan powder. ^{1}H NMR (THF-d_8, 298 K): δ 6.89 (t, J = 15.6 Hz, 1H, C$_2$-H), 2.76 (d, J = 15.3 Hz, 1H, C$_1$-H), 2.53 (d, J = 15.6 Hz, 1H, C$_3$-H), 1.00 (d, J = 5.7 Hz, 18H, SiCC*H*$_3$), 0.95 (m, 3H, SiC*H*), −0.14 (s, 9H, SiMe$_3$-H).

Synthesis of 1,3-(Si(*i*-Pr)$_3$)$_2$C$_3$H$_4$. A 250 mL Schlenk flask equipped with a magnetic stir bar was charged with allyl triisopropylsilane (5.35 g, 27.5 mmol) and TMEDA (3.20 g, 27.5 mmol). The mixture was degassed and hexanes (75 mL) was added. The solution was cooled to 0 °C and *n*-butyllithium (11.0 mL, 27.5 mmol) was added dropwise over the course of 15 min. The reaction was allowed to warm to room temperature while being stirred overnight. The reaction mixture was again cooled to 0 °C, and triisopropylchlorosilane (5.9 mL, 28 mmol) was added dropwise over the course of 10 min. The reaction was allowed to warm to room temperature

while being stirred 6 h. The reaction was hydrolyzed with excess water, and the product was extracted with diethyl ether and dried with magnesium sulfate. Removal of solvent by rotary evaporation afforded the title compound, whose ^{1}H NMR spectrum was consistent with literature values.[77]

Synthesis of K[1,3-(Si(*i*-Pr)$_3$)$_2$C$_3$H$_3$]. A 250 mL Schlenk flask equipped with a magnetic stir bar was charged with 1,3-bis(triisopropylsilyl)propene. The liquid was degassed, and hexane (75 mL) was added. The solution was cooled to 0 °C and one equivalent of *n*-butyllithium was added dropwise over the course of 15 min. The reaction was allowed to warm to room temperature while being stirred overnight. The mixture was then treated with one equivalent of potassium *t*-butoxide and stirred at room temperature for 6 h. The mixture was then filtered over a medium porosity fritted-glass filter, rinsed with fresh hexane, and dried under vacuum, resulting in a red-brown powder. ^{1}H NMR (THF-d_8, 298 K): δ 6.76 (t, J = 15.6 Hz, 1H, C$_2$-H), 2.61 (d, J = 15.6 Hz, 2H, C$_{1,3}$-H), 1.00 (d, J = 5.7 Hz, 32H, SiCC*H*$_3$), 0.95 (m, 6H, SiC*H*).

General Procedures for X-ray Crystallography. Data collection and structure solutions were conducted at one of the following places: the X-Ray Crystallographic Laboratory at the University of California, San Diego; the Crystallographic Laboratory at the University of Minnesota; or the X-Ray Crystallographic Facility of the University of Rochester. Suitable crystals of each compound were located, attached to glass fibers, and mounted on a Siemens SMART system or a Bruker SMART APEX II CCD Platform

diffractometer for data collection. The intensity data were corrected for absorption (SADABS). All calculations were performed with the SHELXTL suite of programs. Final cell constants were calculated from a set of strong reflections measured during the actual data collection. Relevant crystal and data collection parameters and atomic coordinates for each compound are given in Appendix C. The space groups were determined from intensity statistics and where appropriate, systematic absences. The structures were solved by direct methods and refined against F^2 for all observed reflections.

Computational Details. The computations were performed with the Amsterdam Density Functional (ADF) program package.[78-80] The Perdew-Burke-Ernzerhof non-hybrid gradient density functional,[81] modified by the addition of a $1/r^6$ term to model dispersion forces (PBE-D)[82] was employed. Full geometry optimizations were carried out with all-electron valence triple-ζ Slater-type basis sets with double polarization functions for all atoms (TZ2P) from the ADF basis set library. Relevant calculated coordinates for each compound are given in Appendix D.

Results and Discussion

Solid-state structure of {Li[1,1′,3-(SiMe$_3$)$_3$C$_3$H$_2$]}$_2$. Crystals of {Li[1,1′,3-(SiMe$_3$)$_3$C$_3$H$_2$]}$_2$ were grown from hexane, and as depicted in Figure 3, the base-free complex is a dinuclear species in the solid-state in which the two Li atoms are bridged by the allyl ligands. Two independent, but closely similar

molecules are found in the unit cell, and both possess crystallographically imposed inversion centers; only one of them will be discussed here. The coordination of the allyl ligands is probably most accurately described as μ_2-η^1,η^2, with a σ-bonded distance of 2.232(7) Å (Li1–C6′, Li1′–C6).

The Li–C η^2-interaction occurs at distances of 2.230(7) Å (Li1–C4) and 2.241(6) Å (Li–C5). The Li1–C6 contact is appreciably longer at 2.410(6) Å. It should be noted that a precise cut-off distance for an interaction is not possible when a strongly electrostatic (coulombic) component to the bonding exists, as is true with the highly electropositive alkali metals. For example, the structure of $\{Li[1,1',3\text{-}(SiMe_3)_3C_3H_2]\}_2$ is broadly similar to the central core of bis(μ_2-η^3-*N*-(2-(2-allyl)-2-methyl-*n*-propyl)-2-(methoxymethyl)pyrrolidine-*C,N,O*)-di-lithium, in which a bridging allyl ligand bound to lithium spans distances from 2.26–2.45 Å, and the allyl bonding is described as η^3.[83] In that case, the shortest Li–C distance (2.26 Å) involves the central carbon of the allyl ligand, and the terminal carbons are at 2.37 and 2.45 Å. In contrast, the lithium in $\{Li[1,1',3\text{-}(SiMe_3)_3C_3H_2]\}_2$ is centered over the midpoint of the C4–C5 bond, and an η^2 description of the bonding seems more appropriate.

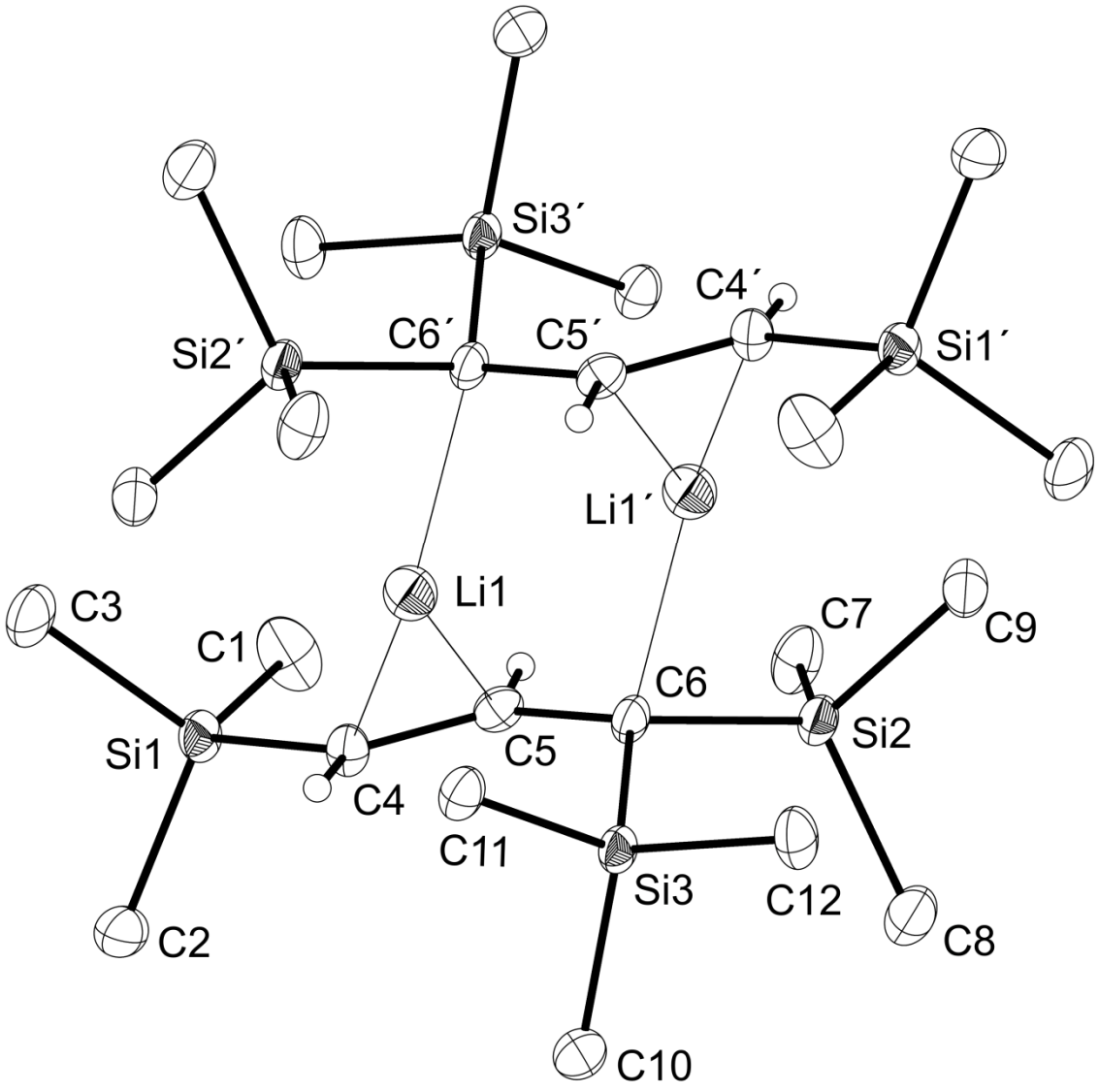

Figure 3. Solid-state structure of the dimeric $\{Li[1,1',3\text{-}(SiMe_3)_3C_3H_2]\}_2$. Thermal ellipsoids are shown at the 50% probability level, and hydrogen atoms on the trimethylsilyl groups have been omitted for clarity.

The bridging allyls (C4–C6) are only partially delocalized, with a 0.085 Å difference between the single and double bonds. Consistent with this, the environment around C6 is noticeably pyramidalized (sum of angles = 347°). The Li···Li′ distance can be used as a marker of the general proximity of the [Li(allyl)] fragments: at 2.59(1) Å, it is interestingly shorter than the Li–Li distance in solid $(LiMe)_4$ (2.68 Å),[84] or the gas-phase Li_2 dimer (2.673 Å).[85]

$\{Li[1,1',3\text{-}(SiMe_3)_3C_3H_2]\}_2$ provides an interesting comparison with the related magnesium counterparts, $\{Mg[1,3\text{-}(SiMe_3)_2C_3H_3]_2\}_2$ and $Mg[1,3\text{-}(SiMe_3)_2C_3H_3]_2(thf)_2$.[48] The former is a bridged dimer that, except for the difference of a terminal allyl ligand on each metal, resembles the framework of $\{Li[1,1',3\text{-}(SiMe_3)_3C_3H_2]\}_2$. The latter is a monomeric complex with σ-bound allyl ligands; i.e., the coordinated bases have completely disrupted the bridging interaction. The Li^+ and Mg^{2+} ions are similar in size,[86] so that the M–μ-C distances provide a measure of the relative strength of the metal–μ-allyl interactions. In $\{Li[1,1',3\text{-}(SiMe_3)_3C_3H_2]\}_2$, they range from 2.23–2.24 Å; in $\{Mg[1,3\text{-}(SiMe_3)_2C_3H_3]_2\}_2$, they range from 2.44–2.51 Å, roughly 10% longer than in the lithium compound. The μ-allyl interactions in the magnesium complex was categorized as (noncovalent) cation-π in character, sufficient to hold the unsolvated dimer together in hydrocarbon solvents, but interrupted in coordinating ethereal solvents. The interactions in $\{Li[1,1',3\text{-}(SiMe_3)_3C_3H_2]\}_2$ are evidently stronger, and probably reflect a higher degree of covalency in the compounds.

Solid-state structure of $\{Na[1,3\text{-}(SiMe_3)_2C_3H_3](thf)\}_4 \cdot 2(C_7H_8)$. Crystals of $\{Na[1,3\text{-}(SiMe_3)_2C_3H_3](thf)\}_4 \cdot 2(C_7H_8)$ were grown from a THF/toluene mixture at 0 °C. The structure is tetranuclear, with Na atoms in a square planar arrangement (Figure 4). The molecule lies on a crystallographic two-fold axis, so there are only two unique sodium sites. There are four (two unique) sodium-coordinated THF molecules; one THF is disordered over three positions and one over two positions. There are four (two unique) bridging allyl ligands. One Na-C distance is longer than the other two for each allyl (2.90 Å vs 2.60 Å and 2.64 Å). This causes the allyl to be slightly slipped with respect to the sodium atom (Figure 5).

This compound represents only the second structurally authenticated sodium-allyl contact ion pair. The first to be characterized, $Na(1\text{-}PhC_3H_4)(pmdta)$, is a monomer with Na–C distances of 2.791(9) Å, 2.577(7) Å, and 2.676(3) Å.[87] The allyl ligand in that complex appears to be η^3-bound, but the C–C bonds are localized (1.31 Å and 1.47 Å), causing some ambiguity about the σ- and π-nature of the sodium-allyl bond. In contrast, in $\{Na[1,3\text{-}(SiMe_3)_2C_3H_3](thf)\}_4 \cdot 2(C_7H_8)$, the C-C bond distances on average are 1.38 Å and 1.41 Å, and the greater delocalization of the allyl ligand is unambiguously consistent with π-bonding. In this context, there should be noted the report of a tetraphenylallylsodium diethyl ether complex.[88] In this compound, the sodium is held between two of the phenyl substituents by cation-π interactions and is not within bonding distance to the allyl backbone.

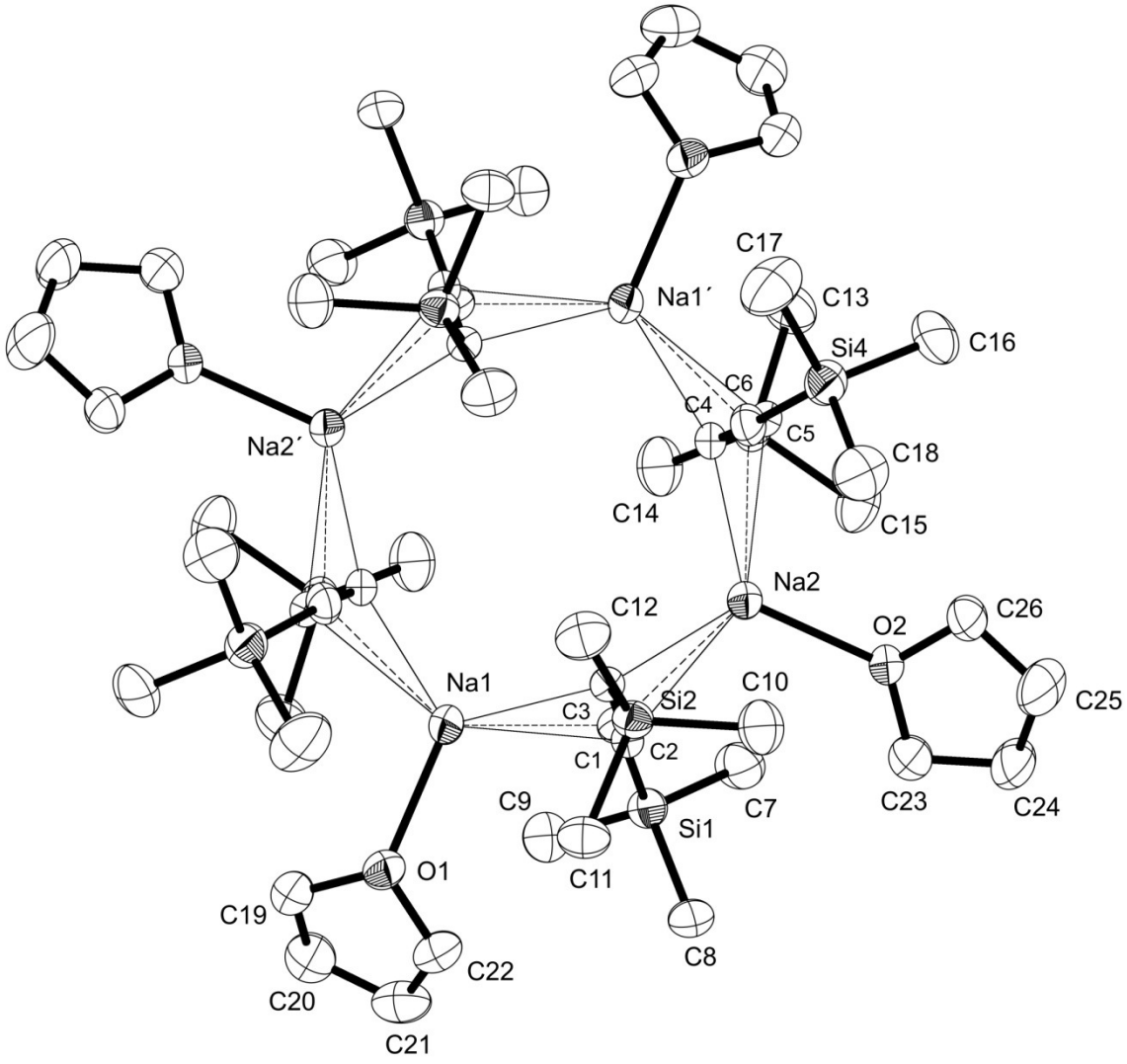

Figure 4. Solid-state structure of the tetrameric $\{Na[1,3\text{-}(SiMe_3)_2C_3H_3](thf)\}_4$. Thermal ellipsoids are shown at the 50% probability level, and hydrogen atoms have been omitted for clarity.

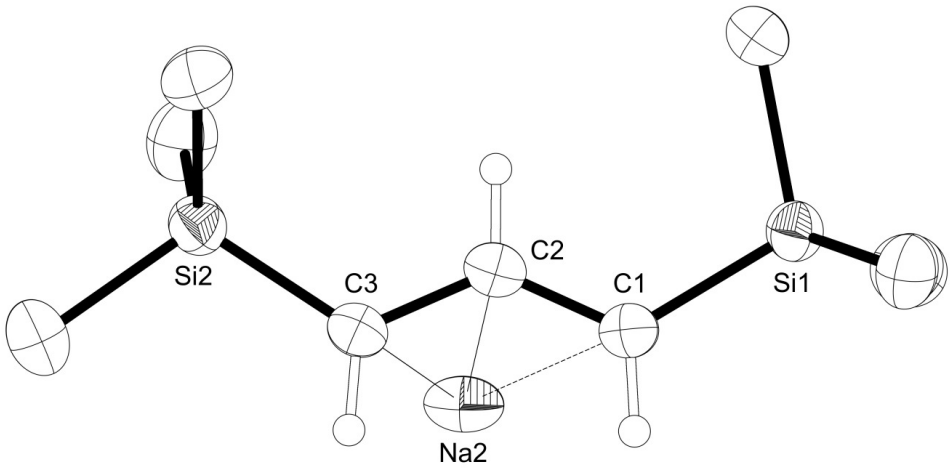

Figure 5. A single Na-allyl unit of $\{Na[1,3\text{-}(SiMe_3)_2C_3H_3](thf)\}_4 \cdot 2(C_7H_8)$, showing the slipped allyl ligand. Selected bond distances [Å] and angles (deg): Na2-C3, 2.598(2); Na2-C2, 2.636(2); Na2-C1, 2.896(3); C1-C2-C3, 131.7(2).

The Na–C distances in $\{Na[1,3\text{-}(SiMe_3)_2C_3H_3](thf)\}_4 \cdot 2(C_7H_8)$ (2.59-2.90 Å) are similar to those in several sodium cyclopentadienides. The Na-C distances in the polymeric $\{Na(C_5H_5)\}_\infty$ and $\{Na(C_5H_5)(tmeda)\}_\infty$ range from 2.63-2.67 Å and 2.83-3.03 Å, respectively,[89,90] and the monomeric silylated complex, $Na(1,2,4\text{-}(SiMe_3)_3C_5H_2)(pmdta)$, shows a Na-C distance range of 2.71-2.85.[91] This similarity indicates a similar degree of ionic bonding to that in $\{Na[1,3\text{-}(SiMe_3)_2C_3H_3](thf)\}_4 \cdot 2(C_7H_8)$. The larger range in Na-C distances in the allyl complex may reflect some steric crowding in the complex.

Solid-state structure of $\{K[1,3\text{-}(SiMe_3)_2C_3H_3](thf)_{3/2}\}_\infty$. Crystals of $\{K[1,3\text{-}(SiMe_3)_2C_3H_3](thf)_{3/2}\}_\infty$ were grown from THF solution at room temperature. Unlike the monomeric lithium species $Li[1,3\text{-}(SiMe_3)_2C_3H_3](tmeda)$,[20] but like the related DME solvate $\{K[1,3\text{-}(SiMe_3)_2C_3H_3](dme)\}_\infty$,[33] the structure of

$\{K[1,3\text{-}(SiMe_3)_2C_3H_3](thf)_{3/2}\}_\infty$ is a one-dimensional coordination polymer, with K(1)(1,3-$(SiMe_3)_2C_3H_3$)$(thf)_2$ units alternating with K(2)(1,3-$(SiMe_3)_2C_3H_3$)(thf) units, running parallel to the *c* axis (Figure 6). Two of the trimethylsilyl groups are disordered over two positions, and all three of the THF molecules are disordered over two positions.

The existence of two different coordination environments around the potassium centers in $\{K[1,3\text{-}(SiMe_3)_2C_3H_3](thf)_{3/2}\}_\infty$ generates distinctive structural features. For example, roughly linear K(1)–K(2)–K(1)′ sections (170.2°) alternate with strongly bent K(2)–K(1)–K(2)′ sequences (103.3°), whereas in $\{K[1,3\text{-}(SiMe_3)_2C_3H_3](dme)\}_\infty$, the corresponding K(1)–K(2)–K(1) and K(2)–K(1)–K(2) angles are more comparable, at 153.3° and 141.9°, respectively.[33,40] The allyl ligands are completely delocalized (Δ_{CC} = 0.014 Å), indicating a high degree of π-bonding. The range of K–C distances in $\{K[1,3\text{-}(SiMe_3)_2C_3H_3](thf)_{3/2}\}_\infty$ (2.93–3.12 Å) is slightly larger than in $\{K[1,3\text{-}(SiMe_3)_2C_3H_3](dme)\}_\infty$ (2.98–3.10 Å), and the average distance to the formally 6-coordinate K(1) (3.05 Å) is marginally larger than the average to the 5-coordinate K(2) (3.01 Å). As with $\{Na[1,3\text{-}(SiMe_3)_2C_3H_3](thf)\}_4 \cdot 2(C_7H_8)$, however, the distances are similar to those for related potassium cyclopentadienides (cf. 2.99 Å to 3.08 Å in $[K(C_5(SiMe_3)H_4)]_\infty$ and 2.93 Å to 3.10 Å in $[K(C_5(SiMe_3)_3H_2)]_\infty$),[92] an indication of the comparably ionic bonding in the complexes.

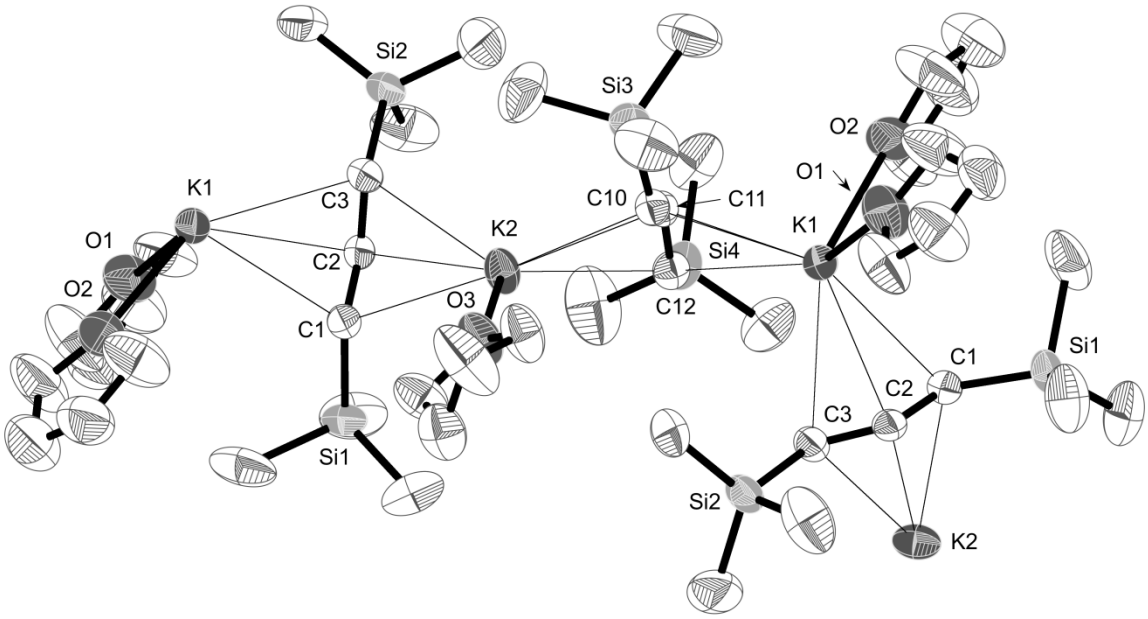

Figure 6. Solid-state structure of the polymeric $\{K[1,3\text{-}(SiMe_3)_2C_3H_3](thf)_{3/2}\}_\infty$. Thermal ellipsoids are shown at the 50% probability level, and hydrogen atoms have been omitted for clarity.

Solid-state structure of $\{K[1,3\text{-}(SiMe_3)_2C_3H_3]\}_\infty$. Crystals of $\{K[1,3\text{-}(SiMe_3)_2C_3H_3]\}_\infty$ were grown from hexane solution at room temperature. Like the related DME and THF solvates $\{K[1,3\text{-}(SiMe_3)_2C_3H_3](dme)\}_\infty$[33] and $\{K[1,3\text{-}(SiMe_3)_2C_3H_3](thf)_{3/2}\}_\infty$, respectively, $\{K[1,3\text{-}(SiMe_3)_2C_3H_3]\}_\infty$ is a coordination polymer with potassium ions linked by bridging π-allyl ligands (Figure 7). $\{K[1,3\text{-}(SiMe_3)_2C_3H_3]\}_\infty$ crystallizes in the polar space group P_2/c, however, and the polymer takes the form of helical chains running parallel to the *a* axis (Figure 8). There are three crystallographically distinct potassium ions in the chains; two of the K–K–K sections have nearly identical bending angles (K(1)–K(2)–K(1)′ = 135.1°; K(2)–K(1)–K(3)′ = 135.7°); the third is more

strongly bent (K(1)–K(3)–K(1)′ = 118.2°) (Figure 7). These are different from the pattern found in $\{K[1,3\text{-}(SiMe_3)_2C_3H_3](thf)_{3/2}\}_\infty$, but it is difficult to ascribe chemical significance to this, given the broader structural difference between the chains (helical vs. simple undulations).

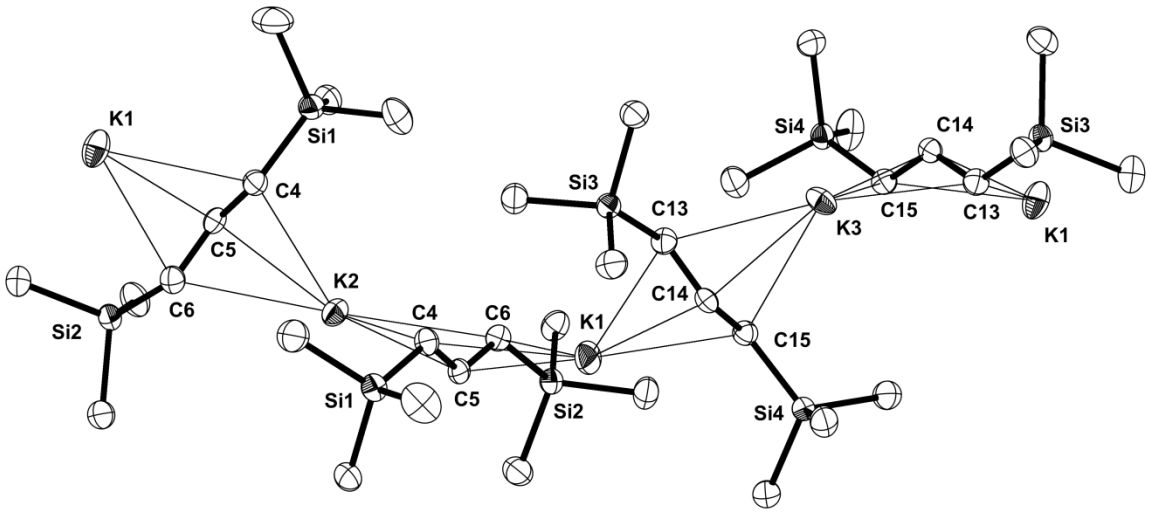

Figure 7. Solid-state structure of the polymeric $\{K[1,3\text{-}(SiMe_3)_2C_3H_3]\}_\infty$. Thermal ellipsoids are shown at the 50% probability level, and hydrogen atoms have been omitted for clarity.

As with $\{K[1,3\text{-}(SiMe_3)_2C_3H_3](thf)_{3/2}\}_\infty$, the allyl ligands are completely delocalized (Δ_{CC} = 0.008 Å), indicating a high degree of π-bonding. The range of K–C distances in $\{K[1,3\text{-}(SiMe_3)_2C_3H_3]\}_\infty$ (2.87–3.15 Å; Δ = 0.28 Å) is the broadest yet observed in K(allyl′) chains, surpassing that in $\{K[1,3\text{-}(SiMe_3)_2C_3H_3](thf)_{3/2}\}_\infty$ (2.93–3.12 Å; Δ = 0.19 Å) and $\{K[1,3\text{-}(SiMe_3)_2C_3H_3](dme)\}_\infty$ (2.98–3.10 Å; Δ = 0.12 Å). In view of the spread in K–C

bond distances, the average K–C distance of 3.01 Å in $\{K[1,3\text{-}(SiMe_3)_2C_3H_3]\}_\infty$ is not a particularly meaningful parameter, although it is interesting that it matches the distance to the 5-coordinate potassium ion in $\{K[1,3\text{-}(SiMe_3)_2C_3H_3](thf)_{3/2}\}_\infty$, even though in $\{K[1,3\text{-}(SiMe_3)_2C_3H_3]\}_\infty$ the potassium ions are formally 4-coordinate. The reduction in the K–C distance that might have been expected from the absence of coordinated THF is perhaps obscured by the conformational changes in the helical chains. In general, however, the distances in $\{K[1,3\text{-}(SiMe_3)_2C_3H_3]\}_\infty$ are comparable to those for potassium cyclopentadienides (cf. 2.99 Å to 3.08 Å in $\{K[C_5(SiMe_3)H_4]\}_\infty$ and 2.93 Å to 3.10 Å in $\{K[C_5(SiMe_3)_3H_2]\}_\infty$),[92] indicating similar ionic bonding in the complexes.

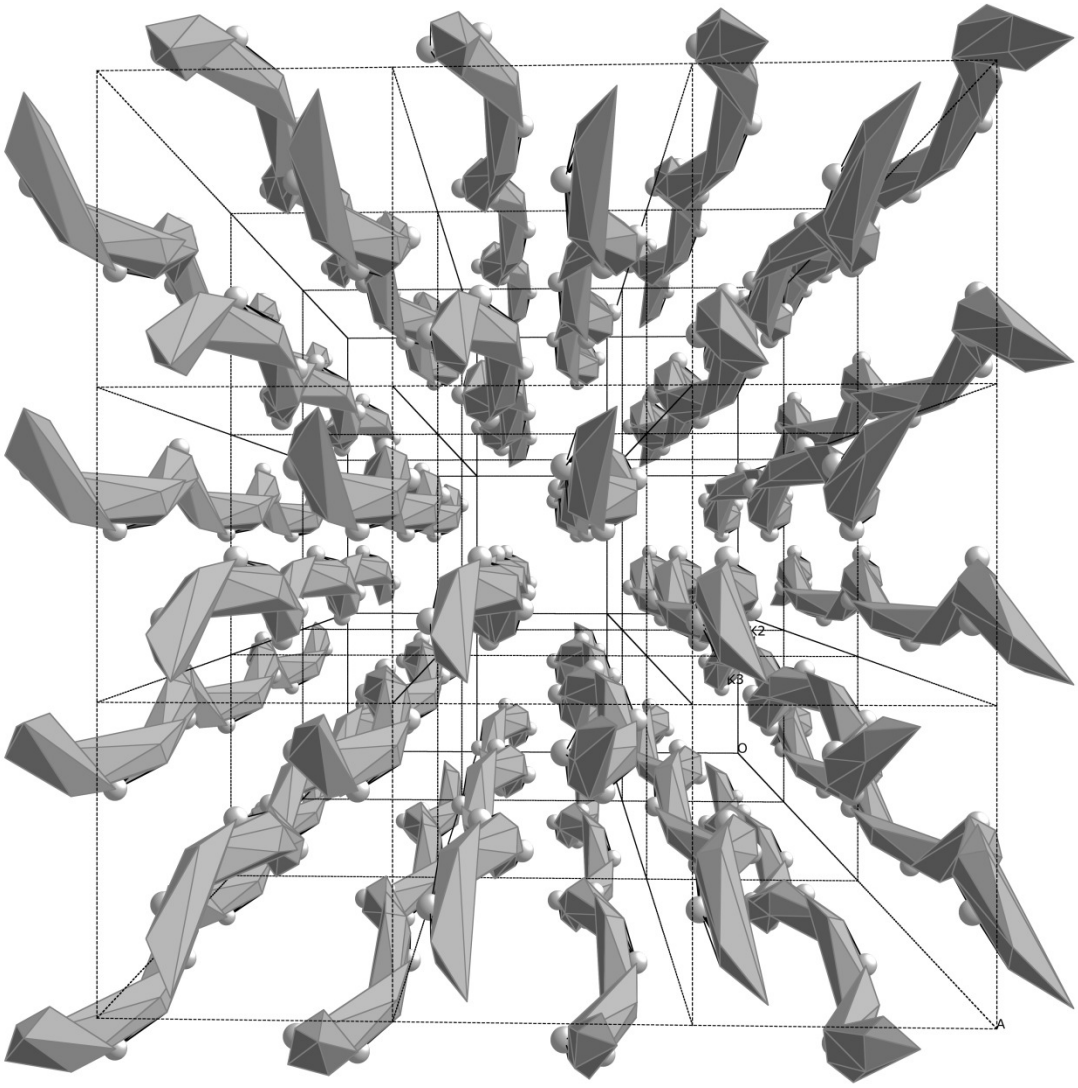

Figure 8. Diagram of several $\{K[1,3\text{-}(SiMe_3)_2C_3H_3]\}_\infty$ unit cells, illustrating the helical nature of the K[allyl′] chains. Polyhedra are constructed around the K^+ ions, with vertices drawn at the atoms of the nearest ligands. The pitch length of the spirals ($K^+\cdots K^+$ distance) is 17.9 Å.

Isopropylsilyl-substituted allyl compounds. The symmetric 1,3-bis(triisopropylsilyl)propene was previously synthesized by Somfai and used purely in organic transformations.[77] In this work, unlike in Somfai's, this molecule and the asymmetric 1-trimethylsilyl-3-triisopropylsilylpropene were prepared and metallated by a procedure similar to that described by Fraenkel in the original preparation of the 1,3-bis(trimethylsilyl)propene (eq 3,4).[16]

$$\text{R-}C_3H_5 \xrightarrow[\text{hex, 0 °C, 18 h}]{\text{n-BuLi, TMEDA}} \xrightarrow[\text{0 °C, 6 h}]{i\text{-}Pr_3SiCl} \text{R-}C_3H_4(Si(i\text{-}Pr)_3)$$

$$(\text{R} = Me_3Si,\ i\text{-}Pr_3Si) \qquad (3)$$

$$\text{R-}C_3H_4(Si(i\text{-}Pr)_3) \xrightarrow[\text{hex, 0 °C, 18 h}]{\text{n-BuLi}} \xrightarrow[\text{RT, 6 h}]{KOt\text{-}Bu} K[\text{R-}C_3H_4(Si(i\text{-}Pr)_3)] \qquad (4)$$

Several attempts were made to synthesize a group II or d-block complex of both the symmetric and asymmetric allyl ligands through metathesis reactions with their respective potassium salt. Many attempts resulted in uncharacterizable decomposition products or unreacted starting material. Upon the attempted synthesis of $(1,3\text{-}(Si(i\text{-}Pr)_3)_2C_3H_3)_2Ni$, (eq 5) the desired bis(allyl)nickel complex was not obtained.

$$NiBr_2(dme) + 2\ K(allyl') \xrightarrow[\text{-78 °C, 18 h}]{\text{THF}} (allyl')_2Ni + 2\ KBr \qquad (5)$$

Instead, the dimerized ligand was the only isolated product, crystals of which yielded a well resolved structure (Figure 9). The structure is a centrosymmetric hexadiene. The C2-C3 distance is 1.333(3) Å, the C1-C2 distance is 1.506(2) Å, and the C1-C1′ distance, the bond formed between the individual allyl units, is 1.579(4) Å. The length of this single bond may be a result of the steric crowding between the *i*-Pr substituents. Ligand dimerization—reflected in the production of the hexadiene—is a common result in the decomposition of allyl-metal complexes.[3,25,76]

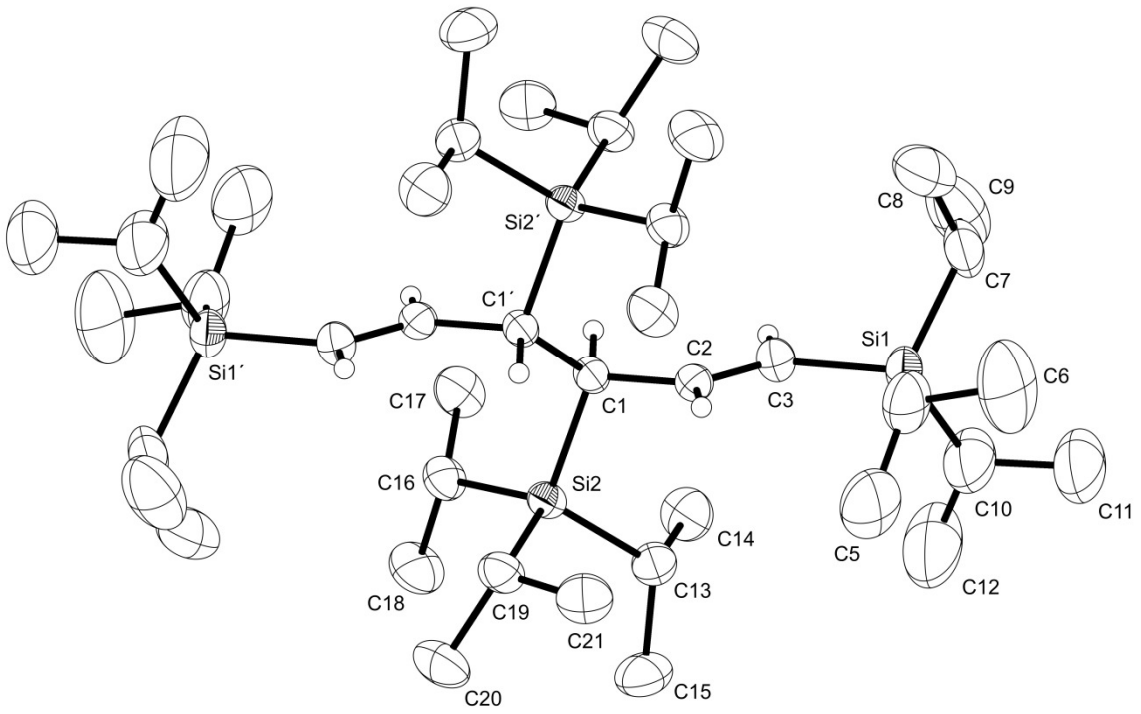

Figure 9. Solid-state structure of 1,3,4,6-tetrakis(triisopropylsilyl)-1,5-hexadiene. Thermal ellipsoids are shown at the 50% probability level, and hydrogen atoms have been omitted from the isopropyl substituents for clarity.

Computational study of allyllithiums. As befits its importance in the family of organolithium reagents, the relative stabilities and geometries of bridged (η^3-bound) and sigma-bonded (η^1-bound) allyllithium, and the influence of coordinated solvent on the structures and barriers to ligand rotation have been the subject of repeated computational studies.[93,94]

The symmetrical π-bound form of $Li(C_3H_5)$ is well established as lower in energy than a "classical" σ-bonded structure.[95] The C_s structure reported by Schleyer at the MP2/6-31G(d,p) level, with Li–C1 = 2.109 Å and Li–C2 = 2.063 Å,[52] is similar to that determined at the PBE-D/TZ2P level used in this study (see experimental section for details); e.g., Li–C1 = 2.102 Å and Li–C2 = 2.067 Å (Figure 10).

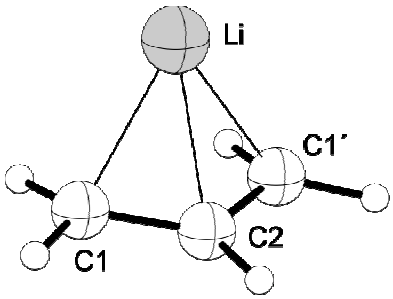

Figure 10. Calculated structure (PBE-D/TZ2P) of π-bound $Li(C_3H_5)$ (imposed C_s symmetry).

Substitution of three of the hydrogens of $Li(C_3H_5)$ with SiH_3 groups to make $Li[1,1',3\text{-}(SiH_3)_3C_3H_2]$ has the effect of lengthening the Li–C interactions by over 4%. The average Li–C(1,3) distances are now 2.213 Å,

and Li–C2 has increased to 2.156 Å (Figure 11), but only slight asymmetry is observed in the Li–allyl interaction, with the Li–C(1,3) and C–C bonds differing by only 0.02 Å.

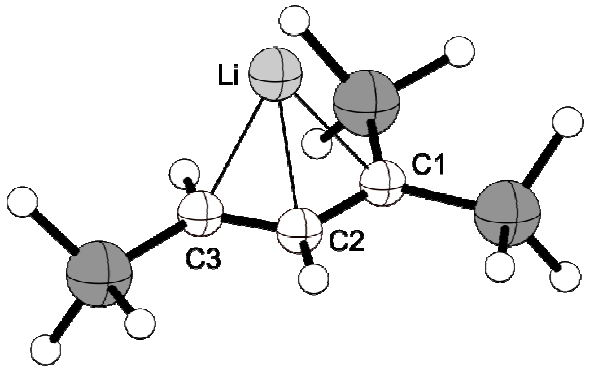

Figure 11. Calculated structure (PBE-D/TZ2P) of π-bound Li[1,1′,3-$(SiH_3)_3C_3H_2$]. Selected bond distances [Å] and angles (deg): Li-C1, 2.220; Li-C2, 2.155; Li-C3, 2.204; C1-C2, 1.425; C2-C3, 1.401; C1-C2-C3, 127.2.

Schleyer found a stable dimeric structure for allyllithium with the use of semiempirical computational methods (MNDO),[96] which were later upgraded to an ab initio (HF/3-21G) level.[52] His results are largely replicated at the PBE-D/TZ2P level, which are depicted in Figure 12. The structure is constructed from the centrosymmetric head-to-tail coupling of two sigma-bonded Li–C units, in which the each allyl also interacts in a polyhapto fashion with the second lithium cation. At the HF/3-21G level, both metals contact the bridging allyls through a σ-bonded distance of 2.19 Å (Li1–C3′, Li1′–C3), and the C–C single and double bonds are clearly localized at 1.35 and 1.45 (Δ = 0.10 Å). As the Li–C1 and L1–C3 distances are similar (2.31,

2.29 Å, respectively), an η^3-description of the bonding is reasonable. At the PBE-D/TZ2P level, the Li–C(σ) bond has contracted only slightly to 2.182 Å, but the C–C bonds have become more delocalized at 1.380 and 1.431 Å (Δ = 0.051 Å). A notable feature of Schleyer's calculated structure is the Li···Li′ distance of 2.400 Å, which is essentially unaltered at the PBE-D/TZ2P level (2.406 Å). This distance is substantially shorter than the comparable distance in $\{Li[1,1',3\text{-}(SiMe_3)_3C_3H_2]\}_2$ (2.59(1) Å).

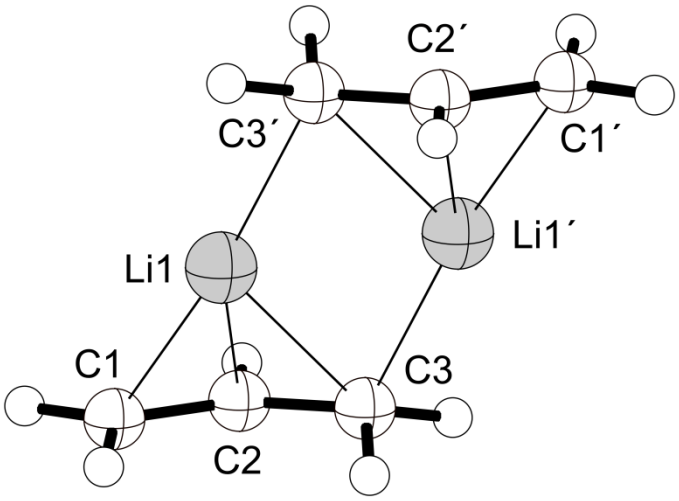

Figure 12. Calculated structure (PBE-D/TZ2P) of $[Li(C_3H_5)]_2$ (imposed C_i symmetry). Selected bond distances [Å] and angles (deg): Li-C1, 2.193; Li-C2, 2.179; Li-C3, 2.274; Li-C3´, 2.182; C1-C2, 1.380; C2-C3, 1.431; C1-C2-C3, 127.5.

Substitution of the dimer with SiH_3 groups to form $\{Li[1,1',3\text{-}(SiH_3)_3C_3H_2]\}_2$ introduces distortions that move the complex in the direction of $\{Li[1,1',3\text{-}(SiMe_3)_3C_3H_2]\}_2$ (Figure 13). The σ-bonded Li–C distance has

substantially lengthened to 2.284 Å, up from 2.182 Å in the unsubstituted model and 2.232 Å in the crystal structure of $\{Li[1,1',3\text{-}(SiMe_3)_3C_3H_2]\}_2$. The distance to the bridging allyls has become more asymmetric; Li–C1 and Li–C2 are 2.222 and 2.262 Å, respectively, but Li–C3 is 2.384 Å, approaching the 2.410(6) Å separation in $\{Li[1,1',3\text{-}(SiMe_3)_3C_3H_2]\}_2$. As a marker of the general proximity of the Li(allyl) fragments, the Li···Li′ distance has increased to 2.646 Å, a nearly 10% increase over the unsubstituted dimer, and roughly similar to the crystallographically observed value of 2.59(1) Å. It appears that the inclusion of SiH_3 groups reproduces most of the features of the $SiMe_3$-substituted complex.

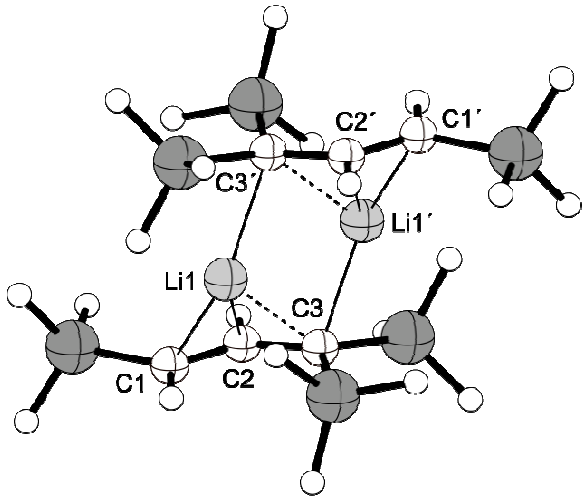

Figure 13. Calculated structure (PBE-D/TZ2P) of $\{Li[1,1',3\text{-}(SiH_3)_3C_3H_2]\}_2$ (imposed C_i symmetry). Selected bond distances [Å] and angles (deg): Li-C1, 2.222; Li-C2, 2.262; Li-C3, 2.384; Li-C3′, 2.284; C1-C2, 1.383; C2-C3, 1.443; C1-C2-C3, 127.7.

Given the broad similarity between the structures of unsolvated {Mg[1,3-$(SiMe_3)_2C_3H_3$]$_2$}$_2$[48] and [Li(allyl′)]$_2$, it is interesting that the magnesium complex dissociates in THF solution, but that the latter remains dimeric.[96] What the structure of such a solvated dimer might be was first investigated by Schleyer, who used H_2O as a computationally expedient proxy for oxygen-based ligands in his semiempirical study of diallyllithium.[96] Although causing large distortions in the framework and strong localization of the C-C/C=C allyl bonds, the presence of two H_2O molecules per lithium did not disrupt the dimeric structure. Water has many inadequacies as an ether substitute,[93] however, and the structure was reinvestigated at the PBE-D/TZ2P level using THF molecules in place of water. The optimized structure with C_1 symmetry indicates that the Li–C bonds have lengthened by roughly 0.1 Å, but that the bonding is still describable as μ_2-η^1,η^3 (Figure 14). The Li1–C1(σ) bond at 2.295 Å remains the shortest in the structure, but the bridging Li1–C(1′,2′,3′) distances span a surprisingly small range (2.34–2.36 Å). The allyl C–C distances are as delocalized (Δ = 0.038 Å) as in the unsolvated dimer. The Li···Li′ distance at 2.65 Å is longer than in the unsolvated [Li(C_3H_5)]$_2$, but comparable to the distance calculated for the {Li[1,1′,3-$(SiH_3)_3C_3H_2$]}$_2$ dimer.

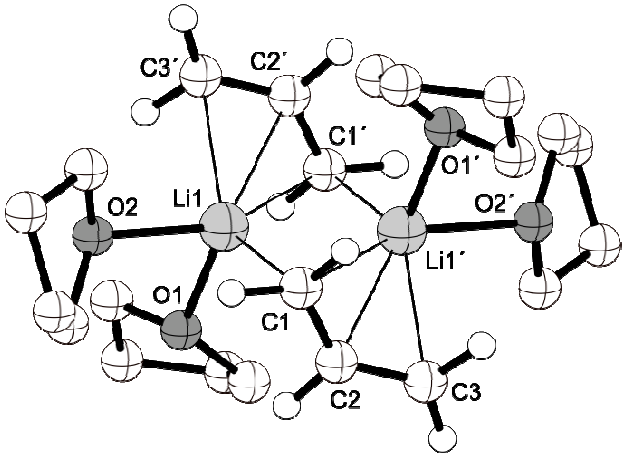

Figure 14. Calculated structure (PBE-D/TZ2P) of $[Li(C_3H_5)(thf)_2]_2$ (imposed C_1 symmetry, numbering changed to facilitate comparison with Figure 12). Selected bond distances [Å] and angles (deg): Li-C1, 2.295; Li-C1´, 2.364; Li-C2´, 2.355; Li-C3´, 2.339; C1-C2, 1.418; C2-C3, 1.380; Li1-O1, 2.091; Li1-O2, 2.141; C1-C2-C3, 129.4.

Adding SiH_3 groups causes further shifts in the geometry of the dimer, such that the allyl ligands bridge the lithium centers more symmetrically. The Li1–C1 and Li1′–C3 distances are 2.288 and 2.334 Å, respectively, but both the Li1–C2 and Li1′–C2 contacts are greater than 2.9 Å and should be considered non-bonding. The metal-allyl bonding is describable as μ_2-η^1,η^1 (Figure 15). Despite the bulk of the SiH_3 groups, the Li–O bonds have shortened to an average of 2.02 Å, but the allyl C–C distances remain delocalized (Δ = 0.033 Å), as in the unsolvated dimer. The symmetrizing of the structure has pushed the Li···Li′ distance to 3.99 Å, 50% longer than the comparable structure without the silyl substituents.

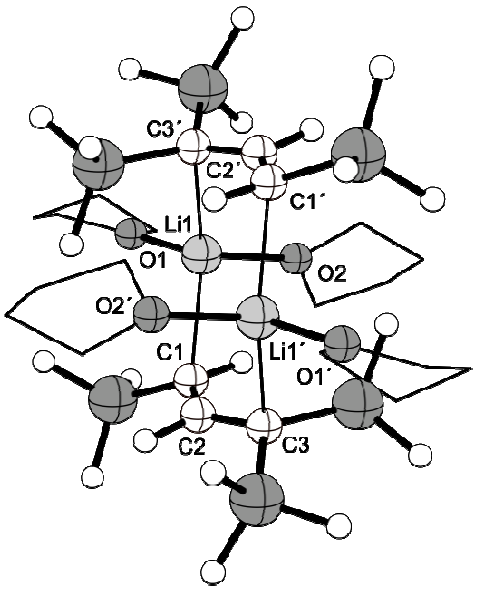

Figure 15. Calculated structure (PBE-D/TZ2P) of {Li[1,1´,3-$(SiH_3)_3C_3H_2$](thf)$_2$}$_2$ (C_i symmetry numbering changed to facilitate comparison with Figure 14). The carbon atoms of the THF ligands have been omitted for clarity. Selected bond distances [Å] and angles (deg): Li-C1, 2.334; Li···C2, 3.293; Li1-C3´, 2.288; Li1···C2´, 2.906; C1-C2, 1.392; C2-C3, 1.425; Li1-O1, 2.006; Li1-O2, 2.032; C1-C2-C3, 130.6.

Conclusions

Trimethylsilylated allyl complexes of the alkali metals show a transition toward higher nuclearity and greater π-character upon descending from lithium to potassium. This is a result of the increase in both the size of the cation and ionicity of the bonding moving down the group. Although there are differences in detail, all known allyl complexes of the heavier alkali metals (K-Cs) form solid-state coordination polymers with π-bound ligands. In the case of potassium, the general structure persists with or without additional coordinated bases (DME, THF). It is difficult to draw general conclusions

about sodium allyl structures, given the limited number in the literature. However, it apparently favors a lower nuclearity than potassium. Even in the presence of a coordinated base, $\{Na[1,3\text{-}(SiMe_3)_2C_3H_3](thf)\}_4$ prefers a tetranuclear structure with highly delocalized allyl ligands. The structural chemistry of allyl complexes of the smaller lithium cation is more complex:[95] monomeric,[20] polymeric,[97] and oligomeric[95] structures can be isolated, depending on the substituents on the ligands and the steric bulk of the associated bases. Nevertheless, the general dinuclear structure of $[Li(allyl)]_2$ with μ_2-allyl ligands appears remarkably resilient to large increases in the steric bulk of the ligands, as observed in $\{Li[1,1',3\text{-}(SiMe_3)_3C_3H_2]\}_2$, or to the addition of THF ligands (as established experimentally in solution[96] and verified computationally). The briding allyl ligands in $\{Li[1,1',3\text{-}(SiMe_3)_3C_3H_2]\}_2$ remain partially delocalized (Δ_{CC} = 0.085 Å), indicating some degree of π-bonding. This is unlike the related $\{Mg[1,3\text{-}(SiMe_3)_2C_3H_3]_2\}_2$, whose bridging allyl ligands are localized (Δ_{CC} = 0.15 Å) and which monomerizes upon coordination of THF.[48]

CHAPTER III

CATION–π BONDING IN ALKALI METAL TRIS-ALLYL COMPLEXES OF ZINC AND CADMIUM

Introduction

The cation-π interaction—a noncovalent attraction between a cation and a substrate that provides π-electron density—is most commonly found between an alkali metal cation and an aromatic ring.[54] The energy of this interaction is typically measured in the gas phase, and can be significant. There are also numerous structural examples in the literature of coordination compounds displaying pronounced alkali cation–arene interactions to coordinated ligands. For example, the reaction of $Ga(PhCH_2)_3$ with CsF in acetonitrile yields $\{Cs[(PhCH_2)_3GaF]\}_2 \cdot 2MeCN$. The structure is constructed around a $(CsF)_2$ ring and displays multiple Cs···phenyl interactions (Figure 16).[98]

Instead of aromatic rings, the source of the electrons in cation-π interactions can be individual double and triple bonds,[57,99-102] but less is known about structural and energetic features in such cases. The gas-phase $Na^+ \cdots C_2H_4$ interaction has been experimentally measured,[101] for example, and the cyclic beltenes (cyclacenes) (Figure 17) display size-selective binding of alkali metal cations mediated by cation-π interactions.[102]

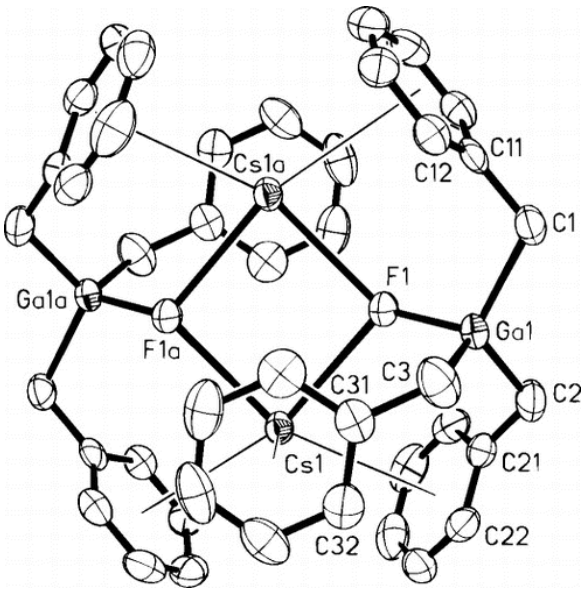

Figure 16. Solid-state structure of $\{Cs[(PhCH_2)_3GaF]\}_2$ showing the cation-π interactions between the Cs atoms and the phenyl moieties.[98]

The allyl fragment is a potentially useful source of π-electrons in cation-π interactions, and Na^+ has been found to bind to the allyl sidearms in the lariat crown ether *N,N'*-dibutenyl-1,10-diaza-18-crown-6 (Figure 18a).[100] Also, Ernst has found that K^+ can bind to the double bonds of pendant pentadienyl ligands in an "allylic like" fashion.[99] A similar role should be possible for allyl ligands in metal complexes, and this work will show that metal bound σ-allyl ligands can also engage in intramolecular cation-π interactions with an electropositive metal cation (Figure 18b). Similar bonding arrangements have been seen in transition metal complexes, but these cases involve covalent d-electron bonding, not noncovalent, cation-π interactions.[103-107]

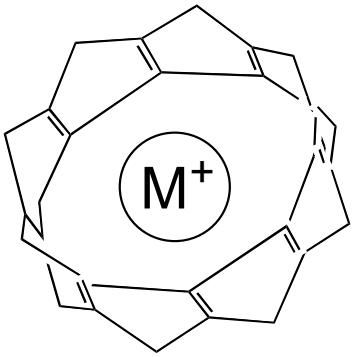

Figure 17. Diagram showing cation-π bonding in a beltene (cyclacene).

This combination of covalent and electrostatic bonding provides an environment in which the geometric requirements of multiple non-arene cation-π interactions can be studied. In this chapter, the synthesis, and resulting structures, and behaviors of these unusual triallylmetalates will be discussed, using both experiment and density functional theory (DFT) calculation to help explain the bonding results.

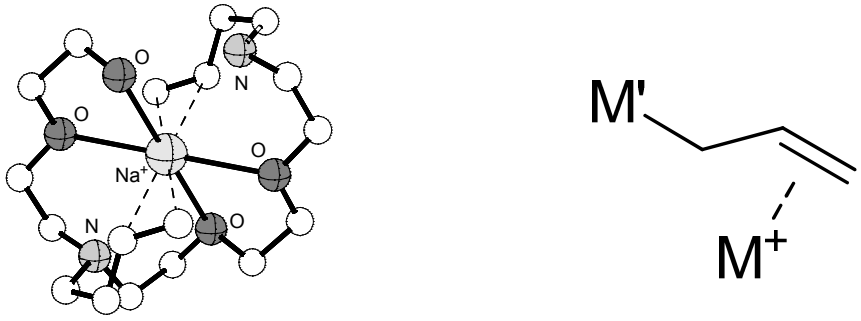

(a) (b)

Figure 18. (a) Na^+ and allyl interaction in a lariat crown ether; (b) simultaneous σ- and cation-π bonding with an allyl ligand.

Experimental

General Considerations. All manipulations were performed with the rigorous exclusion of air and moisture using high-vacuum, Schlenk, or glovebox techniques. Proton (^{1}H) and carbon (^{13}C) NMR experiments were obtained on a Bruker DPX-300 at 300 MHz and 75.5 MHz, or a Bruker DPX-400 at 400 MHz and 100 MHz, respectively, and were referenced to residual proton and ^{13}C resonances of THF-d_8 (δ 3.58 and 67.4), C_6D_6 (δ 7.15 and 128.1), and toluene-d_8 (δ 2.09 and 20.4). Lithium (^{7}Li) and sodium (^{23}Na) NMR data were obtained on the DPX-400 instrument at 155 MHz and 106 MHz, respectively, and were referenced to external 1.0 M LiCl and 1.0 M NaCl in D_2O at 298 K. Elemental analysis was performed by Desert Analytics (Tucson, AZ).

Materials. Hexanes was distilled under nitrogen from potassium benzophenone ketyl. Anhydrous tetrahydrofuran (THF) was purchased from Aldrich and used as received. Anhydrous metal salts were purchased from Strem Chemicals and used as received. D_2O was purchased from Cambridge Isotopic Laboratories, Inc. and used as received. C_6D_6, toluene-d_8, and THF-d_8 were vacuum-distilled from Na/K (22/78) alloy and stored over type 4A molecular sieves prior to use. Li[1,3-$(SiMe_3)_2C_3H_3$],[16] K[1,3-$(SiMe_3)_2C_3H_3$],[33] and Cs[1,3-$(SiMe_3)_2C_3H_3$][41] were prepared following published syntheses.

Synthesis of Li[Zn(1,3-$(SiMe_3)_2C_3H_3)_3$]. A 125 mL Schlenk flask equipped with a magnetic stir bar was charged with $Zn(OTf)_2$ (0.150 g; 0.413 mmol) in

30 mL THF. Li[1,3-$(SiMe_3)_2C_3H_3$] (0.238 g; 1.24 mmol) in 20 mL THF was added to the dropping funnel. The apparatus was cooled to −78 ºC, after which the THF solution of Li[1,3-$(SiMe_3)_2C_3H_3$] was added dropwise with stirring over the course of 15 min. The solution was allowed to warm to room temperature overnight. Removal of solvent under vacuum, followed by extraction of the residue with hexanes, filtration of the extract over a medium-porosity glass frit, and removal of hexanes under vacuum afforded an air- and moisture-sensitive yellow solid (0.150 g, 58%). ^{1}H NMR (C_6D_6, 298 K): δ 6.46 (t, J = 14.1 Hz, 3H, C_2), 3.50 (br, 6H, $C_{1,3}$), 0.15 (s, 54H, $SiMe_3$); (THF-d_8, 298 K): δ 6.51 (t, J = 15.0 Hz, 3H), 3.19 (d J = 15.0 Hz, 6 H), −0.054 (s, 54H, $SiMe_3$). ^{13}C NMR (C_6D_6, 298 K): δ 137.67 ($C_{(2)}$, central), 68.52 ($C_{(1,3)}$, outer), 1.36 ($SiMe_3$), 1.15 ($SiMe_3$). ^{7}Li NMR (C_6D_6, 298 K): δ 1.10 (br); (THF-d_8, 298 K): δ −0.35 (br).

Synthesis of Na[Zn(1,3-$(SiMe_3)_2C_3H_3)_3$]. A 125 mL Schlenk flask equipped with a magnetic stir bar was charged with $Zn(OTf)_2$ (0.152 g; 0.418 mmol) in 30 mL THF. Na[1,3-$(SiMe_3)_2C_3H_3$] (0.253 g; 1.21 mmol) in 20 mL THF was added to the dropping funnel. The apparatus was cooled to −78 ºC, after which the THF solution of Na[1,3-$(SiMe_3)_2C_3H_3$] was added dropwise with stirring over the course of 15 min. The solution was allowed to warm to room temperature overnight. Removal of solvent under vacuum, followed by extraction of the residue with hexanes, filtration of the extract over a medium-porosity glass frit, and removal of hexanes under vacuum afforded

an air- and moisture-sensitive yellow solid (0.220 g, 82%), m.p. 146 °C. Anal. Calcd. for $C_{27}H_{63}NaSi_6Zn$: C, 50.30; H, 9.85; Na, 3.6. Found: C, 50.01; H, 9.85; Na, 3.0. ^{1}H NMR (C_6D_6, 298 K): δ 7.59 (t, J = 15.8 Hz, 3H, C_2), 4.00 (br, 6H, $C_{1,3}$), 0.16 (s, 54H, $SiMe_3$); (THF-d_8, 298 K): δ 6.51 (t, J = 15.0 Hz, 3H), 3.19 (d J = 15.0 Hz, 6 H), −0.054 (s, 54H, $SiMe_3$). ^{13}C NMR (C_6D_6, 298 K): δ 169.64 ($C_{(2)}$, central), 77.8 (v br, $C_{(1,3)}$, outer), 0.99 ($SiMe_3$). ^{23}Na NMR (C_6D_6, 298 K, 0.12 M): δ 12.89 (br); (THF-d_8, 298 K): δ −7.16 (s).

Synthesis of K[Zn(1,3-(SiMe$_3$)$_2$C$_3$H$_3$)$_3$]. A 125 mL Schlenk flask equipped with a magnetic stir bar was charged with $Zn(OTf)_2$ (0.567 g; 1.56 mmol) in 30 mL THF. K[1,3-$(SiMe_3)_2C_3H_3$] (1.05 g; 4.68 mmol) in 20 mL THF was added to the dropping funnel. The apparatus was cooled to −78 °C, after which the THF solution of K[1,3-$(SiMe_3)_2C_3H_3$] was added dropwise with stirring over the course of 15 min. The solution was allowed to warm to room temperature overnight. Removal of solvent under vacuum, followed by extraction of the residue with hexanes, filtration of the extract over a medium-porosity glass frit, and removal of hexanes under vacuum afforded an air- and moisture-sensitive, orange-red solid (0.880 g, 85%). Anal. Calcd. for $C_{27}H_{63}KSi_6Zn$: C, 49.08; H, 9.61. Found: C, 48.66; H, 9.32. ^{1}H NMR (C_6D_6, 298 K): δ 7.05 (t, J = 15.3 Hz, 3H, C_2), 3.42 (d, J = 15.3 Hz, 6H, $C_{1,3}$), 0.23 (s, 54H, $SiMe_3$); (THF-d_8, 298 K, 300 MHz): δ 6.51 (t, J = 15.0 Hz, 3H), 3.19 (d J = 15.0 Hz, 6 H), −0.054 (s, 54H, $SiMe_3$); (tol-d_8, 298 K, 400 MHz): δ

6.95 (t, 3H, C_2), 3.33 (d J = 15.2 Hz, 6 H), 0.15 (s, 54H, $SiMe_3$). ^{13}C NMR (C_6D_6, 298 K): δ 163.91 ($C_{(2)}$, central), 76.40 ($C_{(1,3)}$, outer), 1.00 ($SiMe_3$). Variable temperature ^1H NMR (tol-d_8, 400 MHz, δ): (198 K) 7.1 (t, 3H), 0.28 (s, 54 H, $SiMe_3$); (218 K) 7.06 (t, 3H), 3.38 (broad singlet, 6H), 0.25 (s, 54H, $SiMe_3$); (238 K) 7.04 (t, 3H), 3.36 (broad doublet, J = 10.8 Hz, 6H), 0.22 (s, 54H, $SiMe_3$).

Synthesis of Cs[Zn(1,3-(SiMe$_3$)$_2$C$_3$H$_3$)$_3$]. A 125 mL Schlenk flask equipped with a magnetic stir bar was charged with $Zn(OTf)_2$ (0.115 g; 0.316 mmol) in 30 mL THF. Cs[1,3-$(SiMe_3)_2C_3H_3$] (0.370 g; 1.16 mmol) in 20 mL THF was added to the dropping funnel. The apparatus was cooled to −78 °C, after which the THF solution of Cs[1,3-$(SiMe_3)_2C_3H_3$] was added dropwise with stirring over the course of 15 min. The solution was allowed to warm to room temperature overnight. Removal of solvent under vacuum, followed by extraction of the residue with hexanes, filtration of the extract over a medium-porosity glass frit, and removal of hexanes under vacuum afforded an air- and moisture-sensitive, orange oily solid (0.27 g, quantitative). ^1H NMR (C_6D_6, 298 K): δ 6.95 (t, J = 15.3 Hz, 3H, C_2), 3.31 (d, J = 15.3 Hz, 6H, $C_{1,3}$), 0.26 (s, 54H, $SiMe_3$); (THF-d_8, 298 K, 300 MHz): δ 6.51 (t, J = 15.0 Hz, 3H), 3.19 (d J = 15.0 Hz, 6 H), −0.052 (s, 54H, $SiMe_3$)

Synthesis of Li[Cd(1,3-(SiMe$_3$)$_2$C$_3$H$_3$)$_3$]. A 50 mL Erlenmeyer flask equipped with a stir bar was charged with CdI_2 (0.338 g; 0.923 mmol) in 15

mL THF and cooled to −40 ºC. A solution of Li[1,3-$(SiMe_3)_2C_3H_3$] (0.533 g; 2.77 mmol) in 5 mL THF, also at −40 ºC was added dropwise to the stirring solution of CdI_2 over the course of 5 mins. The reaction was allowed to stir for one hour at −40 ºC. Removal of solvent under vacuum, followed by extraction of the residue with hexanes (cooled to −40 ºC), filtration of the extract over a medium-porosity glass frit, and removal of hexanes under vacuum, afforded an air-, moisture-, and thermally-sensitive yellow oily solid (0.169 g, 27%), which was stored at −40 ºC. ^{1}H NMR (C_6D_6, 298 K): δ 6.80 (t, J = 14.9 Hz, 3H, C_2), 3.70 (d, J = 14.9 Hz, 6H, $C_{1,3}$), 0.27 (s, 54H, $SiMe_3$); (THF-d_8, 298 K): δ 6.55 (t, J = 14.9 Hz, 3H, C_2), 3.36 (d, J = 14.9 Hz, 6H, $C_{1,3}$), −0.01 (s, 54H, $SiMe_3$). ^{13}C NMR (C_6D_6, 298 K): δ 153.38 ($C_{(2)}$, central), 69.14 ($C_{(1,3)}$, outer), 1.27 ($SiMe_3$).

Computational Details. All calculations were performed with the Gaussian 03W suite of programs.[108] For geometry optimization of Li[Zn(1,3-$(SiMe_3)_2C_3H_3)_3$], the B3PW91 functional, which incorporates Becke's three-parameter exchange functional[109] with the 1991 gradient-corrected correlation functional of Perdew and Wang,[110] was used. This hybrid functional has previously been shown to provide realistic geometries for organometallic species.[111-113] The DFT-optimized double-zeta basis sets of Godbout[114] (DGDZVP2) were used with all atoms.

For analysis of the metal-benzene and metal-ethylene cations, an initial goal was the reproduction, within experimental error, of the measured heats

of formation of the gas-phase $[M(C_6H_6)]^+$ species (M = Li, Na, K). Several functional/basis set combinations were evaluated: B3PW91/DGDZVP2 (C,H), DGDZVP (K); PBE1PBE/aug-cc-pVTZ (C,H), CVTZ (K); PBE1PBE/aug-cc-pVDZ (C,H), CVDZ (K); B97-1/DGDZVP2; B97-1/aug-cc-pVTZ. These trials led to the selection of the hybrid PBE1PBE functional[81] and the use of basis sets of at least polarized double zeta quality with diffuse functions on all C, H atoms. Somewhat better results (by 0.1–0.5 kcal mol^{-1}) were obtained if basis sets of triple zeta quality (e.g., aug-cc-pVTZ) were used. The importance of including core valence correlation in reproducing binding energies in alkali metal complexes[115] lead to the use of the cc-pCVTZ basis sets on lithium (11s,5p,2d,1f)/[4s,3p,2d,1f] and sodium ((16s,10p,2d,1f)/[5s,4p,2d,1f]), and the corresponding "Feller Misc. CVTZ" on potassium ((18s,15p,4d,2f)/[8s,7p,4d,2f]) ((*s,p*) exponents from Ahlrichs;[116] polarization and core/valence exponents from Feller[115]). CRENL effective core potential was used for cesium. This does not give adequate agreement with experimental energies; however, comparisons between calculated energies is appropriate. Calculations on $[M(C_6H_6)]^+$ were performed under C_{6v} symmetry; trial calculations for $[M(C_2H_4)_n]^+$ optimized to structures with nearly exact C_{2v}, D_{2d}, and D_3 symmetry for n = 1, 2, and 3, respectively; the symmetry was made exact for subsequent work. All molecules were optimized with ultrafine grids and the GDIIS algorithm.[117,118] Small (less than 20*i*) imaginary frequencies were encountered in the $[M(C_2H_4)_{2,3}]^+$ calculations;

these are considered to be artifactual. The other molecules displayed no imaginary frequencies; all geometries are considered to be minima on their potential energy surfaces.

General Procedures for X-ray Crystallography. Suitable crystals of $Li[Zn(1,3\text{-}(SiMe_3)_2C_3H_3)_3]$, $Na[Zn(1,3\text{-}(SiMe_3)_2C_3H_3)_3]$, and $K[Zn(1,3\text{-}(SiMe_3)_2C_3H_3)_3]$ were located, attached to glass fibers, and mounted on a Siemens SMART system for data collection. The intensity data were corrected for absorption (SADABS). All calculations were performed with the SHELXTL suite of programs.[119] Final cell constants were calculated from a set of strong reflections measured during the actual data collection. Relevant crystal and data collection parameters and atomic coordinates for each compound are given in Appendix C. The space groups were determined from systematic absences and intensity statistics. The structures were solved by direct methods and refined against F^2 for all observed reflections, using SHELXS and SHELXL.

The similarity in chemical environment of the two metal-atom sites in $Li[Zn(1,3\text{-}(SiMe_3)_2C_3H_3)_3]$ and $Na[Zn(1,3\text{-}(SiMe_3)_2C_3H_3)_3]$ led to disorder in their occupancy. At each site there is 30% (for the Li complex) or 16% (for the Na complex) of the character of the other metal. The disorder was modeled using EADP and EXYZ commands that constrained the coordinates and thermal parameters to be identical for each pair, and the occupancies were constrained to unity.

Results and Discussion

Synthesis of tri(allyl)metalates. Allyl ligands containing trimethylsilyl substituents are readily incorporated into thermally stable complexes with metals from across the periodic table,[76] and in an attempt to isolate trimethylsilated allyl compounds of the Group 12 metals, zinc triflate was treated with two equivalents of the potassium salt of the bis(1,3-trimethylsilyl)allyl anion.[33] Potassium triflate was precipitated as a by-product, and the tri(allyl)zincate $K[Zn(1,3\text{-}(SiMe_3)_2C_3H_3)_3]$ was isolated instead of the intended neutral $Zn[1,3\text{-}(SiMe_3)_2C_3H_3]_2$. Adjustment of the stoichiometry of the reaction (eq 6) and the use of lithium, sodium, and cesium allyls as starting materials generated the air- and moisture-sensitive, yellow $Li[Zn(1,3\text{-}(SiMe_3)_2C_3H_3)_3]$, $Na[Zn(1,3\text{-}(SiMe_3)_2C_3H_3)_3]$, and $Cs[Zn(1,3\text{-}(SiMe_3)_2C_3H_3)_3]$ in addition to the orange-red $K[Zn(1,3\text{-}(SiMe_3)_2C_3H_3)_3]$ in moderate to good yields. An analogous lithium cadmiate complex, $Li[Cd(1,3\text{-}(SiMe_3)_2C_3H_3)_3]$, was also synthesized from the addition of three equivalents of bis(1,3-trimethylsilyl)allyl lithium to cadmium iodide (eq 7).

$$Zn(OTf)_2 + 3\ M(allyl') \xrightarrow[-78\ ^oC,\ 18\ h]{THF} M[Zn(allyl')_3] + 2\ M[OTf]\downarrow \quad (M = Li, Na, K, Cs) \qquad (6)$$

$$CdI_2 + 3\ Li(alllyl') \xrightarrow[\text{-40 °C, 18 h}]{\text{THF}} Li[Cd(allyl')_3] + 2\ LiI\downarrow \quad (7)$$

The formation of $K[Zn(1,3\text{-}(SiMe_3)_2C_3H_3)_3]$ when only two equiv of the allyl reagent were available is unusual, given that the parent $Zn(C_3H_5)_2$ is formed even with the use of 2.6 equiv of C_3H_5MgCl per equiv of $ZnCl_2$.[43] There are, however, several known cases in which reactions with electropositive metals and bulky allyl ligands do not give the stoichiometrically expected products.[25,29] For example, in an attempt to synthesize $La[1,3\text{-}(SiMe_3)_2C_3H_3]_3$ from the reaction of three equiv of $K[1,3\text{-}(SiMe_3)_2C_3H_3]$ with $LaCl_3$, only $La[1,3\text{-}(SiMe_3)_2C_3H_3]_2Cl(thf)$ is produced.[29] Conversely, the triallyl complex $Y[1,3\text{-}(SiMe_3)_2C_3H_3]_3$ is formed when only two equiv of $K[1,3\text{-}(SiMe_3)_2C_3H_3]$ are treated with YCl_3.[113] The strong σ-donation properties of the silylated allyl may encourage the formation of tri(allyl′) species; the steric bulk of the substituents obviously do not interfere with the formation of the anion.

When a THF solution of $K[Zn(1,3\text{-}(SiMe_3)_2C_3H_3)_3]$ is treated with lithium iodide, precipitation of KI is accompanied by the formation of $Li[Zn(1,3\text{-}(SiMe_3)_2C_3H_3)_3]$ (eq 8).

$$K[Zn(allyl)_3] + LiI \rightarrow Li[Zn(allyl)_3] + KI\downarrow \quad (8)$$

Although the interaction of the Li^+ cation with the allyl anion is likely stronger than with K^+, this interaction is probably only of minor importance to the metal exchange. The ion separation that occurs in THF (see below) and the precipitation of the insoluble KI are likely the dominant driving forces in the reaction.

Solution behavior. The cadmiate complex was found to be thermally unstable. Cadmium metal precipitates from a solution of $Li[Cd(1,3\text{-}(SiMe_3)_2C_3H_3)_3]$ within minutes of warming to room temperature. However, NMR data indicate that complex $Li[Cd(1,3\text{-}(SiMe_3)_2C_3H_3)_3]$ is analogous to the lithium zincate complex, $Li[Zn(1,3\text{-}(SiMe_3)_2C_3H_3)_3]$. Thus the remaining discussion will focus only on the zincate complexes. All of the Group 12 metallates discussed here are fluxional in solution. Their ^1H and ^{13}C NMR spectra at room temperature indicate that the structures are more symmetrical than in the solid state (see below), with apparently 'π-bound' allyl ligands. For example, the ^1H resonance for all six $SiMe_3$ groups in $K[Zn(1,3\text{-}(SiMe_3)_2C_3H_3)_3]$ appears as a singlet that broadens but does not split on cooling to −75 °C. The hydrogen atoms on the carbons α and γ to the zinc appear as a doublet that coalesces to a single peak on cooling, and disappears into the baseline by −75 °C. These fluxional rearrangements are reminiscent of the patterns observed in the neutral compound $Ga(1,3\text{-}(SiMe_3)_2C_3H_3)_3$[19] described further in chapter IV, and indicate that the $[Zn(allyl)_3]^-$ anion is free to undergo rearrangement largely uninhibited by

the cation. The allyl ligands of Li[Zn(1,3-$(SiMe_3)_2C_3H_3)_3$], Na[Zn(1,3-$(SiMe_3)_2C_3H_3)_3$], Cs[Zn(1,3-$(SiMe_3)_2C_3H_3)_3$], and Li[Cd(1,3-$(SiMe_3)_2C_3H_3)_3$] display the same highly symmetrical structure as does K[Zn(1,3-$(SiMe_3)_2C_3H_3)_3$] in their ^{1}H NMR spectra, although the shifts are at different positions (e.g., in C_6H_6, the C–H triplet at δ 7.05 ppm for K[Zn(1,3-$(SiMe_3)_2C_3H_3)_3$] appears at δ 7.59 ppm for Na[Zn(1,3-$(SiMe_3)_2C_3H_3)_3$]). Such shifts suggest that in C_6D_6 the cations remain associated with the triallyl zinc anion.

Interestingly, in THF-d_8 the ^{1}H NMR chemical shifts for the four zincates are identical, indicating that the alkali metal cations and the zincate anions are now largely solvent-separated. The change in solvation is apparent in the ^{7}Li NMR spectra of Li[Zn(1,3-$(SiMe_3)_2C_3H_3)_3$] (Figure 19) as well as the ^{23}Na NMR spectra of Na[Zn(1,3-$(SiMe_3)_2C_3H_3)_3$]. The ^{7}Li NMR spectrum in C_6D_6 shows a peak at δ 1.10 ppm flanked by a broader resonance at δ 0.6 ppm, demonstrating that at least two similar environments exist for the Li^+ cation, possibly the result of fluxional rearrangements or interaction with the benzene solvent. The shifts are typical for organolithium species (e.g., EtLi is at δ 1.27; *i*-PrLi is at δ 0.69).[120] In THF-d_8, the resonance shifts upfield to approximately δ −0.35 ppm and narrows. Although an upfield shift commonly occurs for alkyllithiums in polar solvents (that for EtLi is at δ 0.79 in Et_2O), the shift in THF for Li[Zn(1,3-$(SiMe_3)_2C_3H_3)_3$] is substantial, and is

indicative of an increase in ionic character. The shift is not far from the value for the solvent-separated pair $[Li(thf)_4][CPh_3]$ (−0.45 ppm in THF-d_8; $\Delta\nu_{1/2}$ = 10.2 Hz),[121] although the width of the line in $Li[Zn(1,3\text{-}(SiMe_3)_2C_3H_3)_3]$ ($\Delta\nu_{1/2} \approx 53$ Hz) and the indications of some unresolved structure on the peak suggests that the latter species is not as symmetric. For $Na[Zn(1,3\text{-}(SiMe_3)_2C_3H_3)_3]$, the ^{23}Na NMR spectra in C_6D_6 shows a peak at δ 12.90 ppm and in THF-d_8 shows a peak at δ −7.16 ppm. The chemical shift in THF-d_8 is similar to that of $NaBPh_4$ in THF (δ −8.12 ppm)[122] and indicative of a solvent-separated ion pair. There are no examples in the literature of a ^{23}Na spectrum of an organometallic complex in benzene. However, Popov notes that NaI in THF represents a contact ion pair, as reflected by a downfield shift in the resonance (δ 6.25 ppm at 0.5 M).[122]

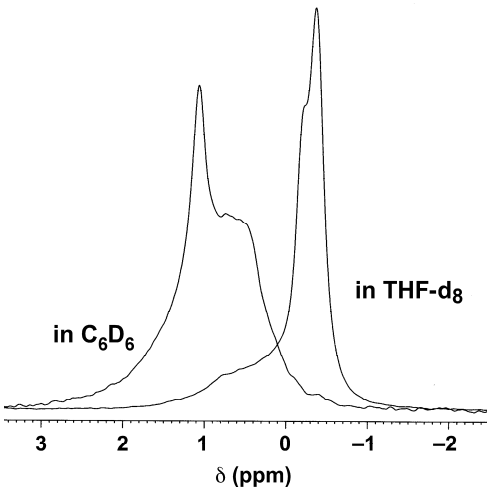

Figure 19. ^7Li NMR spectra of $Li[Zn(allyl')_3]$ in C_6D_6 and THF-d_8.

Solid-state structures of Na[Zn(1,3-$(SiMe_3)_2C_3H_3)_3$] and K[Zn(1,3-$(SiMe_3)_2C_3H_3)_3$]. Single crystal X-ray structures of Na[Zn(1,3-$(SiMe_3)_2C_3H_3)_3$] (Figure 20) and K[Zn(1,3-$(SiMe_3)_2C_3H_3)_3$] (Figure 21) reveal that the three allyl ligands are bound to the zinc in an arrangement with approximate C_3 symmetry, with the alkali metal cation situated between the three double bonds of the allyl ligands. The sodium derivative suffers from some disorder in the Na/Zn positions (see the Experimental Section for details), but it is unquestionably isostructural with the potassium salt, so only K[Zn(1,3-$(SiMe_3)_2C_3H_3)_3$] is discussed in detail here. The average Zn–C distance of 2.068(4) Å is similar to the Zn–C length of 2.09(2) Å found in the trialkyl anion $Zn[CH(SiMe_3)_2]_3^-$.[123] The C–C and C=C bonds in the alkyl groups are localized at 1.462(5) Å and 1.359(6) Å, respectively. The $K^+\cdots$C(olefin) contacts average 3.205(3) Å and 2.945(3) Å to the carbon atoms β (C5, C15, C25) and γ (C6, C16, C26) to the zinc atom, respectively

These contacts are comparable to the $K^+\cdots$C distances to the pentadienyl arms of Ernst's potassium manganate complex (2.983(19) Å to 3.319(17) Å).[99] In Ernst's complex the potassium cation is interacting with three carbons of each ligand instead of only the vinylic carbons. This is seen in spite of the localization of the carbon bonds (C–C and C=C are 1.440(15) Å and 1.335(15) Å, respectively). The distances in K[Zn(1,3-$(SiMe_3)_2C_3H_3)_3$] are also comparable to the range of $K^+\cdots$C contacts usually observed with aromatic

rings (cf. 3.02–3.35 Å to the benzyl group in $\{KZn[N(SiMe_3)_2]_2(CH_2Ph)\}_\infty$[124] or the 3.12–3.35 Å distances to the neutral arenes in $\{[K(toluene)_2]^+[Mg(N(SiMe_3)_2)_3]^-\}_n$[125]), although differences in coordination numbers make exact comparisons difficult.[126] The analogous $Na^+\cdots C$(olefin) contacts in $Na[Zn(1,3\text{-}(SiMe_3)_2C_3H_3)_3]$ average 2.857(3) Å and 2.567(3) Å to the carbon atoms β and γ to the zinc atom, respectively, and are similar to known cation-π $Na^+\cdots C$(arene) distances (cf. 2.91 Å (avg) in $[Na_2(C_2Ph_4)(OEt_2)_2]_n$[127] or 2.88 Å (avg) in $(Et_2O)Na(Ph_2CCHCPh_2)$[88]). There are no contacts in either molecule that are suggestive of $M^+\cdots$C-H agostic interactions.

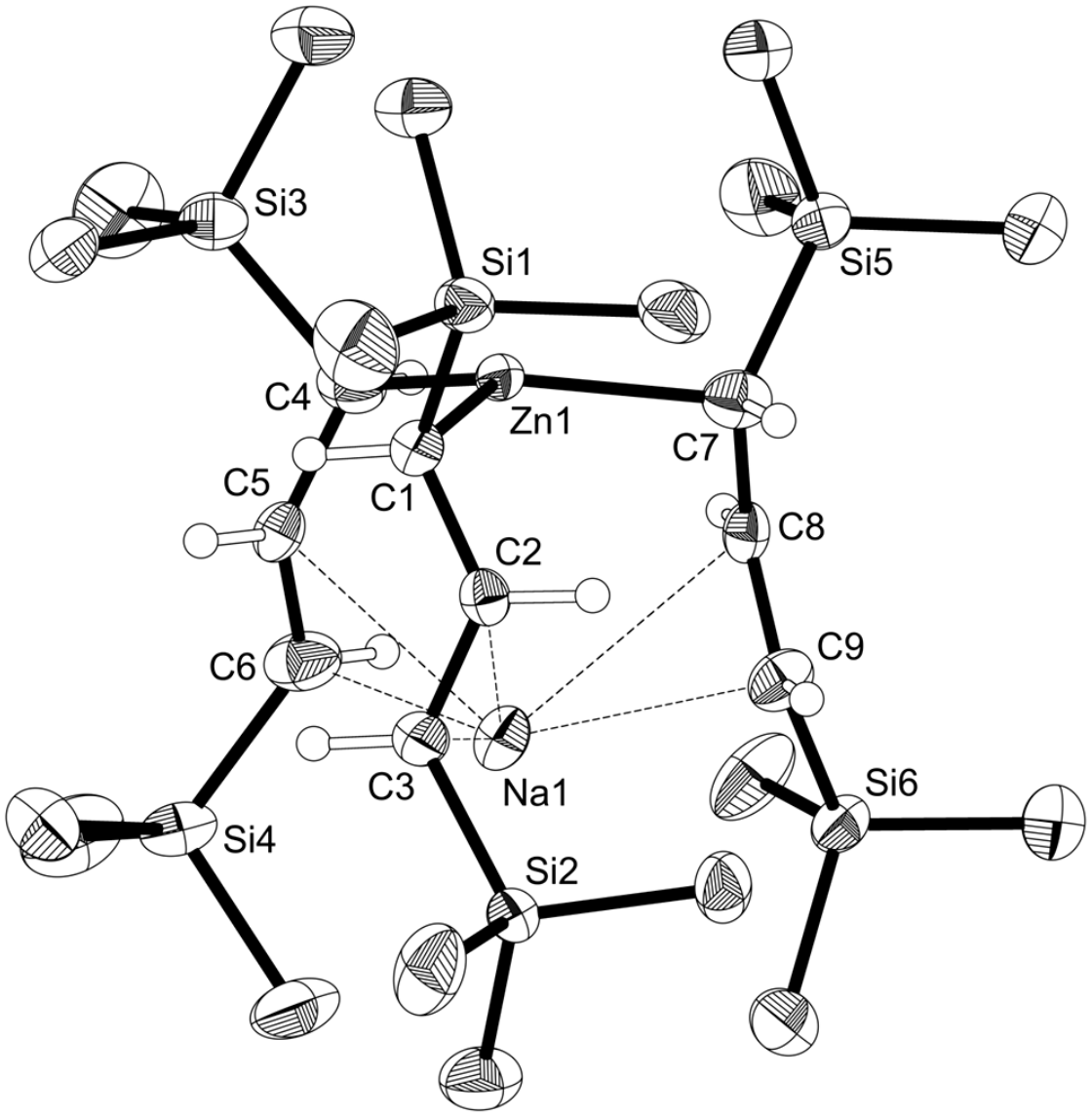

Figure 20. Solid-state structure of $Na[Zn(1,3\text{-}(SiMe_3)_2C_3H_3)_3]$, with thermal ellipsoids at the 50% level. Hydrogen atoms have been removed from the trimethylsilyl groups for clarity. Selected bond distances (Å) and angles (deg): Zn(1)-C(1), 2.100(2); Zn(1)-C(4), 2.101(2); Zn(1)-C(7), 2.108(2); C(1)-C(2), 1.447(2); C(2)-C(3), 1.361(3); C(4)-C(5), 1.441(3); C(5)-C(6), 1.368(3); C(7)-C(8), 1.447(3); C(8)-C(9), 1.365(3); C(2)-C(1)-Zn(1), 104.53(12); C(5)-C(4)-Zn(1), 103.99(13); C(8)-C(7)-Zn(1), 102.45(12).

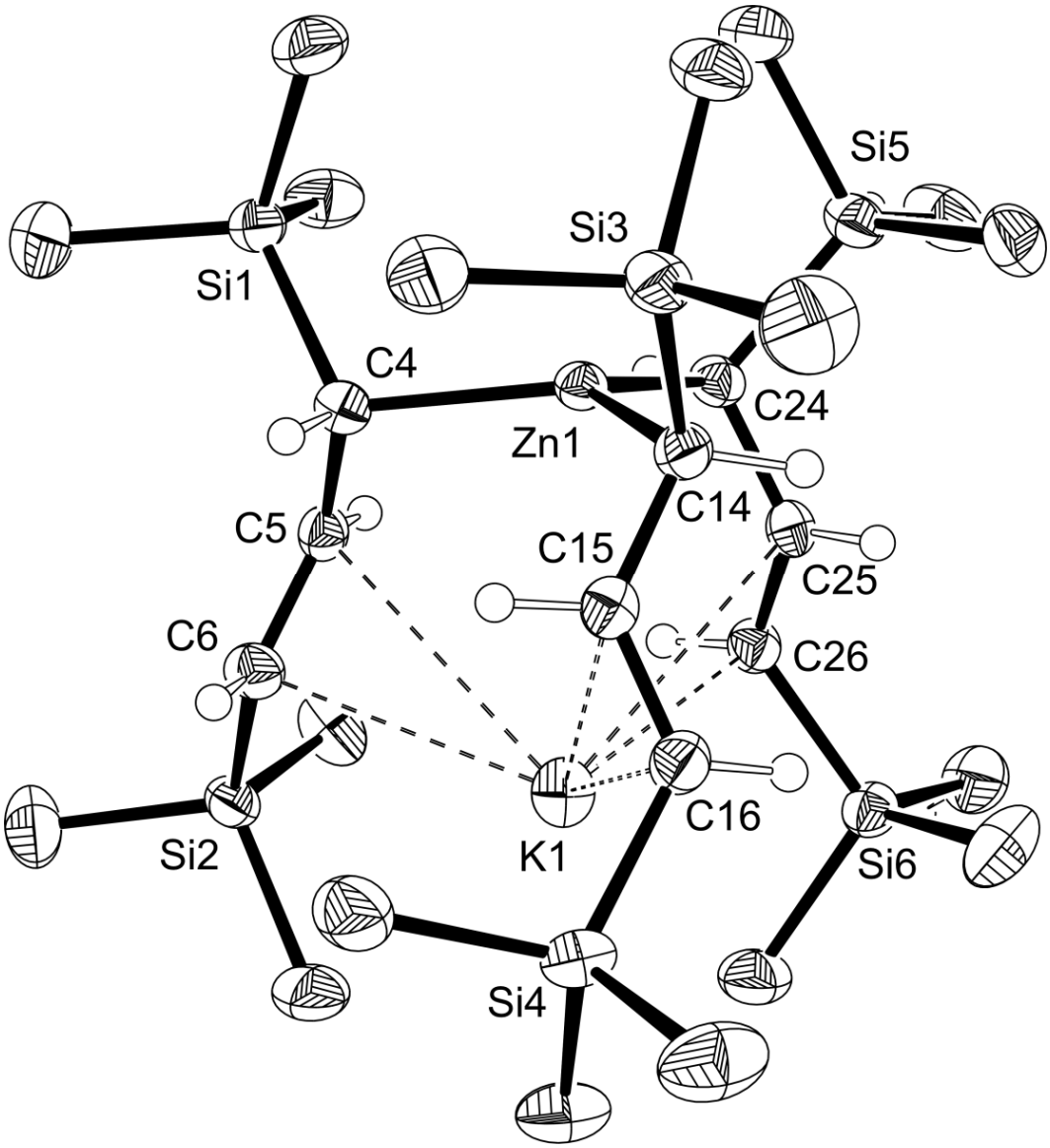

Figure 21. Solid-state structure of $K[Zn(1,3\text{-}(SiMe_3)_2C_3H_3)_3]$, with thermal ellipsoids at the 50% level. Hydrogen atoms have been removed from the trimethylsilyl groups for clarity. Selected bond distances (Å) and angles (deg): Zn(1)-C(4), 2.065(2); Zn(1)-C(14), 2.065(2); Zn(1)-C(24), 2.075(3); C(4)-C(5), 1.467(3); C(5)-C(6), 1.358(4); C(14)-C(15), 1.460(3); C(15)-C(16), 1.355(3); C(24)-C(25),1.460(3); C(25)-C(26), 1.364(3); C(5)-C(4)-Zn(1), 107.83(16); C(15)-C(14)-Zn(1), 108.71(16); C(25)-C(24)-Zn(1),104.75(16).

Solid-state structure of Li[Zn(1,3-(SiMe$_3$)$_2$C$_3$H$_3$)$_3$]. The single crystal X-ray structure of Li[Zn(1,3-(SiMe$_3$)$_2$C$_3$H$_3$)$_3$] (Figure 22) is superficially similar to that of the sodium and potassium derivatives. Like Na[Zn(1,3-(SiMe$_3$)$_2$C$_3$H$_3$)$_3$], the structure of Li[Zn(1,3-(SiMe$_3$)$_2$C$_3$H$_3$)$_3$] is disordered over a two-fold axis, but to a greater extent; refinement leads to occupancies of 70%(Zn)/30%(Li) for the atom marked 'Zn1' and the reverse percentage for 'Li1'. The general structural features of Li[Zn(1,3-(SiMe$_3$)$_2$C$_3$H$_3$)$_3$] are not in doubt, although some of the fine detail cannot be pressed. For example, the average Zn–C distance of 2.117(3) Å is longer than in K[Zn(1,3-(SiMe$_3$)$_2$C$_3$H$_3$)$_3$], and probably reflects the admixture of some Li–C character. Similarly, the direct lithium-carbon bond distance of 2.268(3) Å (avg) is likely somewhat shorter than the undisordered value (but comparable to the 2.28 Å Li–C$_\alpha$ bond found in {Li[CH$_2$CH$_3$]}$_4$).[128] The distance of lithium to the carbons β to the lithium (C2, C5, C8) ranges from 2.70–2.79 Å, which is distinctly longer than normal Li–C bonds. It is, however, similar to Li–aryl distances observed in dibenzylamidolithium, [(PhCH$_2$)$_2$NLi]$_n$ (avg. 2.80 Å),[129] and in the chelating silazane [{Me$_2$Si(Ph)}$_2$N-Li]$_2$, in which Li–C$_\beta$ distances range up to 2.77 Å.[130] Nevertheless, the marked asymmetry of the Li–C distances in Li[Zn(1,3-(SiMe$_3$)$_2$C$_3$H$_3$)$_3$] suggests that the interaction of lithium is not strictly analogous to that of sodium or potassium, but that more pronounced Li–C σ-bonding is involved.

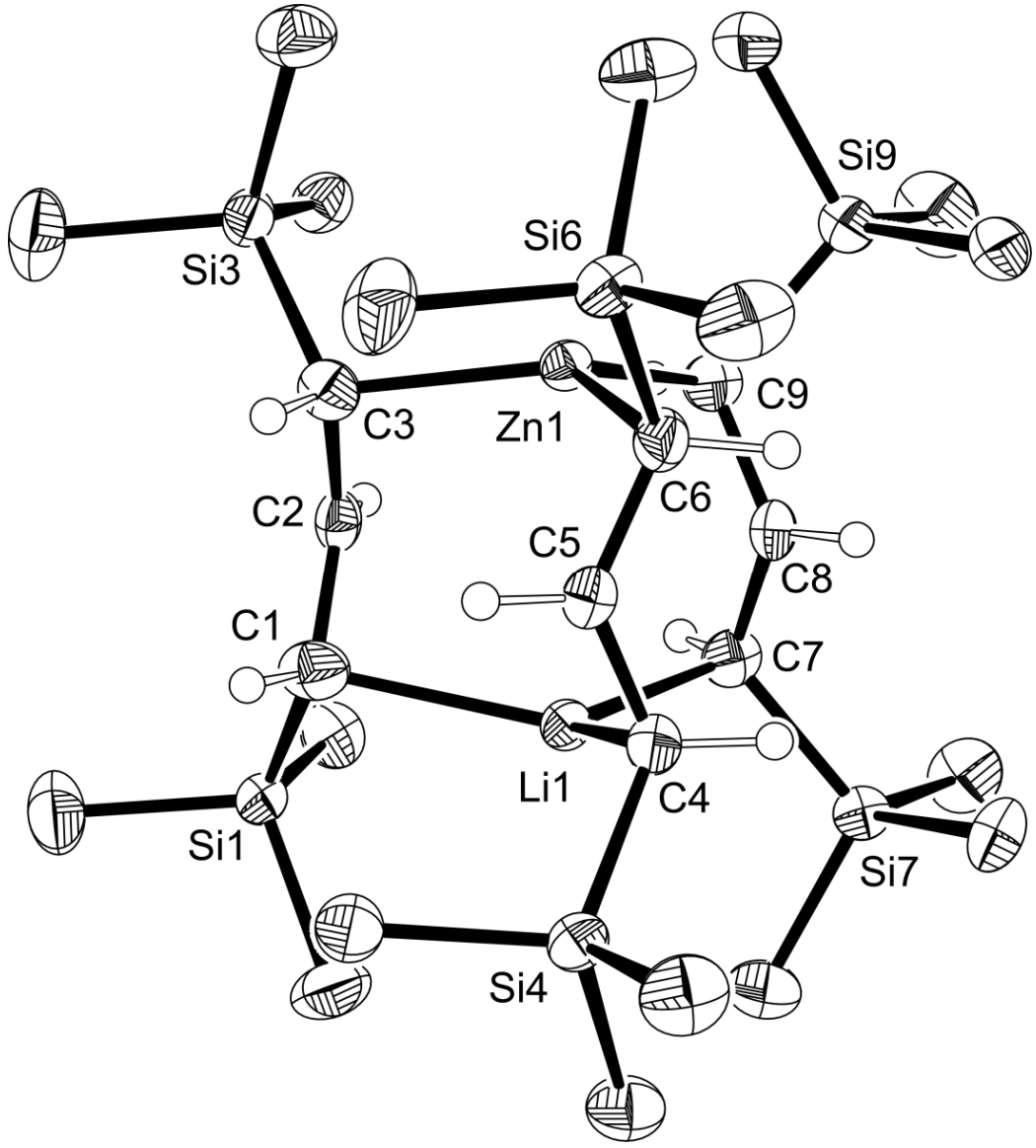

Figure 22. Solid-state structure of $Li[Zn(1,3\text{-}(SiMe_3)_2C_3H_3)_3]$, with thermal ellipsoids at the 50% level. Hydrogen atoms have been removed from the trimethylsilyl groups for clarity. Selected bond distances (Å) and angles (deg): Zn1–C3, 2.1101(19); Zn1–C9, 2.116(2); Zn1–C6, 2.1264(19); Li1–C4, 2.245(2); Li1–C7, 2.252(2); Li1–C1 2.306(2); C2–C1–Li1. 95.24(13); C2–C3–Zn1, 98.99(12); C5–C4–Li1, 95.35(12); C5–C6–Zn1, 99.90(12); C8–C7–Li1, 92.69(12); C8–C9–Zn1, 101.50(12).

Computational study of the geometry of Li[Zn(1,3-(SiMe$_3$)$_2$C$_3$H$_3$)$_3$]. A model of Li[Zn(1,3-(SiMe$_3$)$_2$C$_3$H$_3$)$_3$] was examined at the B3PW91/DGDZVP2 level under C_3 symmetry in an attempt to reconstruct structural features of the undisordered molecule, and to determine how much of the Li–C$_\alpha$/C$_\beta$ bonding asymmetry might be ascribed to the solid-state disorder (Figure 23). The calculated Zn–C$_3$ distance of 2.081 Å has shortened from the solid-state value (2.117(3) Å), and is now close to that in K[Zn(1,3-(SiMe$_3$)$_2$C$_3$H$_3$)$_3$]. The Li–C$_1$ distance has lengthened somewhat to 2.346 Å, whereas the Li···C$_2$ separation remains long at 2.737 Å. Using the optimized values and the experimentally determined occupancies of 70%/30% (see Experimental section), it is possible to calculate the "disordered" values as 0.70(2.081 Å) + 0.30(2.346 Å) = 2.16 Å for the Zn–C$_3$ distance (0.04 Å longer than the crystal structure), and 0.70(2.346 Å) + 0.30(2.081 Å) = 2.27 Å for the Li–C$_1$ distance (matches crystal structure). These values suggest that the geometry optimization has provided a credible restoration of the undisordered structure. The C–C and C=C double bonds of the allyl ligands, at 1.436(5) Å and 1.383(5) Å in the disordered crystal structure, have lengthened and shortened slightly in the optimized model to 1.455 Å (C$_2$–C$_3$) and 1.378 Å (C$_1$–C$_2$), respectively, supporting a largely localized model of the bonding.

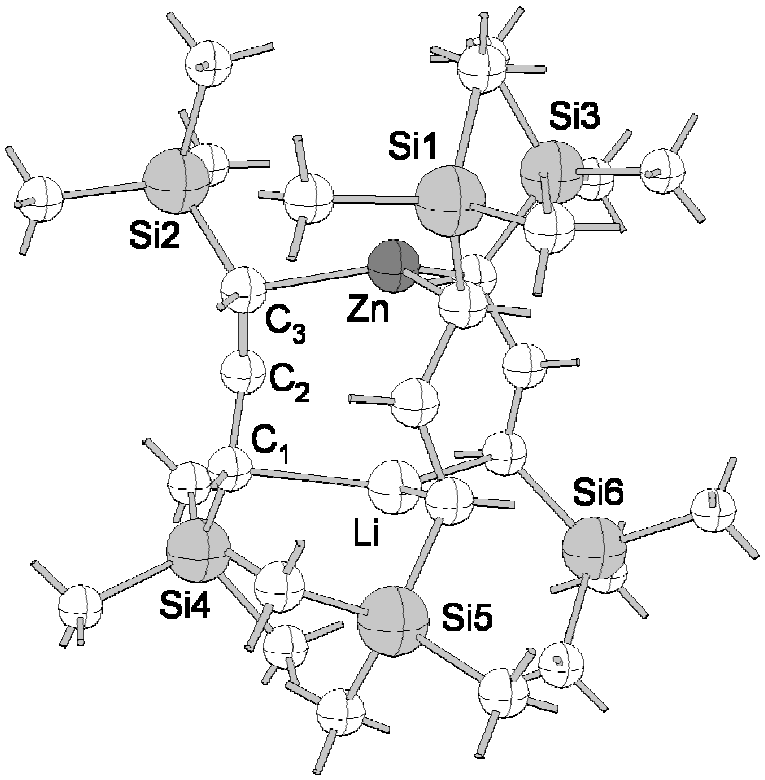

Figure 23. Calculated structure of $Li[Zn(1,3\text{-}(SiMe_3)_2C_3H_3)_3]$ (B3PW91/DGDZVP2), with the numbering scheme used in the text; bonds to hydrogen atoms are indicated as sticks. Selected bond distances (Å) and angles (deg): Zn–C_3, 2.081 Å; Li–C_1, 2.346 Å; C_2–C_1–Li, 90.79°; C_2–C_3–Zn, 102.08°; C_1–C_2–C_3, 129.90°.

Computational study of the geometry of cation-π interactions. DFT studies were conducted on model $[M(C_6H_6)]^+$ and $[M(C_2H_4)_n]^+$ complexes to assess geometric factors in the metal-allyl interactions of $Li[Zn(1,3\text{-}(SiMe_3)_2C_3H_3)_3]$, $Na[Zn(1,3\text{-}(SiMe_3)_2C_3H_3)_3]$, and $K[Zn(1,3\text{-}(SiMe_3)_2C_3H_3)_3]$. It has been noted that the gas-phase binding energies of Na^+ to C_2H_4 (−10.7 kcal mol^{-1})[101] and C_6H_6 (−23.2 kcal mol^{-1})[131] are not in the ratio of 1:3 expected from the relative number of π electrons, a discrepancy partially ascribed to differences

in geometry.[56] The three double bonds in the present tri(allyl)zincates are obviously able to interact with the alkali metal cations in a way different from that of planar benzene, and an estimate of the relative binding energies would be instructive, as the number of available π electrons is the same in both cases.

There have been many previous computational investigations of $M^+\cdots C_6H_6$ interactions with a variety of ab initio and density functional methods.[74,131-135] Although dispersion forces play a role in cation-π interactions, and current density functionals do not describe such forces well,[136-138] dispersion appears to have only a small influence in complexes of Li^+ and Na^+.[56,139] In complexes involving K^+, dispersion effects are more important, but still represent only ~15% of the total interaction energies in $[K(C_6H_6)]^+$,[56] an amount that does not preclude DFT approaches from supplying usefully accurate energies in cation-π systems. The hybrid PBE1PBE functional[81] combined with the basis sets of triple zeta quality gives energies for the $[M(C_6H_6)]^+$ cations that are within the errors limits of experimental values (Table 2).

Table 2. Calculated energies[a] and geometries[b] for $[M(C_2H_4)_n]^+$ and $[M(C_6H_6)]^+$

M^+	$[M(C_2H_4)]^+$ C_{2v}	$[M(C_2H_4)_2]^+$ D_{2d}	$[M(C_2H_4)_3]^+$ D_3	$[M(C_6H_6)]^+$ C_{6v}	Exp. for $[M(C_6H_6)]^+$
Li	−22.3 ($\Delta H°$) −16.0 ($\Delta G°$) 2.342 Å	−40.6 ($\Delta H°$) −25.8 ($\Delta G°$) 2.373 Å	−51.8 ($\Delta H°$) −31.4 ($\Delta G°$) 2.434 Å	−39.8 ($\Delta H°$) −32.0 ($\Delta G°$) 2.287 Å	−39.3±3.3 ($\Delta H°$)[60]
Na	−14.9 ($\Delta H°$) −8.9 ($\Delta G°$) 2.708 Å	−27.4 ($\Delta H°$) −13.8 ($\Delta G°$) 2.740 Å	−37.5 ($\Delta H°$) −12.8 ($\Delta G°$) 2.789 Å	−24.6 ($\Delta H°$) −17.6 ($\Delta G°$) 2.748 Å	−23.2±1.4 ($\Delta H°$)[131]
K	−8.9 ($\Delta H°$) −3.6 ($\Delta G°$) 3.185 Å	−17.1 ($\Delta H°$) −2.2 ($\Delta G°$) 3.225 Å	−23.8 ($\Delta H°$) −1.8 ($\Delta G°$) 3.251 Å	−17.2 ($\Delta H°$) −10.5 ($\Delta G°$) 3.155 Å	−17.7±1.0 ($\Delta H°$)[60]

[a] in kcal mol^{-1}

[b] $M^+\cdots C$ distances

To probe the effect of changing the number and orientation of π-bonds around the metals, the series of $[M(C_2H_4)_n]^+$ cations was investigated (Figure 24). The results of these DFT calculations are generally comparable to other calculations on alkaline earth/ethylene complexes in the literature although they tend to be at the high end of binding strength (Table 3). The only calculation of a $[M(C_2H_4)_3]^+$ species of which we are aware is that of $[Na(C_2H_4)_3]^+$,[58] which predicts a Na–C distance of 2.842 Å (BP86/TZVPP level), 0.053 Å longer than our value of 2.789 Å. We are unaware of any previous calculations for $[M(C_2H_4)_2]^+$ complexes.

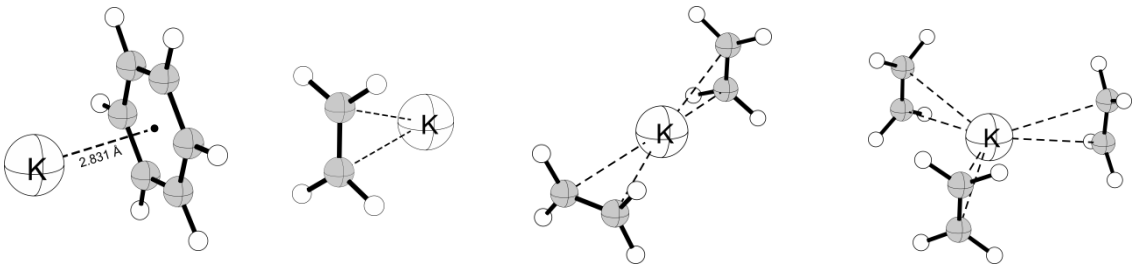

Figure 24. Optimized geometries of cation-π complexes: (a) $[K(C_6H_6)]^+$; (b) $[K(C_2H_4)]^+$; (c) $[K(C_2H_4)_2]^+$; (d) $[K(C_2H_4)_3]^+$

An examination of the trends in binding enthalpies (Figure 25) is instructive. As expected for a largely ionic interaction, the enthalpies decrease in the order $Li^+ > Na^+ > K^+$. There is a roughly additive increase in the interaction energy with each additional ethylene molecule, averaging 20, 14, and 8 kcal mol^{-1} for Li, Na, and K, respectively. It is also clear that three ethylene molecules arranged around the metal center interact more strongly than does a single benzene molecule, presumably because the rigid framework of benzene prevents optimal orientation of the π-electron density toward the cation. In fact, just two ethylene molecules arranged on either side of the metal interact approximately as strongly as does a benzene molecule. It has also been shown computationally that 1,4,7-cyclononatriene—containing three nonconjugated double bonds—interacts with the alkali metals with approximately equal energy to three ethylene molecules.[140] While the three double bonds of this molecule cannot surround the cation as can the individual ethylene molecules, they do have the ability

to twist such that the π-electron density can be optimally directed toward the cation.

This geometrical dependence of the energies of these cation-π interactions appears to diminish with increasing cation size. The percent difference between enthalpies of $[M(C_2H_4)_3]^+$ and $[M(C_6H_6)]^+$ for Li, Na, K, and Cs are 30.2, 52.4, 38.4, and 26.3 kcal mol^{-1}, respectively. Lithium appears to have other factors involved in this energy difference—namely, some degree of covalency. However, with the highly ionic, heavy alkali metals, the trend is clear.

These results must be tempered by the fact that the free energies of formation of $[M(C_6H_6)]^+/[M(C_2H_4)_3]^+$ are always greater for the benzene complexes than for those with ethylene (e.g., −17.6 and −12.8 kcal mol^{-1} for $[Na(C_6H_6)]^+$ and $[Na(C_2H_4)_3]^+$, respectively), owing to the larger number of ethylenes involved. Such comparisons are also complicated by the fact that in the zincates the olefinic functionalities are not completely independent ligands, thus limiting that entropic contribution to the energy.

Table 3. Calculated energies[a] for $[M(C_2H_4)]^+$

Complex	ΔH_{298}	Protocol	Ref.
$[Li(C_2H_4)]^+$	−18.99	MP2/6-31+G(d)//MP2/6-31+G(d)	56
	−20.71[b]	MP2/6-311++G(d,p)// MP2/6-311++G(d,p)	141
	−22.3	see text	this work
$[Na(C_2H_4)]^+$	−12.36	MP2/6-31+G(d)//MP2/6-31+G(d)	56
	−12.7	MP2/6-311+G(2d,2p)//MP2/6-31G(d)	142
	−12.97[b]	MP2/6-311++G(d,p)// MP2/6-311++G(d,p)	141
	−14.6±0.2	CCSD(T)/CBS (est.)//MP2(FC)/CBS	101
	−14.9	see text	this work
	−10.7±1.0	experimental (CID)	101
$[K(C_2H_4)]^+$	−7.05	MP2/6-31+G(d)//MP2/6-31+G(d)	56
	−8.02	MP2/aug-cc-pVDZ//MP2/aug-cc-pVDZ	56
	−8.29	B3LYP/6-311+G(3df,2p)//B3LYP/6-31G(d)	134
	−8.80[b]	MP2/6-311++G(d,p)// MP2/6-311++G(d,p)	141
	−8.9	see text	this work

[a] in kcal mol^{-1}

[b] electronic energies

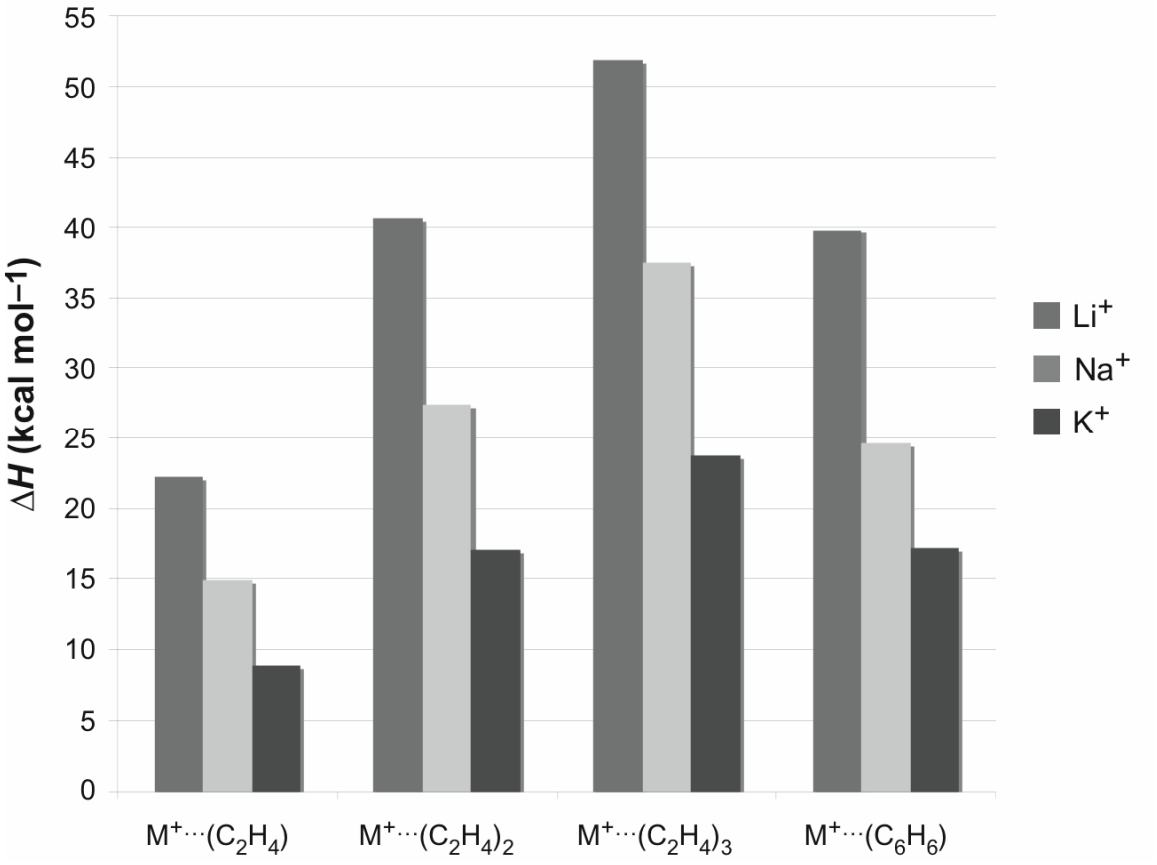

Figure 25. Calculated enthalpies of formation ($\Delta H°$) of $[M(C_2H_4)_n]^+$ and $[M(C_6H_6)]^+$ (PBE1PBE/TZV).

Conclusions

The determination that the olefinic functionality of a σ-bound allyl ligand can engage in cation-π interactions with a second, dissimilar metal, establishes a new combination of bonding modes for the allyl anion in main group metal complexes and new coordination environments for the alkali metal cations. It is possible that similar bonding exists in related complexes with unsubstituted allyl ligands, e.g., $BrMg[Zn(C_3H_5)_3]$,[143] but this has not been structurally authenticated.

In the attempt to understand the formation of the alkali metal (triallyl)zincates, it should be stressed that a principle driving force is the electrostatic attraction between the cations and the $[Zn(1,3\text{-}(SiMe_3)_2C_3H_3)_3]^-$ anion. Although the model $[M(C_2H_4)_n]^+$ complexes are not perfect analogues of the zincates, the finding from density functional studies that two olefinic bonds arranged in a staggered manner around an alkali metal are roughly equal in binding enthalpy to a benzene ring, and that three olefinic units around a metal can surpass the arene binding enthalpy by 30% or more, highlights the importance of geometrical factors in cation-π interactions. This suggests that the strength of such interactions could be improved through judicious ligand design.

CHAPTER IV

BIS(TRIMETHYSILYL)ALLYL COMPLEXES OF P-BLOCK ELEMENTS

Introduction

Much of the early research in organometallic allyl complexes was centered on those of the d-block transition metals. The synthesis and characterization of homoleptic allyl complexes of p-block metals has been a more recent development, and has focused primarily on complexes of silicon,[144-151] germanium,[152-156] boron,[157-164] and tin,[165-176] with the latter two being used predominantly as allylation reagents in organic reactions. Allyl complexes with other p-block metals have received far less attention. For example, there are only a small number of reports describing the use of homoleptic allyl complexes of the heavy group 13 metals (Al, Ga, In). In each, the complexes are formed—typically from the appropriate metal halide and an allyl Grignard reagent—and used in solution with little to no characterization. Their predominant use is as regioselective allylation reagents with α,β-unsaturated nitrile and carbonyl compounds.[177-182] Before this work, there were no structurally authenticated homoleptic allyl complexes of aluminum, gallium, or indium.

It seemed reasonable that p-block allyl compounds—especially those of group 13 metals—could be stabilized by increasing the steric bulk of the

ligands (in this case, by adding trimethylsilyl substituents), as this approach had been well established in transition metal allyl complexes.[21,23,25,27] This work will describe the synthesis and characterization of the first gallium and indium complexes to benefit from such substitution, as well as the first structurally authenticated homoleptic gallium allyl complex. Density functional theory (DFT) calculations have been used to probe the preferences for particular metal-ligand bonding conformations in $(allyl')_3Ga$ compounds.

Experimental

General considerations. All manipulations were performed with the rigorous exclusion of air and moisture using high vacuum, Schlenk, or glovebox techniques. Proton (^1H) and carbon (^{13}C) NMR experiments were obtained on a Bruker DPX-300 spectrometer at 300 and 75.5 MHz, respectively, or on a Bruker DPX-400 at 400 MHz (^1H), and were referenced to residual proton and ^{13}C resonances of toluene-d_8 (δ 2.09 and 20.4) and C_6D_6 (δ 7.15 and 128.1). Elemental analysis was performed at the Micro-Mass Facility, University of California, Berkeley (Berkeley, CA).

Materials. Hexanes were distilled under nitrogen from potassium benzophenone ketyl. Anhydrous tetrahydrofuran (THF) was purchased from Aldrich and stored over type 4A molecular sieves prior to use. Anhydrous metal salts were purchased from Strem Chemicals and used as received. C_6D_6 and toluene-d_8 were vacuum-distilled from Na/K (22/78) alloy and

stored over type 4A molecular sieves prior to use. Li[1,3-$(SiMe_3)_2C_3H_3$] and K[1,3-$(SiMe_3)_2C_3H_3$] were prepared following literature procedures.[33]

Attempted synthesis of [1,3-$(SiMe_3)_2C_3H_3]_3B$. A solution of K[1,3-$(SiMe_3)_2C_3H_3$] (0.800 g; 3.56 mmol) in diethyl ether (7 mL) at −40 °C was added dropwise to a stirring solution of $BF_3 \cdot O(CH_3CH_2)_2$ (0.169 g; 1.19 mmol) in diethyl ether (3 mL) also at −40 °C. The reaction was allowed to warm to room temperature while being stirred for one hour, resulting in a yellow-orange solution. The ether was removed under vacuum, leaving an orange pasty solid. The product was extracted with hexane and filtered over a medium porosity glass frit. Clear, yellow crystals formed in the filtrate within 18 hrs (0.103 g crystalline yield). ^{1}H NMR in THF-d_8 indicated unreacted K[1,3-$(SiMe_3)_2C_3H_3$].[33]

Attempted synthesis of [1,3-$(SiMe_3)_2C_3H_3]_3Al$ via salt metathesis. A 125-mL Schlenk flask equipped with a magnetic stir bar was charged with $AlCl_3$ (0.100 g; 0.750 mmol) in 30 mL THF. K[1,3-$(SiMe_3)_2C_3H_3$] (0.505 g; 2.25 mmol) in 20 mL THF was added to the dropping funnel. The apparatus was cooled to −78 °C. The THF solution of K[1,3-$(SiMe_3)_2C_3H_3$] was added dropwise with stirring over the course of 15 min. The solution was allowed to warm to room temperature while being stirred overnight. Removal of solvent under vacuum, followed by extraction of the residue with hexanes, filtration of the extract over a medium-porosity glass frit, and removal of hexanes

under vacuum, afforded a yellow oil. ^{1}H NMR in THF-d_8 was inconsistent with the desired product and indicated decomposition may have occurred.

Attempted synthesis of [1,3-(SiMe$_3$)$_2$C$_3$H$_3$]$_3$Al via methyl elimination. A 125-mL Schlenk flask equipped with a magnetic stir bar was charged with 1,3-(SiMe$_3$)$_2$C$_3$H$_4$ (8.15 g; 43.7 mmol) in 20 mL hexanes. Me$_3$Al (1.05 g; 14.6 mmol) in 10 mL hexanes was added to the dropping funnel. The apparatus was cooled to −78 °C. The hexanes solution of Me$_3$Al was added dropwise with stirring over the course of 15 min. The solution was allowed to warm to room temperature while being stirred overnight. Most of the hexanes was removed under vacuum, leaving a slightly yellow oil. ^{1}H NMR in C$_6$D$_6$ indicated mostly unreacted 1,3-(SiMe$_3$)$_2$C$_3$H$_4$ and residual hexanes. After allowing the product to rest undisturbed for two days, a white precipitate formed. The ^{1}H NMR spectrum in C$_6$D$_6$ was inconsistent with the desired product.

Synthesis of [1,3-(SiMe$_3$)$_2$C$_3$H$_3$]$_3$Ga. A 125-mL Schlenk flask equipped with a magnetic stir bar was charged with GaCl$_3$ (0.500 g; 2.84 mmol) in 30 mL THF. K[1,3-(SiMe$_3$)$_2$C$_3$H$_3$] (1.90 g; 8.52 mmol) in 20 mL THF was added to the dropping funnel. The apparatus was cooled to −78 °C. The THF solution of K[1,3-(SiMe$_3$)$_2$C$_3$H$_3$] was added dropwise with stirring over the course of 15 min. The solution was allowed to warm to room temperature while being stirred overnight. Removal of solvent under vacuum, followed by extraction of the residue with hexanes, filtration of the extract over a

medium-porosity glass frit, and removal of hexanes under vacuum, afforded air- and moisture-sensitive colorless to pale-yellow crystals (1.67 g, 94%), m.p. 44–46 °C. Anal. Calcd for $C_{27}H_{63}GaSi_6$: C, 51.80; H, 10.14. Found: C, 51.49; H, 10.55. ^{1}H NMR (C_6D_6, 298 K): δ 6.38 (t, J = 14.8 Hz, 3H), 3.94 (d, J = 14.8 Hz, 6H), 0.18 (s, 54H, $SiMe_3$); (tol-d_8, 298 K, 300 MHz): δ 6.35 (t, J = 14.8 Hz, 3H), 3.91 (d J = 14.8 Hz, 6 H), 0.16 (s, 54H, $SiMe_3$). ^{13}C NMR (C_6D_6, 298 K): δ 145.31 ($C_{(2)}$, central), 83.72 ($C_{(1,3)}$, outer), 0.15 ($SiMe_3$). Variable temperature ^{1}H (tol-d_8, 400 MHz, δ): (198 K) 6.43 (t, J = 14.8, 3H), 3.7-4.3 (v br s, 2H), 0.24 (s, 54 H, $SiMe_3$); (213 K) 6.41 (t, J = 14.8 Hz, 3H), 4.01 (broad singlet, 6H), 0.23 (s, 54H, $SiMe_3$); (233 K) 6.40 (t, J = 14.8 Hz, 3H), 3.96 (broad singlet, 6H), 0.21 (s, 54H, $SiMe_3$); (253 K) 6.38 (t, J = 14.8 Hz, 3H), 3.94 (br d, J = 14.2 Hz, 6H), 0.20 (s, 54H, $SiMe_3$); (273 K) 6.37 (t, J = 14.8 Hz, 3H), 3.93 (d, J = 14.8 Hz, 6H), 0.18 (s, 54H, $SiMe_3$).

Synthesis of [1,3-$(SiMe_3)_2C_3H_3$]$_3$In. A 125-mL Schlenk flask equipped with a magnetic stir bar was charged with $InCl_3$ (0.328 g; 1.48 mmol) in 30 mL THF. K[1,3-$(SiMe_3)_2C_3H_3$] (1.00 g; 4.45 mmol) in 20 mL THF was added to the dropping funnel. The apparatus was cooled to −78 °C. The THF solution of K[1,3-$(SiMe_3)_2C_3H_3$] was added dropwise with stirring over the course of 15 min. The solution was allowed to warm to room temperature overnight. Removal of solvent under vacuum, followed by extraction of the residue with hexanes, filtration of the extract over a medium-porosity glass frit, and removal of hexanes under vacuum, afforded an air- and moisture-

sensitive yellow oil (0.781 g, 78.6%). ^{1}H NMR (C_6D_6, 298 K): δ 6.52 (t, J = 14.8 Hz, 3H, C_2), 3.98 (d, J = 14.8 Hz, 6H), 0.18 (s, 54H, $SiMe_3$).

Attempted synthesis of [1,3-$(SiMe_3)_2C_3H_3$]Tl. A 125-mL Schlenk flask equipped with a magnetic stir bar was charged with TlCl (0.500 g; 2.08 mmol) in 30 mL THF. K[1,3-$(SiMe_3)_2C_3H_3$] (0.468 g; 2.08 mmol) in 20 mL THF was added to the dropping funnel. The apparatus was cooled to −78 °C. The THF solution of K[1,3-$(SiMe_3)_2C_3H_3$] was added dropwise with stirring over the course of 15 min. The solution was allowed to warm to room temperature while being stirred overnight. Removal of solvent under vacuum, followed by extraction of the residue with hexanes, filtration of the extract over a medium-porosity glass frit, and removal of hexanes under vacuum, afforded a crude product mixture. ^{1}H NMR in C_6D_6 indicated a mixture of starting material and decomposition products.

Attempted synthesis of [1,3-$(SiMe_3)_2C_3H_3$]$_2$Pb. A 125-mL Schlenk flask equipped with a magnetic stir bar was charged with $PbCl_2$ (0.500 g; 1.80 mmol) in 30 mL THF. K[1,3-$(SiMe_3)_2C_3H_3$] (0.807 g; 3.60 mmol) in 20 mL THF was added to the dropping funnel. The apparatus was cooled to −78 °C. The THF solution of K[1,3-$(SiMe_3)_2C_3H_3$] was added dropwise with stirring over the course of 15 min. The solution was allowed to warm to room temperature while being stirred overnight. Removal of solvent under vacuum, followed by extraction of the residue with hexanes, filtration of the extract over a medium-porosity glass frit, and removal of hexanes under

vacuum, afforded air- and moisture-sensitive colorless crystals, identified by ^{1}H NMR as the solvated starting material, K[1,3-$(SiMe_3)_2C_3H_3$](thf).

Attempted synthesis of [1,3-$(SiMe_3)_2C_3H_3$]$_3$As. A 125-mL Schlenk flask equipped with a magnetic stir bar was charged with AsI_3 (0.500 g; 1.10 mmol) in 30 mL THF. K[1,3-$(SiMe_3)_2C_3H_3$] (0.739 g; 3.29 mmol) in 20 mL THF was added to the dropping funnel. The apparatus was cooled to −78 °C. The THF solution of K[1,3-$(SiMe_3)_2C_3H_3$] was added dropwise with stirring over the course of 15 min. The solution was allowed to warm to room temperature while being stirred overnight. Removal of solvent under vacuum, followed by extraction of the residue with hexanes, filtration of the extract over a medium-porosity glass frit, and removal of hexanes under vacuum, afforded a yellow oily solid. The product was identified as 1,3,4,6-tetrakis(trimethylsilyl)-1,5-hexadiene. ^{1}H NMR resonances were consistent with the previously published values.[25]

General Procedures for X-ray Crystallography. Crystals of [1,3-$(SiMe_3)_2C_3H_3$]$_3$Ga were obtained as pale yellow plates upon removal of hexanes. A suitable crystal was located, placed onto the tip of a 0.1 mm diameter glass capillary and mounted on a Bruker SMART Platform CCD diffractometer for a data collection at 173(2) K. The intensity data were corrected for absorption (SADABS),[183] and the structure was solved using SIR97 and refined using SHELXL-97. Relevant crystal and data collection parameters and atomic coordinates are given in Appendix C. The triclinic

space group $P\bar{1}$ was indicated from intensity statistics and the lack of systematic absences. A direct-methods solution was calculated that provided most non-hydrogen atoms from the E-map. Full-matrix least squares / difference Fourier cycles were performed that located the remaining non-hydrogen atoms. All non-hydrogen atoms were refined with anisotropic displacement parameters. All methyl hydrogen atoms were placed in ideal positions and refined as riding atoms with relative isotropic displacement parameters. The allylic hydrogen atoms were found from the difference map and refined with individual isotropic displacement parameters.

Computational Details. Calculations were performed using the GAUSSIAN 03W suite of programs.[108] The B3PW91 functional, which incorporates Becke's three-parameter exchange functional[109] with the 1991 gradient-corrected correlation functional of Perdew and Wang,[110] was used. This hybrid functional has previously been shown to provide realistic geometries for organometallic species.[111,112] The correlation consistent double zeta basis set cc-pVDZ was used for geometry optimization and final energy calculations.[184] Zero-point corrections were applied to the energies of the final geometries.

Results and Discussion

Synthesis of $[1,3\text{-}(SiMe_3)_2C_3H_3]_3M$ (M = Ga, In). The synthesis of trimethylsilyl-substituted triallyl complexes of gallium and indium was

achieved by a halide metathesis reaction performed under an inert atmosphere at −78 °C (eq 9).

$$3\ \mathrm{K(allyl)} + \mathrm{MCl_3} \xrightarrow[\text{-78 °C, 18 h}]{\text{THF}} (\mathrm{allyl})_3\mathrm{M} + 3\ \mathrm{KCl}$$

$$(\mathrm{M = Ga,\ In}) \qquad (9)$$

The triallylgallium compound was recovered in good yield as air- and moisture-sensitive pale yellow crystals, while the indium compound was isolated only as an oil. Both complexes are soluble in ethers and in both aromatic and aliphatic hydrocarbons. Both are also stable indefinitely under an inert atmosphere at room temperature and can survive brief (minutes) exposure to air before substantial decomposition occurs.

Solution behavior of $[1,3\text{-}(SiMe_3)_2C_3H_3]_3M$ (M = Ga, In). Both the gallium and indium allyl complex are diamagnetic and ^{1}H NMR spectra at room temperature have the appearance of a structure with symmetrically bound ("π-type") allyl ligands; e.g., the resonance for the $SiMe_3$ groups appears as a sharp singlet, and the central hydrogen atom on the allyl ligands appears as a triplet. Such a structure differs from that found in the solid state for the triallylgallium complex, and is unlikely from theoretical considerations (see below); a variable temperature ^{1}H NMR study of the gallium species (Figure 26) confirmed the fluxionality of the molecule in solution.

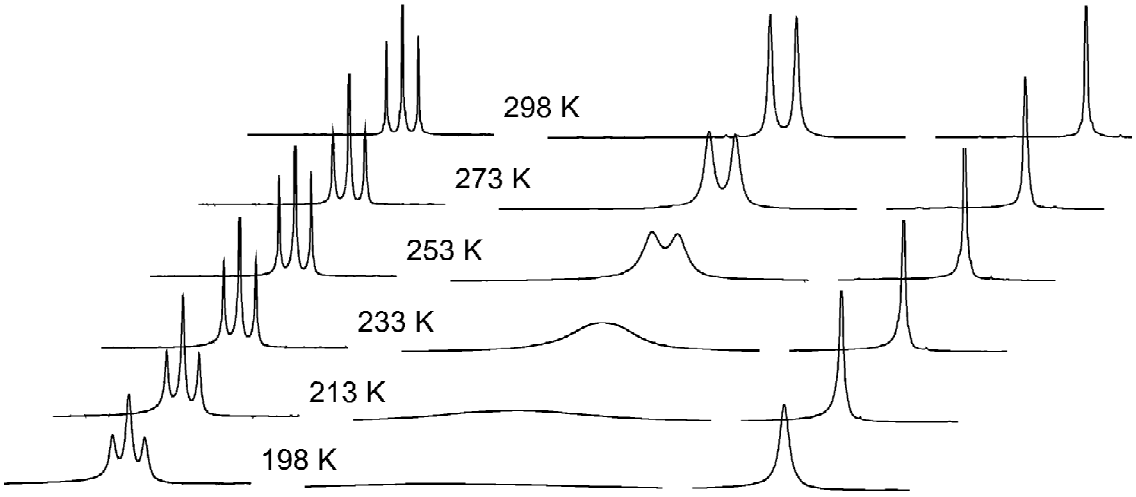

Figure 26. Variable temperature NMR spectra of $[1,3\text{-}(SiMe_3)_2C_3H_3]_3Ga$ (tol-d_8). Resonances (left to right) represent the central carbon ($C_{(2)}$), the outer carbons ($C_{(1,3)}$), and the trimethylsilyl carbons. The peak heights of the three resonances are not to scale.

The central doublet resonance at δ 3.91 broadens and coalesces to a single peak at −40 °C, and then almost disappears into the baseline by −75 °C. The triplet resonance at δ 6.35 and the trimethylsilyl peak at δ 0.16, however, only shift slightly downfield and broaden on cooling to −75 °C. Most notably, the $SiMe_3$ signal shows no sign of splitting into a more complex set of resonances. Obviously, a limiting spectrum is not reached, which is in contrast to the behavior of the related Group 13 allyl compound triallylboron, $(C_3H_5)_3B$. The latter exhibits a symmetric AX_4 NMR pattern at room temperature, but displays a static A_2BX_2 spectrum at −40 °C;[75] the activation barrier for the 1,3-sigmatropic shifts involved is estimated at 10±1

kcal mol^{-1}. Evidently the rearrangements represented in the spectra of [1,3-$(SiMe_3)_2C_3H_3]_3Ga$ must have a lower activation barrier.

X-ray crystal structure of [1,3-$(SiMe_3)_2C_3H_3]_3Ga$. The complex crystallizes from hexanes as well-separated monomers with the gallium atom σ-bound to the bis(trimethylsilyl)allyl ligands in a trigonal planar manner (Figure 26). All three ligands are roughly perpendicular to the GaC_3 plane, with one antiparallel to the other two. The terminal trimethylsilyl groups are *syn* to the central hydrogen atoms of the allyl ligands.

The average Ga–C distance of 1.980(5) Å is typical for gallium-carbon single bonds; cf. those of trimethylgallium (1.957(3) Å),[185] trimesitylgallium (1.968(4) Å),[186] and triethylgallium (1.966(3)–1.996(3) Å).[185] The Ga–C bonds in $(\sigma\text{-}Cp)_3Ga$ are slightly longer (2.05(3) Å).[187] The near perfect planarity of the central GaC_3 unit in [1,3-$(SiMe_3)_2C_3H_3]_3Ga$ is indicated by the sum of the C–Ga–C′ angles of 359.7°; the gallium atom lies only 0.058 Å from the C_3 plane. The fully localized C–C bonding in the allyl ligands is suggested by the average C=C bond distance of 1.329(7) Å and the average C–C bond length of 1.497(6) Å. The Ga–C–C angles average 106.6°, far less than the values observed in $GaEt_3$ (113.2–118.8°); in the latter compound, hyperconjugative effects between the gallium *p* orbital and C–H bond orbitals may be operative.[185]

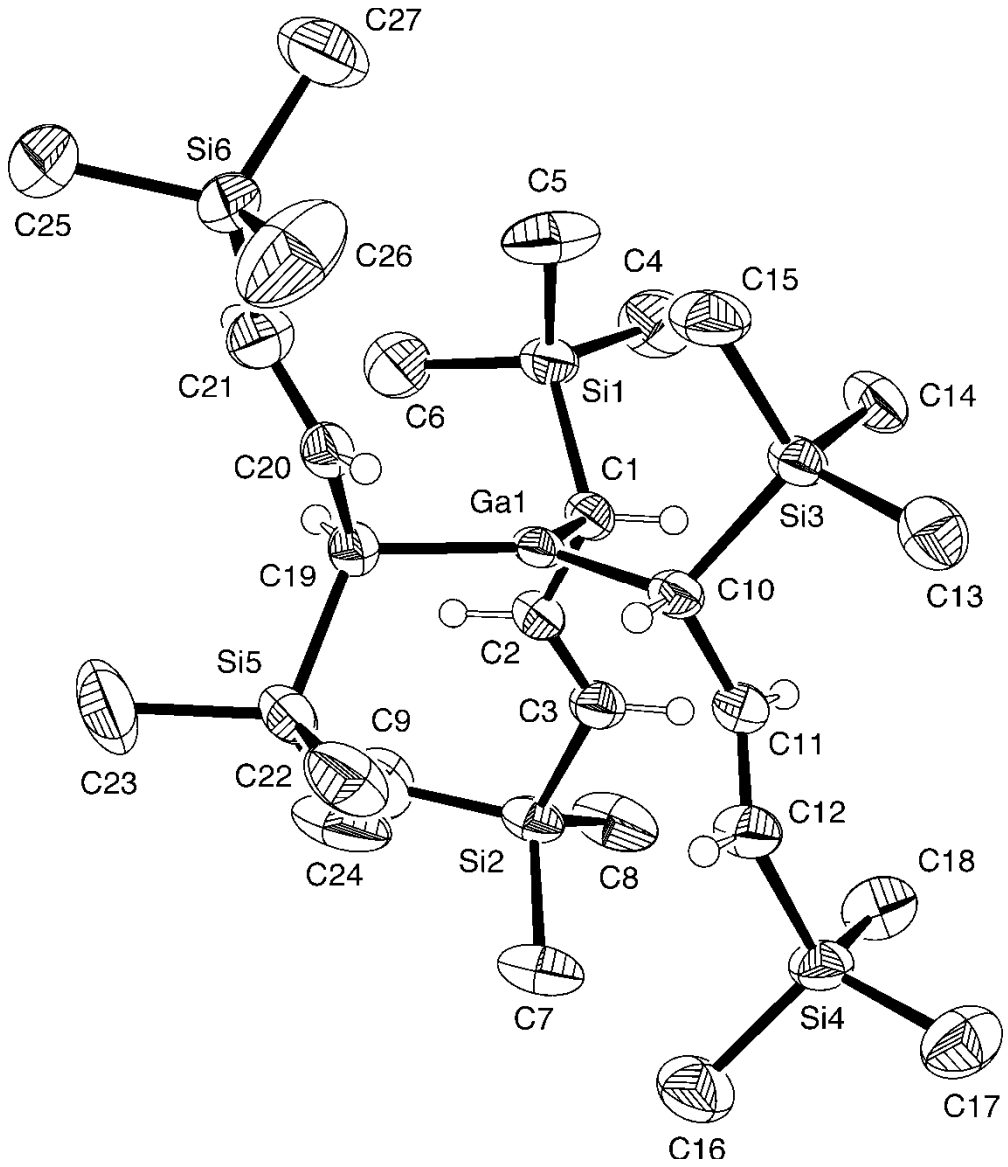

Figure 27. Solid-state structure of $[1,3\text{-}(SiMe_3)_2C_3H_3]_3Ga$. Thermal ellipsoids are shown at the 50% probability level, and hydrogen atoms have been removed from the trimethylsilyl groups for clarity. Selected bond distances (Å) and angles (deg): Ga(1)-C(1), 1.983(3); Ga(1)-C(10), 1.981(3); Ga(1)-C(19), 1.975(3); C(1)-C(2), 1.499(3); C(2)-C(3), 1.326(4); C(10)-C(11), 1.499(3); C(11)-C(12), 1.330(4); C(19)-C(20), 1.493(4); C(20)-C(21), 1.330(4); C(2)-C(1)-Ga(1), 107.26(17); C(11)-C(10)-Ga(1), 104.40(17); C(20)-C(19)-Ga(1), 108.43(17).

Computational modeling of $(R_2C_3H_5)_3Ga$ (R = H, SiH_3, $SiMe_3$). The occurrence in the solid state of the antiparallel "2 up, 1 down" arrangement of the allyl ligands, and the evidently low energy required for rearrangements in solution, prompted a computational study on the relative energies of possible configurations of the complex. Structures of triallylgallium complexes using $C_3H_5^-$, 1,3-$(SiH_3)_2C_3H_3^-$, and 1,3-$(SiMe_3)_2C_3H_3^-$ ligands were calculated at the B3PW91/cc-pVDZ level (Figure 28).

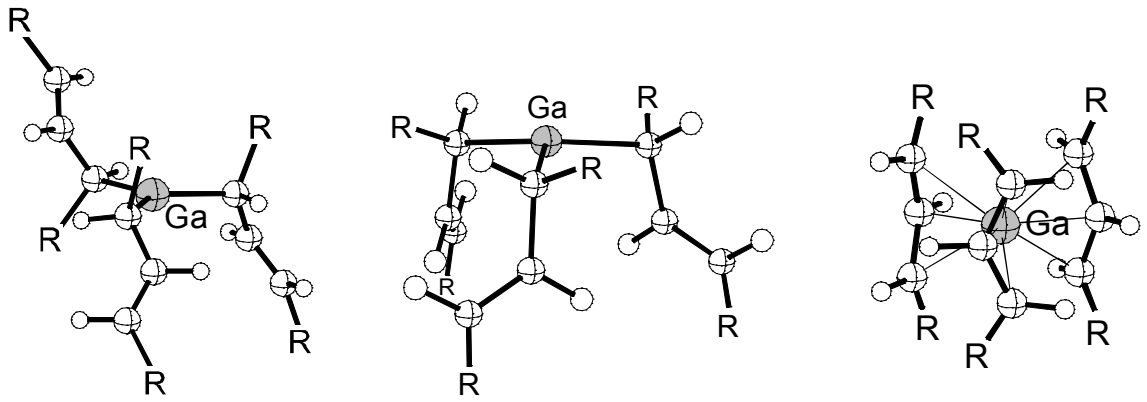

(a) (b) (c)

Figure 28. Schematics of the three structural types examined for (1,3-$R_2C_3H_3)_3Ga$ (R = H, SiH_3, $SiMe_3$): all σ-bound ("2 up, 1 down", C_1 symmetry); all σ-bound ("3 up", C_3 symmetry); all π-bound (C_{3h} symmetry).

Two all σ-bound geometries were examined, one of which had one ligand initially antiparallel to the other two ("2 up, 1 down"), similar to the asymmetric conformation (C_1 symmetry) found in the crystal structure. In the second all-σ conformation, the ligands were grouped together ("3 up"),

with C_3 symmetry. Although it was not found to be an energetically realistic alternative, a π-bound geometry with C_{3h} symmetry was also computed for all three ligand types; such a structure would match the symmetry observed in the room temperature NMR spectra.

Key features of the geometry calculated for $[1,3\text{-}(SiMe_3)_2C_3H_3]_3Ga$ (Figure 29) agree well with those observed in the crystal structure. These include the Ga–C bond distances (2.012 Å (av)), the C_α–C_β single bond distance (1.495 Å (av)), and the C_β=C_γ double bond distance (1.351 Å (av)). The calculated distances change relatively little as the $SiMe_3$ groups are replaced with SiH_3 and then H substituents. In $(C_3H_5)_3Ga$, for example, the Ga–C bond length is 2.007 Å, and the average C–C and C=C distances are 1.490 Å and 1.341 Å, respectively, all of which differ by less than 0.01 Å from the $SiMe_3$ version. The major change on substitution of SiH_3 and then H for $SiMe_3$ is a rotation of one of the allyl ligands so that the C_β atom is closer to the plane defined by the gallium and three C_α atoms. In the experimental and calculated structures of $[1,3\text{-}(SiMe_3)_2C_3H_3]_3Ga$, the C_β atoms are > 1.1 Å from the GaC_3 plane; in the SiH_3-substituted model, C(2) is 0.51 Å from the plane; in $(C_3H_5)_3Ga$, C(2) is 0.38 Å from the plane. Apparently the bulk of the substituents serve to keep the allyl ligands roughly perpendicular to the central GaC_3 plane.

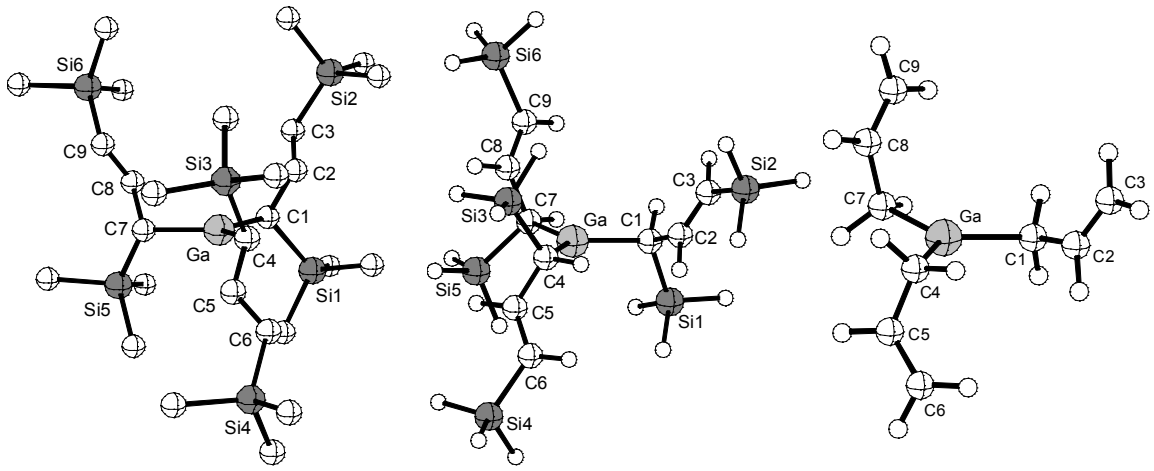

(a) (b) (c)

Figure 29. Optimized lowest energy structures of $[1,3\text{-}(SiMe_3)_2C_3H_3]_3Ga$ (a), $[1,3\text{-}(SiH_3)_2C_3H_3]_3Ga$ (b), and $(C_3H_5)_3Ga$ (c). For clarity, the hydrogen atoms (open circles in b and c) have been omitted from the drawing of $[1,3\text{-}(SiMe_3)_2C_3H_3]_3Ga$.

Regardless of the identity of the allyl substituents, $\Delta G°$ of the C_1 form is the lowest, although that of the "3 up" C_3 form is at most only 2.6 kcal mol^{-1} higher in energy (Table 4). This difference is on the edge of being computationally significant, so that the two forms are nearly equienergetic. The "2 up, 1 down" form found for $[1,3\text{-}(SiMe_3)_2C_3H_3]_3Ga$ in the solid state is possibly reinforced by packing forces.

Table 4. Energies of (allyl′)$_3$Ga conformations[a]

Ligand		π (C_{3h})	σ (C_3)	σ (C_1)
$[C_3H_5]^-$	$\Delta H°$	−2276.288137 (+81.4)	−2276.416999 (+0.5)	−2276.417834 (0.0)
	$\Delta G°$	−2276.335697 (+90.4)	−2276.476641 (+2.0)	−2276.479762 (0.0)
$[(SiH_3)_2C_3H_3]^-$	$\Delta H°$	−4020.156916 (+75.3)	−4020.276907 (0.0)	−4020.276101 (+0.5)
	$\Delta G°$	−4020.237254 (+85.4)	−4020.372047 (+0.8)	−4020.373333 (0.0)
$[(SiMe_3)_2C_3H_3]^-$	$\Delta H°$	−4727.225657 (+97.7)	−4727.37849 (0.0)	−4727.381309 (+1.8)
	$\Delta G°$	−4727.374070 (+108.2)	−4727.54244 (+2.6)	−4727.546544 (0.0)

[a] Energies are in a.u. Values in parentheses are calculated relative to the most stable form of each molecule (listed as "0.0") and given in kcal mol^{-1}. All the π-bound forms had 4 imaginary frequencies; the σ-bound forms had none.

That the two σ-bound forms are close in energy is significant in the context of the solution fluxionality of the complex, as they are reasonable limiting structures in the rearrangement process. The energy of transition structures that involve delocalized allyl ligands depends critically on the identity of all the ligands in a complex. Correlated ab initio calculations have been used to find that the energy of (π-C_3H_5)BH_2 (C_s) is only 1.8 kcal mol^{-1} above that of (σ-C_3H_5)BH_2 (C_1), for example, but that (π-C_3H_5)BMe_2 is 9.2 kcal mol^{-1} above (σ-C_3H_5)BMe_2 (C_1).[188] Considering that the vacant *p* orbital on the metal is involved in stabilizing a "π-bound" ligand, it is not surprising

that threefold π-bound geometries (C_{3h} symmetry) can play no role in the fluxional process. They represent high-order transition structures (N_{imag} = 4) that are more than 85 kcal mol^{-1} above the lowest energy σ-bonded configurations (Table 4). Structures with only one π-bound ligand are more reasonable, and a preliminary search of the potential energy surface using the parent allyl ligand has identified a (π-C_3H_5)(σ-C_3H_5)$_2$Ga configuration (C_s symmetry) that is 7.3 kcal mol^{-1} above the lowest energy σ-bound form. It is a second order saddle point (N_{imag} = 2), but may be close to a transition structure of slightly lower symmetry.

Conclusions

Several attempts were made to isolate allyl complexes of some p-block metals using a bulky trimethylsilyl-substituted ligand. While most attempts were unsuccessful, this work has afforded the first isolated examples of thermally stable, heavy Group 13 allyl complexes in [1,3-(SiMe$_3$)$_2$C$_3$H$_3$]$_3$Ga and [1,3-(SiMe$_3$)$_2$C$_3$H$_3$]$_3$In. The solid-state structure of [1,3-(SiMe$_3$)$_2$C$_3$H$_3$]$_3$Ga indicates the allyl ligands are σ-bound in an asymmetric fashion, but DFT calculations show that a more symmetrical C_3 form is only a few kcal mol^{-1} higher in energy. This result is consistent with variable temperature NMR measurements, which suggest that the molecule has a low energy of activation for rearrangement.

CONCLUSION

In the course of this research, several new organometallic complexes were synthesized and characterized. In an attempt to evaluate the criteria initially set by this work, the structural characteristics of those complexes have been compiled (Table 5).

Table 5. Bond distances (Å) of main group organometallic allyl complexes.

Complex	**C–C**	**C=C**	**M–C_{t1}**	**M–C_c**	**M–C_{t2}**
$\{Li(A')\}_2$	1.456(4)	1.368(4)	2.226(6)	–	–
	–	–	2.235(6)	2.245(6)	2.413(6)
$\{Na(A')\}_4$	1.414(3)	1.386(3)	2.864(3)	2.629(2)	2.611(3)
	1.398(3)	1.381(4)	2.627(3)	2.618(2)	2.787(3)
	–	–	2.896(3)	2.656(2)	2.598(2)
	–	–	2.591(3)	2.635(3)	2.885(3)
$\{K(A')\}_\infty$	1.399(4)	1.396(4)	3.100(3)	2.872(3)	3.030(3)
	–	–	2.977(3)	2.882(3)	3.147(3)
	1.403(4)	1.390(4)	2.981(3)	2.881(3)	3.049(3)
	–	–	3.093(3)	2.902(3)	2.987(3)
$\{K(A')(thf)_{1.5}\}_\infty$	1.394(4)	1.387(4)	3.095(3)	3.014(3)	3.062(3)
	–	–	3.090(3)	2.957(3)	2.987(3)
	1.392(4)	1.371(4)	3.042(3)	2.990(3)	3.116(3)
	–	–	3.024(3)	2.930(3)	3.067(3)

Table 5, continued.

Complex	C–C	C=C	M–C_{t1}	M–C_c	M–C_{t2}
Li[A′$_3$Zn]	1.439(3)	1.377(3)	2.1101(19)	–	–
	1.429(3)	1.388(3)	2.1264(19)	–	–
	1.440(2)	1.383(3)	2.116(2)	–	–
Na[A′$_3$Zn]	1.447(2)	1.361(3)	2.100(2)	–	–
	1.441(3)	1.368(3)	2.101(2)	–	–
	1.447(3)	1.365(3)	2.108(2)	–	–
K[A′$_3$Zn]	1.467(3)	1.358(4)	2.065(2)	–	–
	1.460(3)	1.355(3)	2.065(2)	–	–
	1.460(3)	1.364(3)	2.075(3)	–	–
GaA′$_3$	1.499(3)	1.326(4)	1.983(3)	–	–
	1.499(3)	1.330(4)	1.981(3)	–	–
	1.493(4)	1.330(4)	1.975(3)	–	–

In the criteria set forth by this work, the delocalization of the π electron density is evaluated by the difference between the C–C bond lengths, $\Delta_{(C-C)}$. A value less than 0.1 Å is indicative of a π-bonding complex. The other criterion for π-bonding is that the metal atom is centered over the region of π electron density. This can be evaluated by comparing the M–C bond lengths with the two terminal carbons of the allyl ligand (C_{t1} and C_{t2} from Table 5). In an ideal π-bonding complex, these distances would be equal. Both of these comparisons must be made taking into account statistically significant values. For the purposes of this work, statistical significance is measured at the 3σ level. This data is compiled in Table 6.

Table 6. Statistical evaluation of bond distances (Å) at the 3σ level.[a]

Complex	$\Delta_{(C-C)min}$	$\Delta_{(C-C)max}$	$\Delta_{(M-Ct)min}$
$\{Li(A')\}_2$	0.064	0.112	< 0 (η^2)
	–	–	0.142 (η^3)
$\{Na(A')\}_4$	0.010	0.046	0.235
	0	0.038	0.142
	–	–	0.283
	–	–	0.276
$\{K(A')\}_\infty$	0	0.027	0.052
	–	–	0.152
	0	0.037	0.050
	–	–	0.088
$\{K(A')(thf)_{1.5}\}_\infty$	0	0.031	0.015
	–	–	0.085
	0	0.045	0.056
	–	–	0.025
$Li[A'_3Zn]$[b]	0.044	0.080	–
	0.023	0.059	–
	0.039	0.075	–
$Na[A'_3Zn]$	0.071	0.101	–
	0.055	0.091	–
	0.064	0.100	–
$K[A'_3Zn]$	0.091	0.127	–
	0.087	0.123	–
	0.078	0.114	–
GaA'_3	0.152	0.194	–
	0.148	0.190	–
	0.139	0.187	–

[a] Nonzero values are the amount by which bond length differences exceed the 3σ level.

[b] This structure shows a 30% geometrical disorder. The calculated structure reveals a $\Delta_{(C-C)}$ of 0.077 Å.

For the determination of σ- versus π-bonding, a $\Delta_{(C–C)min}$ value of zero (from Table 6) indicates that the bonds are equal within 3σ. This shows completely delocalized π electron density, indicating a π-bonding complex. A $\Delta_{(C–C)max}$ value of 0.1 Å or more suggests a σ-bonding complex. From this measure, it can be seen that the homoleptic allyl complexes of sodium and potassium contain purely π-bound ligands. The lithium allyl dimer, the sodium and potassium tri(allyl)zincates, and the tri(allyl)gallium complexes contain σ-bound ligands. However, based on these criteria, the lithium tri(allyl)zincate is somewhat ambiguous.

The other set of criteria for σ- versus π-bonding set in this work involved the position of the metal relative to the ligand. Based on this measure, only a $\Delta_{(M–Ct)min}$ value of zero (or less) indicates purely π-bound ligands. The only structure that fits this condition is the lithium allyl dimer, if it is considered to be an η^2 interaction between each lithium and one allyl ligand.

It is clear from the failure of these criteria to accurately describe the bonding in all structures shown in this work, that the criteria itself must be appended or that it simply is not possible to hold all complexes to rigidly defined bonding modes. It would take a detailed study of a wider sample of similar organometallic complexes to determine a more accurate set of guidelines for this purpose. It would also be interesting to study whether the difference in the bonding modes of similar organometallic complexes affects their reactivities.

Appendix A

SYNTHESIS AND STRUCTURE OF BIS(1,2,4-TRIS(TRIMETHYLSILYL)CYCLOPENTADIENYL)ZINC

Introduction

$(1,2,4\text{-}(SiMe_3)_3C_5H_2)_2Zn$ was synthesized as a preliminary step in research on the synthesis and study of dizinc(I) complexes.[189]

Experimental

General Considerations. All manipulations were performed with the rigorous exclusion of air and moisture using high-vacuum, Schlenk, or glovebox techniques. Proton (^1H) NMR data were obtained on a Bruker DPX-300 at 300 MHz and were referenced to residual proton resonances of C_6D_6 (δ 7.15).

Materials. Hexanes, toluene, and diethyl ether were distilled under nitrogen from potassium benzophenone ketyl. ZnI_2 and $KN(SiMe_3)_2$ were purchased from Strem Chemicals and used as received. C_6D_6 was vacuum-distilled from Na/K (22/78) alloy and stored over type 4A molecular sieves prior to use. $K[(1,2,4\text{-}(SiMe_3)_3C_5H_2)]$ was prepared following published synthesis.[190]

Synthesis of $(1,2,4\text{-}(SiMe_3)_3C_5H_2)_2Zn$. A 125 mL Erlenmeyer flask, equipped with a magnetic stir bar, was charged with ZnI_2 (0.080 g, 0.25 mmol) and $K[(1,2,4\text{-}(SiMe_3)_3C_5H_2)]$ (0.161 g, 0.500 mmol). The solid mixture was dissolved in 25 mL diethyl ether and allowed to react overnight at room temperature while stirring. Removal of solvent under vacuum, followed by extraction of the residue with toluene, filtration of the extract over a medium-

porosity glass frit, and removal of toluene under vacuum afforded air- and moisture-sensitive off-white, feathery crystals. The product was then recrystallized from hexanes, producing colorless crystals. ^{1}H NMR (C_6D_6, 298 K): δ 7.00 (s, 4H, Cp), 0.29 (s, 36H, $C_{1,2}$-$SiMe_3$), 0.24 (s, 18H, C_4-$SiMe_3$).

X-ray Crystallography of [1,2,4-(SiMe$_3$)$_3$C$_5$H$_2$]$_2$Zn. [1,2,4-$(SiMe_3)_3C_5H_2]_2Zn$ crystallizes from hexanes. Suitable crystals were located, attached to glass fibers, and mounted on a Siemens SMART system for data collection. The intensity data were corrected for absorption (SADABS). All calculations were performed with the SHELXTL suite of programs.[119] Final cell constants were calculated from a set of strong reflections measured during the actual data collection. Relevant crystal and data collection parameters and atomic coordinates are given in Appendix C. The space groups were determined from systematic absences and intensity statistics. The structures were solved by direct methods and refined against F^2 for all observed reflections, using SHELXS and SHELXL.

The zinc atom is σ-bound to one tris(trimethylsilyl)cyclopentadienyl ligand and π-bound to another. A summary of bond distances and angles for [1,2,4-$(SiMe_3)_3C_5H_2]_2Zn$ is given in Table 7, and the solid-state structure of the complex is displayed as Figure 30.

Table 7. Selected bond distances (Å) and angles (°) for (1,2,4-$(SiMe_3)_3C_5H_2)_2Zn$

Atoms	Distance	Atoms	Angles
Zn(1)-C(1)	2.218(2)	C(1)-Zn-C(6)	162.17(7)
Zn(1)-C(2)	2.236(3)	C(7)-C(6)-Zn(1)	110.00(15)
Zn(1)-C(3)	2.285(2)	C(10)-C(6)-Zn(1)	102.70(15)
Zn(1)-C(4)	2.331(2)		
Zn(1)-C(5)	2.249(2)		
Zn(1)-C(6)	1.957(2)		

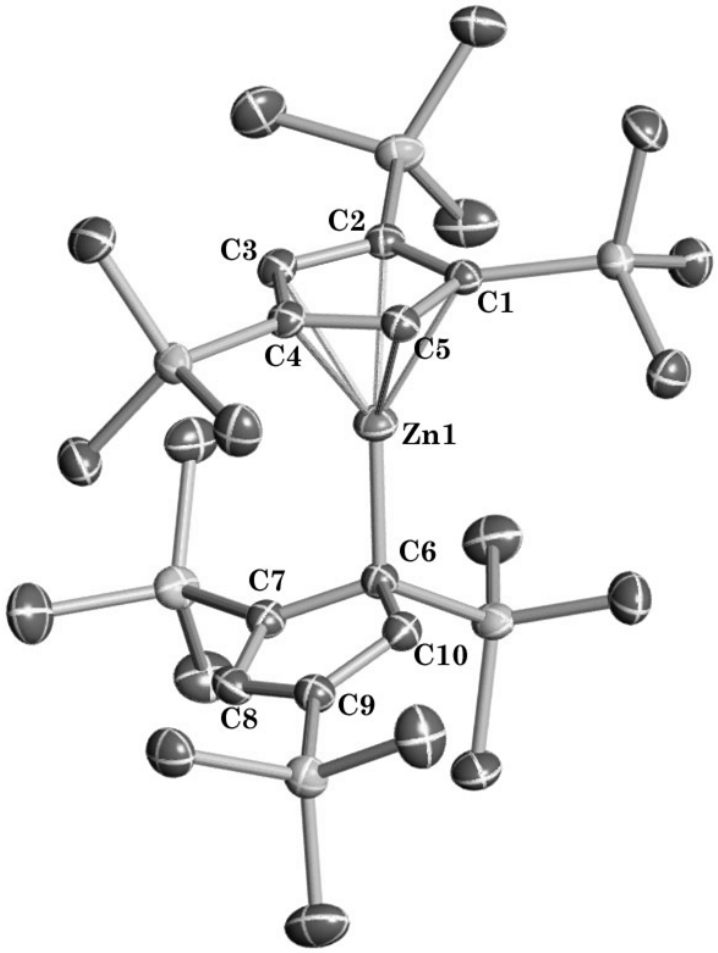

Figure 30. Solid-state structure of (1,2,4-$(SiMe_3)_3C_5H_2)_2Zn$, giving the numbering scheme used in the text. Thermal ellipsoids are shown at the 50% level, and hydrogen atoms have been omitted for clarity.

Appendix B

PROGRESS TOWARD A MULTI-FLORINATED METALLOCENE

Introduction

The C–F bond is the most robust of all single bonds (120-125 kcal mol^{-1}), and organometallic compounds containing partially fluorinated or perfluorinated ligands often possess strongly altered chemical, thermal, and structural properties when compared to their hydrocarbon counterparts.[34] Methods for preparing such complexes usually involve fluorinated precursors (e.g., CF_3I, *cyclo*-C_8F_8, C_2F_4); examples of direct fluorine addition to metal-bound ligands are relatively rare.

In particular, unlike the heavier halogens, fluorine is notoriously difficult to incorporate into metal-coordinated cyclopentadienyl rings. For example, perchloryl fluoride (ClO_3F) will convert lithioferrocene to fluoroferrocene in low (10%) yield,[191] although the reaction is potentially explosive. Attempts to transform the related 1,1´-$(C_5H_4Li)_2Fe$ to 1,1´-$(C_5H_4F)_2Fe$ have been unsuccessful.[192]

Perfluorinated molecules $(C_5F_5)_2M$ remain unknown, despite repeated attempts to obtain them. For example, no reaction occurs between the $[C_5F_5]^-$ anion and NiI_2, $FeBr_2$, or $MnCl_2$, or between C_5F_5H and either $M(OEt)_2$ (M = Fe, Ni) or $M\{N[SiMe_3]_2\}_2$ (M = Fe, Mn, Ni).[193] Attempts to convert $(C_5Cl_5)_2Fe$ (or $(C_5Cl_5)_2Ru$) to $(C_5F_5)_2Fe(Ru)$ by heating with CsF have been unsuccessful,[194] as have experiments to convert $[C_5(HgOAc)_5]_2Fe$ with various fluorinating agents.[195]

The repeated failure of seemingly reasonable routes to decafluorinated metallocenes at one time raised doubts about the intrinsic stability of the (η^5-C_5F_5)M unit.[193] Hughes has shown, however, that thermally stable *penta*fluorinated ruthenocenes (i.e., (C_5F_5)RuCp*, (C_5F_5)RuCp) are available from the flash photolysis of fluorinated (oxocyclohexadienyl)RuCp´ precursors; in these cases the C_5F_5 ligand is constructed *in situ*, using the metal as a template.[196,197]

Nevertheless, it remains difficult to prepare fluorinated metallocenes, especially in view of the ease with which Cl, Br, and I derivatives can be synthesized. This work investigates several exchange reactions that could potentially yield fluorinated ferrocenes.

Experimental

General Considerations. All manipulations of air-sensitive materials were performed with the rigorous exclusion of air and moisture using high-vacuum, Schlenk, or glovebox techniques. Proton (^{1}H) and fluorine (^{19}F) NMR data were obtained on a Bruker DPX-300 at 300 MHz or a Bruker DPX-400 at 400 and 376 MHz, respectively, and were referenced to residual proton resonances of C_6D_6 (δ 7.15) or $CDCl_3$ (δ 7.24).

Materials. Hexanes and toluene were distilled under nitrogen from potassium benzophenone ketyl. C_6D_6 was vacuum-distilled from Na/K (22/78) alloy and stored over 4A molecular sieves prior to use. Anhydrous

tetrahydrofuran, $CDCl_3$, and fluorinating agents were purchased from Sigma Aldrich and used as received. Cobalt (II) chloride and bis(cyclopentadienyl)cobalt were purchased from Strem Chemicals and used as received. $(C_5H_4Li)_2Fe$,[198] $(C_5H_4Br)_2Fe$,[199] $(C_5H_4(MgBr))_2Fe$,[200] $[(C_5H_5)_2Co]F$[201] were prepared following published syntheses. (1,2,4-$(SiMe_3)_3C_5H_2)_2Co$ was prepared from $CoCl_2$ and the KCp′ salt, which was prepared from 1,2,4-$(SiMe_3)_3C_5H_3$[202] by treatment with *n*-BuLi followed by KO(*t*-Bu) in hexane.

Attempted syntheses of 1,1′-difluoroferrocene. Several exchange reactions were attempted in THF to either afford a halogen exchange from bromine to fluorine or make use of an electrophilic fluorine source (Selectfluor™) to attack a C-Li or C-MgBr bond. Products were evaluated by comparing their ^1H, or in some cases ^{19}F, NMR spectra with those of starting materials. These attempts are summarized in Table 8.

Table 8. Attempted syntheses of 1,1′-difluoroferrocene.

$(C_5H_4X)_2Fe$	Flourinating agent	Result	Ref
X = Br	$[Cp'_2Co]F$[a]	no reaction	201
X = Br	KF/18-crown-6/Ph_4PBr	no reaction	203
X = Br	Me_4NF	no reaction	204
X = Li	Selectfluor™	no reaction	205,206
X = MgBr	Selectfluor™	no reaction	205-207

[a] Substituted cobaltocenes used were $(C_5H_5)_2Co$, $(C_5H_2(SiMe_3)_3)_2Co$, and $(C_5H(i\text{-}Pr)_4)_2Co$.[208]

Computational Detail. All calculations were performed with the Gaussian 03W suite of programs.[108] All DFT methods used the BP86 or B3PW91 functionals with the DGDZVP2 (all atoms) or the combination of cc-pwCVTZ(Fe) and cc-pVTZ (others) basis sets. These give satisfactory reproduction of the gas-phase parameters of ferrocene (e.g., with B3PW91 and the triple-zeta basis sets, Fe–C = 2.054(3) Å (exp); 2.057 Å (calc)).

Results and Discussion

Exchange reactions with 1,1´-$(C_5H_4X)_2Fe$. All attempts at halogen exchange using nucleophilic fluoride sources and 1,1´-dibromoferrocene resulted in the persistence of starting materials as seen by proton or fluorine NMR. Attempted substitution reactions using an electrophilic fluorine source (Selectfluor™) also resulted in persistence of starting material as seen by proton or fluorine NMR.

Attempts to use the electrophilic fluorinating agent XeF_2 at low temperature with ferrocene have led to the formation of trace (~2%) amounts of neutral orange materials.[209] Mass spectrometric evidence suggests these may contain fluorinated metallocenes. The formation of these products is not always reproducible, however.

Computational Considerations. DFT calculations indicate that both $(\eta^5\text{-}C_5H_4F)_2Fe$ and $(\eta^5\text{-}C_5F_5)_2Fe$ are minima on their respective potential

energy surfaces (N_{imag} = 0). (Figure 31) The Fe–C length is consistently shorter (up to 0.6%) than in ferrocene itself.

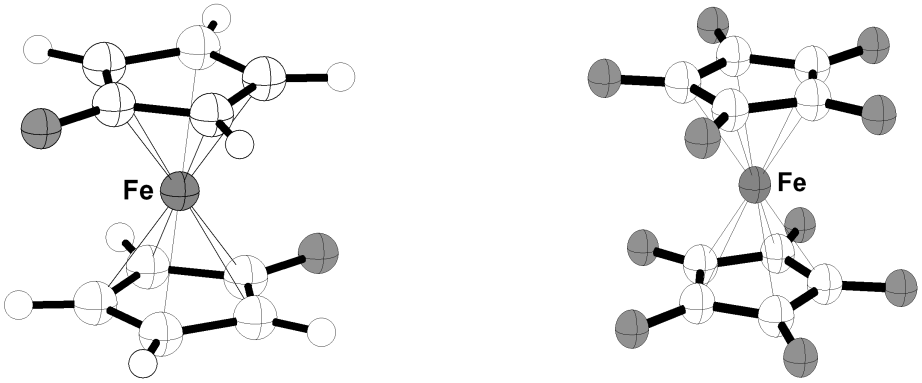

(a) (b)

Figure 31. Calculated structure of (a) $(\eta^5\text{-}C_5H_4F)_2Fe$ and (b) $(\eta^5\text{-}C_5F_5)_2Fe$. Selected bond distances (Å) and angles (°): (a) Fe-C = 2.053; $Fe\text{-}Cp_{(centroid)}$ = 1.660; C-C = 1.420; C-F = 1.336; C_5-F = 0.85 (away from Fe). (b) Fe-C = 2.029, $Fe\text{-}Cp_{(centroid)}$ = 1.625, C-C = 1.429, C-F = 1.329, C_5-F = 2.6 (away from Fe).

Conclusions

Fluorinated metallocenes do not appear to be intrinsically unstable compounds, although there are still no general routes available to generate them. Methods that are appropriate for H/F or X/F exchange in organic molecules often fail with metallocenes, especially where oxidation of the metal center is an alternative reaction outcome.

Appendix C

CRYSTAL DATA, ATOMIC FRACTIONAL COORDINATES AND ISOTOPIC THERMAL PARAMETERS FOR X-RAY STRUCTURAL DETERMINATIONS

Table 9. Crystal data and structure refinement for $\{Li[1,3,3'\text{-}(SiMe_3)_3C_3H_2]\}_2$.

Empirical formula	C12 H28 Li Si3	
Formula weight	263.55	
Temperature	100(2) K	
Wavelength	0.71073 Å	
Crystal system	Triclinic	
Space group	P−1	
Unit cell dimensions	a = 9.5882(10) Å	α= 94.813(2)°
	b = 10.4166(11) Å	β= 102.068(2)°
	c = 18.4130(19) Å	γ=104.7130(10)°
Volume	1721.1(3) $Å^3$	
Z	4	
Density (calculated)	1.017 g/cm^3	
Absorption coefficient	0.253 mm^{-1}	
F(000)	580	
Crystal size	0.30 x 0.25 x 0.20 mm^3	
Crystal color, habit	Colorless rods	
Theta range for data collection	2.04 to 25.31°	
Index ranges	−11≤h≤11, −12≤k≤12, −20≤l≤22	
Reflections collected	15994	
Independent reflections	6185 [R(int) = 0.0413]	
Completeness to theta = 25.00°	99.0 %	
Absorption correction	Multi−scan	
Max. and min. transmission	0.9512 and 0.9280	
Refinement method	Full−matrix least−squares on F^2	
Data / restraints / parameters	6185 / 0 / 303	
Goodness−of−fit on F^2	1.042	
Final R indices [I>2sigma(I)]	R1 = 0.0537, wR2 = 0.1384	
R indices (all data)	R1 = 0.0700, wR2 = 0.1523	
Largest diff. peak and hole	0.693 and −0.704 e $Å^{-3}$	

Table 10. Atomic coordinates (x 10^4) and equivalent isotropic displacement parameters (Å^{2}x 10^3) for {Li[1,3,3′-$(SiMe_3)_3C_3H_2$]}$_2$. U_{eq} is defined as one third of the trace of the orthogonalized U_{ij} tensor.

atom	x	y	z	U_{eq}
Si(1)	2264(1)	7349(1)	1353(1)	19(1)
Si(2)	3047(1)	11577(1)	45(1)	17(1)
Si(3)	5806(1)	12455(1)	1445(1)	18(1)
Si(4)	8347(1)	7299(1)	3740(1)	20(1)
Si(5)	11568(1)	8072(1)	4811(1)	20(1)
Si(6)	8117(1)	7466(1)	6682(1)	22(1)
Li(1)	6221(6)	10965(5)	143(3)	25(1)
Li(2)	10425(6)	9885(5)	5707(3)	27(1)
C(1)	3953(3)	9841(3)	1052(2)	17(1)
C(2)	2707(3)	8776(3)	823(2)	18(1)
C(3)	8852(3)	7867(3)	5286(2)	20(1)
C(4)	4448(3)	11066(3)	739(2)	17(1)
C(5)	2191(3)	10320(3)	−846(2)	20(1)
C(6)	7434(3)	13337(3)	1078(2)	25(1)
C(7)	3936(4)	13130(3)	−318(2)	24(1)
C(8)	1459(3)	11825(3)	434(2)	23(1)
C(9)	1990(4)	5682(3)	793(2)	29(1)
C(10)	9371(3)	7896(3)	6040(2)	22(1)
C(11)	12879(3)	9356(3)	5615(2)	26(1)
C(12)	6144(4)	7115(4)	6143(2)	32(1)
C(13)	4973(4)	13794(3)	1757(2)	27(1)
C(14)	8859(4)	5833(3)	3311(2)	27(1)
C(15)	6373(4)	6618(3)	3796(2)	27(1)
C(16)	8353(4)	8488(3)	3015(2)	24(1)
C(17)	12297(4)	8572(3)	3977(2)	28(1)
C(18)	477(3)	7263(3)	1631(2)	25(1)
C(19)	6582(4)	11840(3)	2329(2)	28(1)
C(20)	9598(3)	8109(3)	4677(2)	20(1)
C(21)	3793(4)	7596(4)	2212(2)	35(1)

Table 10, continued.

atom	x	y	z	U_{eq}
C(22)	11872(4)	6416(3)	5008(2)	32(1)
C(23)	8359(5)	5945(4)	7106(2)	39(1)
C(24)	8484(4)	8848(3)	7473(2)	34(1)

Table 11. Crystal data and structure refinement for {Na[1,3-$(SiMe_3)_2C_3H_3$](thf)}$_4$ • 2(C_7H_8).

Empirical formula	C66 H132 Na4 O4 Si8	
Formula weight	1306.40	
Temperature	100.0(1) K	
Wavelength	0.71073 Å	
Crystal system	Orthorhombic	
Space group	*Pnna*	
Unit cell dimensions	a = 11.080(2) Å	α = 90°
	b = 27.497(6) Å	β = 90°
	c = 27.207(6) Å	γ = 90°
Volume	8289(3) Å^3	
Z	4	
Density (calculated)	1.047 Mg/m^3	
Absorption coefficient	0.189 mm^{-1}	
F(000)	2864	
Crystal color, morphology	colorless, rod	
Crystal size	0.38 x 0.16 x 0.08 mm^3	
Theta range for data collection	1.48 to 29.57°	
Index ranges	$-15 \le h \le 15$, $-38 \le k \le 38$, $-37 \le l \le$ 37	
Reflections collected	100412	
Independent reflections	11636 [R(int) = 0.0747]	
Observed reflections	7676	
Completeness to theta = 29.57°	100.0%	
Absorption correction	Multi−scan	
Max. and min. transmission	0.9850 and 0.9317	
Refinement method	Full−matrix least−squares on F^2	
Data / restraints / parameters	11636 / 97 / 368	
Goodness−of−fit on F^2	1.058	
Final R indices [I>2sigma(I)]	R1 = 0.0712, wR2 = 0.1684	
R indices (all data)	R1 = 0.1110, wR2 = 0.1842	
Largest diff. peak and hole	0.589 and −0.376 e.Å^{-3}	

Table 12. Atomic coordinates (x 10^4) and equivalent isotropic displacement parameters ($Å^2$x 10^3) for $\{Na[1,3\text{-}(SiMe_3)_2C_3H_3](thf)\}_4 \cdot 2(C_7H_8)$. U_{eq} is defined as one third of the trace of the orthogonalized U_{ij} tensor.

	x	y	z	U_{eq}
Na1	4037(1)	1395(1)	2024(1)	42(1)
Na2	4154(1)	2952(1)	1391(1)	39(1)
Si1	6520(1)	957(1)	3092(1)	33(1)
Si2	1577(1)	1422(1)	3015(1)	34(1)
Si3	6678(1)	2058(1)	1350(1)	38(1)
Si4	1728(1)	1811(1)	961(1)	44(1)
C1	5350(2)	1394(1)	2931(1)	32(1)
C2	4123(2)	1313(1)	2986(1)	29(1)
C3	3108(2)	1607(1)	2879(1)	30(1)
C4	5131(2)	2116(1)	1572(1)	32(1)
C5	4130(2)	2000(1)	1282(1)	34(1)
C6	2906(2)	2032(1)	1373(1)	36(1)
C7	7553(3)	1180(1)	3583(1)	53(1)
C8	5822(2)	380(1)	3324(1)	39(1)
C9	7516(3)	805(1)	2555(1)	46(1)
C10	1291(3)	1381(1)	3695(1)	53(1)
C11	1266(3)	803(1)	2755(1)	48(1)
C12	480(3)	1862(1)	2750(1)	54(1)
C13	7051(3)	1422(1)	1150(1)	63(1)
C14	7741(3)	2250(1)	1843(1)	56(1)
C15	6926(3)	2446(1)	789(1)	55(1)
C16	2439(4)	1574(1)	379(1)	65(1)
C17	830(4)	1305(2)	1250(2)	80(1)
C18	608(3)	2285(1)	777(1)	62(1)
O1	4018(5)	634(1)	1693(2)	40(4)
C19	4457(14)	511(5)	1206(3)	66(3)
C20	5491(7)	173(2)	1302(3)	67(2)
C21	5193(7)	−60(3)	1786(3)	57(2)
C22	4138(11)	203(3)	1978(3)	58(3)
O2	4186(10)	3291(2)	638(1)	44(2)

Table 11, continued.

atom	x	y	z	U_{eq}
C23	4486(6)	3778(2)	511(2)	55(2)
C24	4416(9)	3810(2)	−35(2)	83(2)
C25	3647(9)	3409(2)	−183(2)	96(3)
C26	3684(6)	3046(2)	210(2)	48(1)
O1'	3650(20)	637(4)	1718(7)	40(4)
C19'	3534(18)	481(5)	1221(5)	66(3)
C20'	3923(15)	−33(5)	1223(5)	67(2)
C21'	4862(17)	−44(7)	1635(7)	57(2)
C22'	4380(30)	307(8)	1993(7)	58(3)
O2'	3970(40)	3307(7)	654(4)	44(2)
C23'	3950(20)	3807(7)	526(6)	55(2)
C24'	3660(20)	3811(7)	−1(6)	83(2)
C25'	4350(20)	3396(7)	−178(6)	96(3)
C26'	4203(18)	3035(6)	221(6)	48(1)
O1"	4370(30)	649(4)	1670(8)	40(4)
C19"	4160(40)	536(15)	1156(8)	66(3)
C20"	4980(20)	127(6)	1047(6)	67(2)
C21"	5539(16)	−18(7)	1526(7)	57(2)
C22"	4690(20)	181(8)	1889(7)	58(3)

Table 13. Crystal data and structure refinement for $\{K[1,3\text{-}(SiMe_3)_2C_3H_3]\}_\infty$.

Empirical formula	C18 H38 K2 Si4	
Formula weight	445.04	
Temperature	100(2) K	
Wavelength	0.71073 Å	
Crystal system	Monoclinic	
Space group	P2/c	
Unit cell dimensions	a = 17.9074(15) Å	α= 90°
	b = 13.0671(11) Å	β= 91.4270(10)°
	c = 12.2835(10) Å	γ = 90°
Volume	2873.4(4) $Å^3$	
Z	4	
Density (calculated)	1.029 g/cm^3	
Absorption coefficient	0.497 mm^{-1}	
F(000)	960	
Crystal size	0.33 x 0.30 x 0.23 mm^3	
Crystal color, habit	Colorless block	
Theta range for data collection	1.56 to 25.22°	
Index ranges	$-21\leq h\leq 21$, $-15\leq k\leq 15$, $-14\leq l\leq 14$	
Reflections collected	44965	
Independent reflections	5204 [R(int) = 0.0417]	
Completeness to theta = 25.00°	99.9 %	
Refinement method	Full−matrix least−squares on F^2	
Data / restraints / parameters	5204 / 0 / 218	
Goodness−of−fit on F^2	1.068	
Final R indices [I>2sigma(I)]	R1 = 0.0474, wR2 = 0.1386	
R indices (all data)	R1 = 0.0548, wR2 = 0.1445	
Largest diff. peak and hole	0.852 and −0.583 e $Å^{-3}$	

Table 14. Atomic coordinates (x 10^4) and equivalent isotropic displacement parameters (Å^{2}x 10^3) for $\{K[1,3\text{-}(SiMe_3)_2C_3H_3]\}_\infty$. U_{eq} is defined as one third of the trace of the orthogonalized U_{ij} tensor.

atom	x	y	z	U_{eq}
K(1)	2617(1)	7711(1)	840(1)	39(1)
K(2)	0	9342(1)	2500	28(1)
K(3)	5000	5565(1)	2500	30(1)
Si(1)	335(1)	7549(1)	−28(1)	26(1)
Si(2)	2349(1)	10357(1)	2137(1)	24(1)
Si(3)	2701(1)	4767(1)	1665(1)	24(1)
Si(4)	4902(1)	7534(1)	3(1)	23(1)
C(1)	790(2)	6569(3)	−915(3)	50(1)
C(2)	−553(2)	6966(3)	443(3)	42(1)
C(3)	109(2)	8680(3)	−928(3)	32(1)
C(4)	913(2)	7963(2)	1135(2)	25(1)
C(5)	1300(2)	8889(2)	1250(2)	23(1)
C(6)	1732(2)	9245(2)	2133(3)	26(1)
C(7)	3337(2)	10022(3)	1796(3)	34(1)
C(8)	2414(2)	10934(3)	3540(3)	32(1)
C(9)	2036(2)	11350(3)	1127(3)	35(1)
C(10)	1720(2)	5165(3)	1970(3)	36(1)
C(11)	2927(2)	3703(2)	2649(3)	31(1)
C(12)	2711(2)	4236(3)	247(3)	34(1)
C(13)	3341(2)	5856(2)	1805(2)	25(1)
C(14)	3812(2)	6238(2)	1019(2)	22(1)
C(15)	4261(2)	7117(2)	1050(2)	24(1)
C(16)	5069(2)	6426(3)	−944(3)	34(1)
C(17)	4559(2)	8620(3)	−863(3)	41(1)
C(18)	5810(2)	7977(3)	632(3)	34(1)

Table 15. Crystal data and structure refinement for {K[1,3-$(SiMe_3)_2C_3H_3$]$(thf)_{3/2}$}$_\infty$.

Empirical formula	C30 H66 K2 O3 Si4	
Formula weight	665.39	
Temperature	173(2) K	
Wavelength	0.71073 Å	
Crystal system	Orthorhombic	
Space group	*Pna*2$_1$	
Unit cell dimensions	*a* = 23.151(2) Å	α = 90°
	b = 11.0862(9) Å	β = 90°
	c = 16.9491(14) Å	γ = 90°
Volume	4350.1(6) Å^3	
Z	4	
Density (calculated)	1.016 Mg/m^3	
Absorption coefficient	0.352 mm^{-1}	
F(000)	1456	
Crystal color, morphology	colorless, block	
Crystal size	0.50 x 0.32 x 0.30 mm^3	
Theta range for data collection	1.76 to 25.04°	
Index ranges	$-27 \le h \le 27$, $-13 \le k \le 13$, $-20 \le l \le 19$	
Reflections collected	31324	
Independent reflections	7483 [*R*(int) = 0.0350]	
Observed reflections	6288	
Completeness to theta = 25.04°	99.9%	
Absorption correction	Multi−scan	
Max. and min. transmission	0.9019 and 0.8438	
Refinement method	Full−matrix least−squares on F^2	
Data / restraints / parameters	7483 / 115 / 438	
Goodness−of−fit on F^2	1.019	
Final *R* indices [*I*>2sigma(*I*)]	*R*1 = 0.0422, *wR*2 = 0.1054	
R indices (all data)	*R*1 = 0.0559, *wR*2 = 0.1177	
Absolute structure parameter	0.01(5)	
Largest diff. peak and hole	0.363 and −0.174 e.Å^{-3}	

Table 16. Atomic coordinates (x 10^4) and equivalent isotropic displacement parameters (Å^{2}x 10^3) for $\{K[1,3\text{-}(SiMe_3)_2C_3H_3](thf)_{3/2}\}_\infty$. U_{eq} is defined as one third of the trace of the orthogonalized U_{ij} tensor.

atom	x	y	z	U_{eq}
K1	3649(1)	8887(1)	2604(1)	56(1)
K2	4828(1)	10049(1)	5240(1)	64(1)
C1	3798(1)	9064(3)	4396(2)	45(1)
C2	4258(1)	8357(3)	4138(2)	46(1)
C3	4729(1)	8648(3)	3669(2)	52(1)
Si1	3229(1)	8606(1)	5062(1)	60(1)
C4	2494(7)	8830(20)	4541(13)	115(3)
C5	3128(13)	9390(20)	6002(11)	119(3)
C6	3270(20)	6945(14)	5250(30)	110(4)
Si1'	3229(1)	8606(1)	5062(1)	60(1)
C4'	2565(3)	9498(9)	4930(7)	115(3)
C5'	3453(5)	8951(10)	6122(4)	119(3)
C6'	3093(7)	6965(6)	5015(9)	110(4)
Si2	5308(1)	7642(1)	3370(1)	67(1)
C7	5294(8)	7070(20)	2344(9)	93(2)
C8	5148(10)	6061(15)	3902(16)	120(2)
C9	6015(8)	8090(30)	3796(17)	119(2)
Si2'	5308(1)	7642(1)	3370(1)	67(1)
C7'	5702(2)	8368(6)	2479(4)	93(2)
C8'	5025(3)	6192(6)	2986(6)	120(2)
C9'	5878(3)	7447(9)	4128(5)	119(2)
C10	5899(1)	11210(3)	5921(2)	51(1)
C11	5920(1)	9990(3)	6113(2)	48(1)
C12	5598(1)	9319(3)	6632(2)	53(1)
Si3	6292(1)	11959(1)	5139(1)	67(1)
C13	6265(2)	13623(4)	5269(4)	113(2)
C14	7062(2)	11460(6)	5100(5)	130(2)
C15	5970(3)	11633(6)	4129(3)	124(2)
Si4	5654(1)	7709(1)	6825(1)	68(1)

Table 16, continued.

atom	x	y	z	U_{eq}
C16	5705(3)	7394(4)	7908(3)	99(2)
C17	6308(2)	7051(4)	6332(3)	102(2)
C18	5003(3)	6861(5)	6450(5)	145(3)
O1	3028(3)	6819(6)	2622(5)	97(2)
C19	3318(4)	5757(12)	2846(15)	116(2)
C20	2874(6)	4854(15)	2992(15)	127(4)
C21	2346(3)	5508(7)	3014(6)	108(3)
C22	2436(4)	6588(8)	2599(9)	143(5)
O1'	3205(12)	6650(30)	2470(20)	97(2)
C19'	3454(16)	5690(60)	2890(60)	116(2)
C20'	2990(20)	4900(70)	3120(60)	127(4)
C21'	2514(14)	5200(30)	2640(30)	108(3)
C22'	2652(15)	6300(40)	2240(40)	143(5)
O2	2626(6)	10030(20)	2476(15)	116(3)
C23	2053(4)	9701(12)	2326(11)	140(5)
C24	1692(5)	10753(15)	2561(12)	132(4)
C25	2076(5)	11651(12)	2761(9)	131(4)
C26	2656(5)	11203(13)	2807(11)	139(4)
O2'	2657(8)	10190(30)	2640(20)	116(3)
C23'	2344(6)	10061(18)	1934(13)	140(5)
C24'	1735(6)	10183(19)	2229(12)	132(4)
C25'	1756(6)	10850(30)	2902(12)	131(4)
C26'	2375(7)	11222(19)	2974(15)	139(4)
O3	4366(13)	12240(20)	5310(40)	86(3)
C27	3764(12)	12435(18)	5190(30)	91(2)
C28	3677(7)	13678(15)	5475(13)	95(3)
C29	4208(10)	14260(20)	5160(40)	146(4)
C30	4609(9)	13400(30)	5506(15)	95(4)
O3'	4271(8)	12184(13)	5220(20)	86(3)
C27'	3682(7)	12513(11)	5220(20)	91(2)
C28'	3677(4)	13784(8)	4976(9)	95(3)

Table 16, continued.

atom	x	y	z	U_{eq}
C29'	4232(6)	14270(14)	5260(30)	146(4)
C30'	4614(5)	13264(14)	5152(9)	95(4)

Table 17. Crystal data and structure refinement for 1,3,4,6-$(Si(^{i}Pr)_3)_4C_6H_6$.

Empirical formula	C42 H90 Si4	
Formula weight	707.50	
Temperature	198(2) K	
Wavelength	0.71073 Å	
Crystal system	Monoclinic	
Space group	P2(1)/n	
Unit cell dimensions	a = 14.7352(7) Å	α= 90°
	b = 12.2053(5) Å	β= 117.8230(10)°
	c = 14.8173(7) Å	γ = 90°
Volume	2356.78(19) $Å^3$	
Z	2	
Density (calculated)	0.997 g/cm^3	
Absorption coefficient	0.151 mm^{-1}	
F(000)	796	
Crystal size	0.40 x 0.30 x 0.30 mm^3	
Theta range for data collection	1.61 to 26.25°	
Index ranges	$-18\leq h\leq 17$, $-14\leq k\leq 6$, $-18\leq l\leq 18$	
Reflections collected	12751	
Independent reflections	4695 [R(int) = 0.0357]	
Completeness to theta = 25.00°	99.1 %	
Absorption correction	Multi−scan	
Max. and min. transmission	0.9561 and 0.9421	
Refinement method	Full−matrix least−squares on F^2	
Data / restraints / parameters	4695 / 0 / 208	
Goodness−of−fit on F^2	1.123	
Final R indices [I>2sigma(I)]	R1 = 0.0588, wR2 = 0.1663	
R indices (all data)	R1 = 0.0676, wR2 = 0.1758	
Largest diff. peak and hole	0.703 and −0.467 e $Å^{-3}$	

Table 18. Atomic coordinates (x 10^4) and equivalent isotropic displacement parameters (Å^{2}x 10^3) for 1,3,4,6-(Si(^{i}Pr)$_3$)$_4$C$_6$H$_6$. U_{eq} is defined as one third of the trace of the orthogonalized U_{ij} tensor.

atom	x	y	z	U_{eq}
Si(1)	1726(1)	−1697(1)	−1691(1)	43(1)
Si(2)	1310(1)	1346(1)	691(1)	30(1)
C(1)	590(1)	−28(2)	157(1)	28(1)
C(2)	778(1)	−439(2)	−701(1)	31(1)
C(3)	1459(2)	−1186(2)	−651(2)	37(1)
C(4)	725(2)	−1170(3)	−2970(2)	63(1)
C(5)	752(4)	58(3)	−3133(3)	96(1)
C(6)	721(4)	−1781(4)	−3882(3)	113(2)
C(7)	1658(2)	−3243(2)	−1690(2)	57(1)
C(8)	569(3)	−3665(3)	−2046(4)	92(1)
C(9)	2373(4)	−3755(3)	−658(3)	96(1)
C(10)	3076(3)	−1307(4)	−1382(4)	100(2)
C(11)	3440(4)	−1811(5)	−2110(5)	146(3)
C(12)	3494(4)	−335(5)	−1027(5)	175(3)
C(13)	2568(2)	1286(2)	634(2)	40(1)
C(14)	3330(2)	464(2)	1399(2)	54(1)
C(15)	3114(2)	2388(2)	723(2)	57(1)
C(16)	1525(2)	1527(2)	2053(2)	38(1)
C(17)	1839(2)	486(2)	2713(2)	48(1)
C(18)	2277(2)	2444(2)	2652(2)	59(1)
C(19)	467(2)	2482(2)	−160(2)	41(1)
C(20)	741(3)	3656(2)	227(3)	64(1)
C(21)	362(2)	2408(2)	−1239(2)	53(1)

Table 19. Crystal data and structure refinement for Li[Zn(1,3-$(SiMe_3)_2C_3H_3)_3$].

Empirical formula	C27 H63 Li Si6 Zn	
Formula weight	628.62	
Temperature	100(2) K	
Wavelength	0.71073 Å	
Crystal system	Triclinic	
Space group	P−1	
Unit cell dimensions	a = 12.2863(6) Å	α= 81.1310(10)°
	b = 12.5849(7) Å	β= 71.0810(10)°
	c = 13.8068(7) Å	γ = 88.5420(18)°
Volume	1994.67(18) $Å^3$	
Z	2	
Density (calculated)	1.047 g/cm^3	
Absorption coefficient	0.809 mm^{-1}	
F(000)	684	
Crystal size	0.40 x 0.20 x 0.10 mm^3	
Theta range for data collection	1.58 to 27.50°	
Index ranges	−15≤h≤15, −16≤k≤16, −17≤l≤17	
Reflections collected	17371	
Independent reflections	8729 [R(int) = 0.0190]	
Completeness to theta = 27.50°	95.4 %	
Absorption correction	Semi−empirical from equivalents	
Max. and min. transmission	0.8549 and 0.7933	
Refinement method	Full−matrix least−squares on F^2	
Data / restraints / parameters	8729 / 0 / 316	
Goodness−of−fit on F^2	1.060	
Final R indices [I>2sigma(I)]	R1 = 0.0364, wR2 = 0.0970	
R indices (all data)	R1 = 0.0434, wR2 = 0.1005	
Largest diff. peak and hole	0.455 and −0.338 e $Å^{-3}$	

Table 20. Atomic coordinates (x 10^4) and equivalent isotropic displacement parameters (Å^{2}x 10^3) for Li[Zn(1,3-$(SiMe_3)_2C_3H_3)_3$]. U_{eq} is defined as one third of the trace of the orthogonalized U_{ij} tensor.

atom	x	y	z	U_{eq}
Zn1	3597.8(2)	2919.11(19)	3018.12(19)	20.9(8)
Zn2	1226.1(6)	3111.6(5)	2536.6(5)	21.01(14)
Si1	1365.5(5)	1619.9(4)	712.2(4)	28.81(12)
Si3	5398.4(4)	1457.1(4)	1446.6(4)	26.75(12)
Si4	828.4(4)	5669.9(4)	1725.8(4)	25.3(12)
Si6	4716.8(4)	5327.9(4)	2723(4)	26.3(12)
Si7	-970.8(4)	2321.1(4)	4668.6(4)	24.58(12)
Si9	3074.4(4)	1795.2(4)	5401.3(4)	26.13(12)
C1	2353.6(17)	2432.8(17)	1088(16)	34.8(5)
C2	3129.9(15)	1964.8(14)	1542.5(13)	24.2(4)
C3	4193.3(16)	2406.8(15)	1554.7(15)	28.4(4)
C4	1467.7(16)	4849.6(15)	2633.5(14)	26.9(4)
C5	2652.9(15)	4811.1(13)	2405.6(14)	22.1(3)
C6	3317.5(16)	4583.8(15)	3088.5(14)	27.5(4)
C7	553.8(16)	1981.9(15)	4044.9(15)	28.2(4)
C8	1417.7(15)	2283(13)	4394.2(13)	22.1(3)
C9	2535.5(16)	1838.7(15)	4281.8(15)	27.8(4)
C11	2051(2)	1436(2)	-672.9(18)	57.4(7)
C12	4.4(19)	2346(2)	785(2)	48.8(6)
C13	1021.6(19)	283.6(17)	1552.6(17)	38.2(5)
C31	6061(2)	1286(2)	54.5(18)	51.8(6)
C32	6535.9(18)	1986.7(19)	1883.8(19)	42.1(5)
C33	4862.9(17)	119.4(15)	2246.5(16)	32.3(4)
C41	768(2)	7101.7(16)	1944.2(19)	40.9(5)
C42	-676.5(18)	5209.4(17)	1944.7(18)	37(5)
C43	1742(2)	5591.8(19)	364.4(16)	41.1(5)
C61	5445(2)	5485(2)	1296.7(18)	46.9(6)
C62	4480.5(19)	6702.8(17)	3101(2)	42.8(5)

Table 20, continued.

atom	x	y	z	U_{eq}
C63	5679.9(19)	4600.3(17)	3396(2)	42(5)
C71	-1062(17)	3645.9(16)	5141.3(16)	34(4)
C72	-1811.7(19)	2388.7(19)	3752.3(18)	41.4(5)
C73	-1640(2)	1250.7(18)	5791.8(18)	44.5(5)
C91	2391(2)	640(2)	6432(2)	56.2(7)
C92	2737.4(19)	3065.5(18)	5970.3(17)	37.9(5)
C93	4667.5(18)	1603.5(18)	4979.6(17)	37.1(5)

Table 21. Crystal data and structure refinement for Na[Zn(1,3-$(SiMe_3)_2C_3H_3)_3$].

Empirical formula	C27 H63 Na Si6 Zn	
Formula weight	644.67	
Temperature	173(2) K	
Wavelength	0.71073 Å	
Crystal system	Triclinic	
Space group	P−1	
Unit cell dimensions	a = 12.1734(17) Å	α= 80.647(2)°
	b = 12.7745(18) Å	β= 71.666(2)°
	c = 13.9023(19) Å	γ = 88.586(2)°
Volume	2024.1(5) $Å^3$	
Z	2	
Density (calculated)	1.058 g/cm^3	
Absorption coefficient	0.809 mm^{-1}	
F(000)	700	
Crystal size	0.40 x 0.20 x 0.10 mm^3	
Theta range for data collection	1.56 to 28.26°	
Index ranges	−15≤h≤16, −16≤k≤16, −18≤l≤18	
Reflections collected	24888	
Independent reflections	9119 [R(int) = 0.0226]	
Completeness to theta = 25.00°	99.6 %	
Absorption correction	Semi−empirical from equivalents	
Max. and min. transmission	0.9235 and 0.7380	
Refinement method	Full−matrix least−squares on F^2	
Data / restraints / parameters	9119 / 0 / 371	
Goodness−of−fit on F^2	1.082	
Final R indices [I>2sigma(I)]	R1 = 0.0369, wR2 = 0.0920	
R indices (all data)	R1 = 0.0432, wR2 = 0.0955	
Largest diff. peak and hole	0.888 and −0.432 e $Å^{-3}$	

Table 22. Atomic coordinates (x 10^4) and equivalent isotropic displacement parameters (Å^{2}x 10^3) for Na[Zn(1,3-$(SiMe_3)_2C_3H_3)_3$]. U_{eq} is defined as one third of the trace of the orthogonalized U_{ij} tensor.

atom	x	y	z	U_{eq}
Zn(1)	1453(1)	7094(1)	1984(1)	19(1)
Na(1A)	1453(1)	7094(1)	1984(1)	19(1)
Si(1)	1916(1)	8221(1)	−403(1)	28(1)
Si(2)	6051(1)	7725(1)	225(1)	27(1)
Si(3)	−376(1)	8498(1)	3537(1)	31(1)
Si(4)	3652(1)	8518(1)	4332(1)	33(1)
Si(5)	284(1)	4722(1)	2269(1)	31(1)
Si(6)	4191(1)	4278(1)	3297(1)	28(1)
Na(1)	3838(1)	6937(1)	2482(1)	28(1)
Zn(1A)	3838(1)	6937(1)	2482(1)	28(1)
C(1)	2468(2)	8156(2)	716(2)	31(1)
C(2)	3631(2)	7768(1)	532(1)	22(1)
C(3)	4552(2)	8159(2)	732(2)	33(1)
C(4)	873(2)	7592(2)	3424(2)	33(1)
C(5)	1884(2)	8089(1)	3503(1)	24(1)
C(6)	2577(2)	7721(2)	4084(2)	38(1)
C(7)	1692(2)	5465(2)	1917(2)	31(1)
C(8)	2363(2)	5159(1)	2606(1)	23(1)
C(9)	3528(2)	5021(2)	2377(1)	30(1)
C(10)	319(2)	8404(2)	5(2)	38(1)
C(11)	2246(2)	6974(2)	−969(2)	39(1)
C(12)	2606(2)	9367(2)	−1418(2)	57(1)
C(13)	6071(2)	6412(2)	−197(2)	39(1)
C(14)	6880(2)	8727(2)	−882(2)	53(1)
C(15)	6800(2)	7598(2)	1225(2)	46(1)
C(16)	121(2)	9834(2)	2751(2)	38(1)
C(17)	−1498(2)	7947(2)	3086(2)	44(1)
C(18)	−1046(3)	8644(2)	4911(2)	60(1)

Table 22, continued.

atom	x	y	z	U_{eq}
C(19)	3962(2)	9798(2)	3433(2)	44(1)
C(20)	3109(2)	8752(3)	5697(2)	62(1)
C(21)	5030(2)	7782(2)	4182(2)	51(1)
C(22)	−656(2)	5416(2)	1546(2)	42(1)
C(23)	512(2)	3345(2)	1964(2)	51(1)
C(24)	−485(2)	4620(2)	3673(2)	47(1)
C(25)	3279(2)	4388(2)	4631(2)	50(1)
C(26)	4296(2)	2852(2)	3133(2)	44(1)
C(27)	5698(2)	4785(2)	3064(2)	44(1)

Table 23. Crystal data and structure refinement for K[Zn(1,3-$(SiMe_3)_2C_3H_3)_3$].

Empirical formula	C27 H63 K Si6 Zn	
Formula weight	660.78	
Temperature	100(2) K	
Wavelength	0.71073 Å	
Crystal system	Triclinic	
Space group	P−1	
Unit cell dimensions	a = 11.982(2) Å	α= 79.258(3)°
	b = 13.160(3) Å	β= 72.505(3)°
	c = 13.942(3) Å	γ = 89.654(3)°
Volume	2057.1(7) $Å^3$	
Z	2	
Density (calculated)	1.067 g/cm^3	
Absorption coefficient	0.887 mm^{-1}	
F(000)	716	
Crystal size	0.20 x 0.20 x 0.20 mm^3	
Theta range for data collection	1.56 to 27.48°	
Index ranges	−15≤h≤15, −16≤k≤16, −18≤l≤18	
Reflections collected	17881	
Independent reflections	8975 [R(int) = 0.0203]	
Completeness to theta = 27.48°	95.3 %	
Absorption correction	None	
Max. and min. transmission	0.8426 and 0.8426	
Refinement method	Full−matrix least−squares on F^2	
Data / restraints / parameters	8975 / 0 / 316	
Goodness−of−fit on F^2	1.071	
Final R indices [I>2sigma(I)]	R1 = 0.0441, wR2 = 0.1208	
R indices (all data)	R1 = 0.0521, wR2 = 0.1266	
Largest diff. peak and hole	1.647 and −0.496 e $Å^{-3}$	

Table 24. Atomic coordinates (x 10^4) and equivalent isotropic displacement parameters (Å^{2}x 10^3) for K[Zn(1,3-(SiMe$_3$)$_2$C$_3$H$_3$)$_3$]. U_{eq} is defined as one third of the trace of the orthogonalized U_{ij} tensor.

atom	x	y	z	U_{eq}
K(1)	5765(1)	7983(1)	2429(1)	31(1)
Zn(1)	8423(1)	7915(1)	3017(1)	21(1)
Si(1)	8024(1)	6757(1)	5390(1)	27(1)
Si(2)	3753(1)	7227(1)	4964(1)	26(1)
Si(3)	10357(1)	6700(1)	1501(1)	29(1)
Si(4)	6403(1)	6281(1)	576(1)	28(1)
Si(5)	9711(1)	10207(1)	2718(1)	28(1)
Si(6)	5705(1)	10750(1)	1722(1)	27(1)
C(1)	7281(3)	5621(3)	6397(2)	49(1)
C(2)	9634(3)	6560(3)	4996(2)	42(1)
C(3)	7758(3)	7944(3)	5966(2)	40(1)
C(4)	7435(2)	6868(2)	4280(2)	24(1)
C(5)	6229(2)	7205(2)	4554(2)	23(1)
C(6)	5237(2)	6743(2)	4518(2)	27(1)
C(7)	3847(3)	8512(2)	5316(3)	40(1)
C(8)	3037(3)	7390(3)	3922(3)	45(1)
C(9)	2807(3)	6286(2)	6080(3)	47(1)
C(11)	9955(3)	5362(2)	2282(3)	41(1)
C(12)	11471(2)	7298(3)	1947(2)	40(1)
C(13)	11058(3)	6601(3)	130(2)	53(1)
C(14)	9028(2)	7473(2)	1612(2)	24(1)
C(15)	8086(2)	6886(2)	1461(2)	22(1)
C(16)	7467(2)	7147(2)	791(2)	27(1)
C(17)	6887(3)	6138(3)	−789(3)	52(1)
C(18)	4908(3)	6823(3)	854(3)	42(1)
C(19)	6249(3)	5002(2)	1455(3)	42(1)
C(21)	10618(3)	9584(2)	3518(2)	38(1)
C(22)	10528(3)	10275(3)	1331(2)	40(1)

Table 24, continued.

atom	x	y	z	U_{eq}
C(23)	9506(3)	11574(2)	2925(3)	46(1)
C(24)	8271(2)	9477(2)	3072(2)	24(1)
C(25)	7584(2)	9858(2)	2387(2)	23(1)
C(26)	6425(2)	10064(2)	2632(2)	25(1)
C(27)	6532(3)	10585(3)	396(2)	48(1)
C(28)	5645(3)	12150(2)	1795(3)	42(1)
C(29)	4156(3)	10230(3)	2040(3)	41(1)

Table 25. Crystal data and structure refinement for $[1,3\text{-}(SiMe_3)_2C_3H_3]_3Ga$.

Empirical formula	C27 H63 Ga Si6	
Formula weight	626.03	
Temperature	173(2) K	
Wavelength	0.71073 Å	
Crystal system	Triclinic	
Space group	*P*–1	
Unit cell dimensions	*a* = 10.253(2) Å	α = 76.797(2)°
	b = 12.840(2) Å	β = 88.265(2)°
	c = 16.054(3) Å	γ = 81.855(2)°
Volume	2036.9(5) Å^3	
Z	2	
Density (calculated)	1.021 Mg/m^3	
Absorption coefficient	0.865 mm^{-1}	
F(000)	680	
Crystal color, morphology	colorless, block	
Crystal size	0.28 x 0.26 x 0.18 mm^3	
Theta range for data collection	1.30 to 26.37°	
Index ranges	$-12 \le h \le 12$, $-16 \le k \le 16$, $-19 \le l \le 19$	
Reflections collected	18668	
Independent reflections	8225 [*R*(int) = 0.0362]	
Observed reflections	6299	
Completeness to theta = 26.37°	99.0%	
Absorption correction	Multi–scan	
Max. and min. transmission	1.000000 and 0.880580	
Refinement method	Full–matrix least–squares on F^2	
Data / restraints / parameters	8225 / 0 / 361	
Goodness–of–fit on F^2	1.033	
Final *R* indices [*I*>2sigma(*I*)]	*R*1 = 0.0396, *wR*2 = 0.0956	
R indices (all data)	*R*1 = 0.0615, *wR*2 = 0.1068	
Largest diff. peak and hole	0.725 and –0.431 e.Å^{-3}	

Table 26. Atomic coordinates (x 10^4) and equivalent isotropic displacement parameters (Å^{2}x 10^3) for [1,3-$(SiMe_3)_2C_3H_3$]$_3$Ga. U_{eq} is defined as one third of the trace of the orthogonalized U_{ij} tensor.

atom	x	y	z	U_{eq}
Ga1	6035(1)	2435(1)	7671(1)	30(1)
Si1	7547(1)	1607(1)	9505(1)	39(1)
Si2	2642(1)	3752(1)	9918(1)	40(1)
Si3	8124(1)	3833(1)	6467(1)	35(1)
Si4	3433(1)	6348(1)	6628(1)	41(1)
Si5	3577(1)	1455(1)	7075(1)	41(1)
Si6	8175(1)	−1106(1)	6634(1)	50(1)
C1	6304(2)	2659(2)	8832(2)	32(1)
C2	4977(2)	2765(2)	9247(2)	35(1)
C3	4280(3)	3654(2)	9398(2)	39(1)
C4	8282(4)	2216(3)	10284(2)	72(1)
C5	8864(3)	1065(3)	8826(2)	75(1)
C6	6734(4)	459(3)	10104(2)	70(1)
C7	1348(3)	4536(3)	9145(2)	63(1)
C8	2708(3)	4459(3)	10798(2)	69(1)
C9	2197(4)	2375(3)	10350(3)	74(1)
C10	6363(2)	3603(2)	6677(2)	32(1)
C11	5512(2)	4588(2)	6838(2)	36(1)
C12	4497(3)	5170(2)	6375(2)	43(1)
C13	8157(3)	5012(3)	5541(2)	52(1)
C14	8850(3)	4155(2)	7409(2)	47(1)
C15	9098(3)	2601(3)	6210(2)	55(1)
C16	1701(3)	6044(3)	6696(2)	65(1)
C17	3538(4)	7572(3)	5758(2)	64(1)
C18	3912(3)	6636(3)	7645(2)	58(1)
C19	5300(2)	1147(2)	7525(2)	34(1)
C20	6242(2)	562(2)	7004(2)	36(1)
C21	6961(3)	−401(2)	7261(2)	46(1)

Table 26, continued.

atom	x	y	z	U_{eq}
C22	3566(3)	2166(3)	5931(2)	66(1)
C23	2908(4)	165(3)	7166(3)	83(1)
C24	2533(3)	2306(3)	7698(3)	78(1)
C25	7812(3)	−2494(3)	6691(3)	72(1)
C26	8150(5)	−354(3)	5501(3)	101(2)
C27	9828(4)	−1172(4)	7098(4)	107(2)

Table 27. Crystal data and structure refinement for (η^5-1,2,4-$(SiMe_3)_3C_5H_2$) (η^1-1,2,4-$(SiMe_3)_3C_5H_2$)Zn.

Empirical formula	C28 H58 Si6 Zn	
Formula weight	628.65	
Temperature	218(2) K	
Wavelength	0.71073 Å	
Crystal system	Triclinic	
Space group	P−1	
Unit cell dimensions	a = 10.3083(12) Å	α= 90.943(2)°
	b = 11.4333(13) Å	β= 95.924(2)°
	c = 16.688(2) Å	γ = 103.885(2)°
Volume	1897.4(4) $Å^3$	
Z	2	
Density (calculated)	1.100 g/cm^3	
Absorption coefficient	0.851 mm^{-1}	
F(000)	680	
Crystal size	0.30 x 0.30 x 0.30 mm^3	
Theta range for data collection	2.05 to 28.21°	
Index ranges	−13≤h≤13, −15≤k≤15, −21≤l≤20	
Reflections collected	8121	
Independent reflections	4819 [R(int) = 0.0272]	
Completeness to theta = 28.21°	51.6 %	
Absorption correction	None	
Max. and min. transmission	0.7842 and 0.7842	
Refinement method	Full−matrix least−squares on F^2	
Data / restraints / parameters	4819 / 0 / 316	
Goodness−of−fit on F^2	0.925	
Final R indices [I>2sigma(I)]	R1 = 0.0336, wR2 = 0.0683	
R indices (all data)	R1 = 0.0429, wR2 = 0.0696	
Largest diff. peak and hole	0.287 and −0.214 e $Å^{-3}$	

Table 28. Atomic coordinates (x 10^4) and equivalent isotropic displacement parameters (Å^{2}x 10^3) for (η^5-1,2,4-$(SiMe_3)_3C_5H_2$) (η^1-1,2,4-$(SiMe_3)_3C_5H_2$)Zn. U_{eq} is defined as one third of the trace of the orthogonalized U_{ij} tensor.

atom	x	y	z	U_{eq}
Zn(1)	4902(1)	7223(1)	2564(1)	36(1)
Si(1)	6378(1)	4504(1)	2508(1)	33(1)
Si(2)	6923(1)	9244(1)	1225(1)	34(1)
Si(3)	7710(1)	9561(1)	3627(1)	39(1)
Si(4)	2095(1)	8055(1)	2319(1)	37(1)
Si(5)	2563(1)	6135(1)	4202(1)	40(1)
Si(6)	1388(1)	3540(1)	1096(1)	38(1)
C(1)	7018(2)	8224(2)	2906(1)	29(1)
C(2)	6768(2)	8123(2)	2027(1)	27(1)
C(3)	6510(2)	6862(2)	1814(1)	28(1)
C(4)	6568(2)	6168(2)	2504(1)	29(1)
C(5)	6883(2)	7021(2)	3171(1)	31(1)
C(6)	2936(2)	6757(2)	2455(1)	29(1)
C(7)	2466(2)	5907(2)	3083(1)	31(1)
C(8)	1941(2)	4781(2)	2712(1)	34(1)
C(9)	2017(2)	4820(2)	1850(1)	32(1)
C(10)	2601(2)	5982(2)	1699(2)	31(1)
C(11)	5077(3)	3799(2)	3162(2)	54(1)
C(12)	8013(3)	4193(2)	2912(2)	52(1)
C(13)	5874(3)	3895(2)	1456(2)	50(1)
C(14)	5774(3)	8539(2)	314(2)	47(1)
C(15)	8668(3)	9616(3)	935(2)	50(1)
C(16)	6475(3)	10666(2)	1536(2)	47(1)
C(17)	8166(3)	8986(3)	4630(2)	62(1)
C(18)	6510(3)	10503(2)	3777(2)	57(1)
C(19)	9261(3)	10527(3)	3281(2)	56(1)
C(20)	4198(3)	7197(3)	4598(2)	52(1)
C(21)	2476(4)	4652(3)	4657(2)	63(1)

Table 28, continued.

atom	x	y	z	U_{eq}
C(22)	1153(3)	6705(3)	4526(2)	60(1)
C(23)	2700(3)	9270(2)	3131(2)	60(1)
C(24)	2451(3)	8762(3)	1348(2)	58(1)
C(25)	250(3)	7423(3)	2290(2)	53(1)
C(26)	2047(4)	3992(3)	125(2)	62(1)
C(27)	1957(3)	2193(2)	1459(2)	53(1)
C(28)	−491(3)	3148(3)	951(2)	68(1)

Appendix D

ATOMIC FRACTIONAL COORDINATES FOR DENSITY FUNCTIONAL THEORY OPTIMIZED STRUCTURES

Table 29. Atomic coordinates for optimized structure of $Li(C_3H_5)$; (PBE-D/T2ZP).

atom	x	y	z
C1	0.84786	0.93434	0.00052
C2	-0.39737	0.28870	0.06496
C3	-0.62661	-1.09509	0.00052
H1	0.91819	2.01858	0.04100
H2	-1.63604	-1.49703	0.04100
H3	1.74982	0.37971	0.29495
H4	-1.28062	0.93042	-0.03531
H5	0.17960	-1.78152	0.29495
Li1	0.64382	-0.46776	-1.55236

Table 30. Atomic coordinates for optimized structure of Li[1,1´,3-$(SiH_3)_3C_3H_2$]; (PBE-D/T2ZP).

atom	x	y	z
C1	-0.60587	-2.31573	-0.50539
C2	0.52955	-1.67452	-1.08125
C3	-1.95328	-2.08394	-0.80943
H1	3.05230	-0.84691	-0.28215
H2	-0.36631	-1.13903	-3.75535
H3	-0.67402	0.52628	-2.10623
H4	1.57099	0.10798	-2.92395
H5	-0.41188	-2.96875	0.35736
H6	-2.78079	-3.57377	1.30266
H7	-4.06893	-3.92824	-0.72197
H8	-4.38638	-1.92745	0.53612
H9	-2.17506	-1.54986	-1.74602
H10	2.12523	-2.80620	0.82082
H11	3.01897	-2.93989	-1.42358
Li1	-0.93449	-0.19525	-0.30760
Si1	-3.33880	-2.90158	0.08769
Si2	2.22615	-2.08053	-0.48588
Si3	0.30885	-0.58489	-2.54088

Table 31. Atomic coordinates for optimized structure of $[Li(C_3H_5)]_2$; (PBE-D/T2ZP).

atom	x	y	z
C1	2.25958	1.68885	1.09586
C2	0.25623	-1.58298	-0.97306
C3	1.00621	1.50528	1.64283
C4	-1.00621	-1.50528	-1.64283
C5	-0.25623	1.58298	0.97306
C6	-2.25958	-1.68885	-1.09586
H1	-1.13562	1.67238	1.61965
H2	3.16414	1.55900	1.68514
H3	-3.16414	-1.55900	-1.68514
H4	-0.30149	2.25383	0.10209
H5	0.98029	1.12361	2.67048
H6	1.13562	-1.67238	-1.61965
H7	2.37062	2.16963	0.11520
H8	-2.37062	-2.16963	-0.11520
H9	-0.98029	-1.12361	-2.67048
H10	0.30149	-2.25383	-0.10209
Li1	1.18871	0.17129	-0.07074
Li2	-1.18871	-0.17129	0.07074

Table 32. Atomic coordinates for optimized structure of {Li[1,1´,3-$(SiH_3)_3C_3H_2$]}$_2$; (PBE-D/T2ZP).

atom	x	y	z
C1	-0.70317	1.01771	1.47356
C2	0.70317	-1.01771	-1.47356
C3	1.75016	1.32195	2.04237
C4	-1.75016	-1.32195	-2.04237
C5	0.51674	0.71236	2.18083
C6	-0.51674	-0.71236	-2.18083
H1	-2.08852	-0.39686	3.41091
H2	2.08852	0.39686	-3.41091
H3	-3.39070	1.32847	2.24120
H4	3.39070	-1.32847	-2.24120
H5	-2.81272	-0.70478	1.14278
H6	2.81272	0.70478	-1.14278
H7	-0.55523	3.83636	0.97380
H8	0.55523	-3.83636	-0.97380
H9	-0.35367	-2.35487	0.64968
H10	0.35367	2.35487	-0.64968
H11	2.04933	-2.48365	0.41261
H12	-2.04933	2.48365	-0.41261
H13	1.79898	2.25095	1.45310
H14	-1.79898	-2.25095	-1.45310
H15	0.48305	-0.15659	2.85249
H16	-0.48305	0.15659	-2.85249
H17	2.92791	-0.50980	3.66268
H18	-2.92791	0.50980	-3.66268
H19	3.89356	1.72172	3.78645
H20	-3.89356	-1.72172	-3.78645
H21	4.34806	0.34283	1.88758
H22	-4.34806	-0.34283	-1.88758
Li1	1.14432	0.66413	0.00810
Li2	-1.14432	-0.66413	-0.00810

Table 32, continued.

atom	x	y	z
Si1	-3.28006	-0.70992	-2.87230
Si2	-2.28435	0.33430	2.12388
Si3	2.28435	-0.33430	-2.12388
Si4	-0.77728	2.48603	0.36673
Si5	0.77728	-2.48603	-0.36673
Si6	3.28006	0.70992	2.87230

Table 33. Atomic coordinates for optimized structure of $[Li(C_3H_5)(thf)_2]_2$; (PBE-D/T2ZP).

atom	x	y	z
C1	-0.95155	-2.26874	-2.07728
C2	2.82938	1.95354	3.50839
C3	-1.30375	-2.12944	-3.55704
C4	1.30375	2.12944	3.55704
C5	0.35235	-1.97690	0.97953
C6	0.95155	2.26874	2.07728
C7	3.36255	-0.87780	-1.86431
C8	4.25617	-0.24373	-2.92635
C9	3.84313	1.23237	-2.82581
C10	3.64635	1.40673	-1.31812
C11	-3.64635	-1.40673	1.31812
C12	-3.84313	-1.23237	2.82581
C13	-4.25617	0.24373	2.92635
C14	-3.36255	0.87780	1.86431
C15	-1.66592	2.26659	-0.67095
C16	2.98625	1.07107	2.27308
C17	-0.18106	-0.87525	1.69443
C18	-2.82938	-1.95354	-3.50839
C19	-2.98625	-1.07107	-2.27308
C20	-0.35235	1.97690	-0.97953
C21	0.18106	0.87525	-1.69443
C22	1.66592	-2.26659	0.67095
H23	1.92291	-3.11511	0.03972
H24	2.49604	-1.73233	1.14262
H25	-1.21004	-0.95173	2.04236
H26	-0.39505	-2.62712	0.50920
H27	-0.48078	0.33465	-2.37610
H28	1.21004	0.95173	-2.04236
H29	-2.49604	1.73233	-1.14262
H30	-1.92291	3.11511	-0.03972

Table 33, continued.

atom	x	y	z
H31	0.39505	2.62712	-0.50920
H32	0.48078	-0.33465	2.37610
Li1	1.32266	-0.02989	0.07831
Li2	-1.32266	0.02989	-0.07831
O1	3.26882	0.10268	-0.80295
O2	-3.26882	-0.10268	0.80295
O3	1.95440	1.50197	1.35382
O4	-1.95440	-1.50197	-1.35382

Table 34. Atomic coordinates for optimized structure of {Li[1,1´,3-$(SiH_3)_3C_3H_2$]$(thf)_2$}$_2$; (PBE-D/T2ZP).

atom	x	y	z
C1	1.66012	-0.37482	-3.94740
C2	-3.05799	-0.08149	4.35216
C3	-1.66012	0.37482	3.94740
C4	0.53721	2.30517	0.23580
C5	-0.62064	2.46248	-0.58048
C6	2.44357	1.16613	-2.32052
C7	-3.24599	1.36019	-3.14816
C8	-3.79392	1.34488	-4.56975
C9	-2.57257	1.81827	-5.37203
C10	-1.43695	1.08749	-4.66182
C11	1.43695	-1.08749	4.66182
C12	2.57257	-1.81827	5.37203
C13	3.79392	-1.34488	4.56975
C14	3.24599	-1.36019	3.14816
C15	-2.44357	-1.16613	2.32052
C16	-0.68445	-1.73559	-1.49731
C17	3.05799	0.08149	-4.35216
C18	-3.64255	-0.50544	2.99664
C19	3.64255	0.50544	-2.99664
C20	-0.53721	-2.30517	-0.23580
C21	0.68445	1.73559	1.49731
C22	0.62064	-2.46248	0.58048
H8	2.33416	-2.30577	-1.62412
H17	0.24097	-1.42316	-1.99589
H18	-1.46098	-2.73818	0.17991
H19	-0.24097	1.42316	1.99589
H20	1.46098	2.73818	-0.17991
H30	0.26160	4.88276	-1.66591
H31	0.25108	3.08363	-3.20374
H32	-1.83397	4.02689	-2.50143

Table 34, continued.

atom	x	y	z
H33	-3.33289	2.98243	-0.47570
H34	-2.77513	0.70294	-0.08485
H35	-2.33416	2.30577	1.62412
H36	-0.25108	-3.08363	3.20374
H37	-0.26160	-4.88276	1.66591
H38	1.83397	-4.02689	2.50143
H39	-1.87983	-1.81244	-3.97499
H40	-2.53497	-3.58201	-2.48895
H41	-3.41430	-1.41341	-2.15510
H50	2.77513	-0.70294	0.08485
H51	3.33289	-2.98243	0.47570
H52	1.87983	1.81244	3.97499
H53	3.41430	1.41341	2.15510
H54	2.53497	3.58201	2.48895
Li1	0.49285	-0.56382	1.85070
Li2	-0.49285	0.56382	-1.85070
O1	1.26460	0.50986	-2.86905
O2	-1.26460	-0.50986	2.86905
O3	1.84472	-0.98355	3.27266
O4	-1.84472	0.98355	-3.27266
Si1	-2.27907	2.11032	0.13467
Si2	-2.15005	-2.13053	-2.53589
Si3	2.27907	-2.11032	-0.13467
Si4	0.48160	-3.62038	2.00361
Si5	-0.48160	3.62038	-2.00361
Si6	2.15005	2.13053	2.53589

Table 35. Atomic coordinates for optimized structure of Li[Zn(1,3-$(SiMe_3)_2C_3H_3)_3$]; (B3PW91/DGDZVP2).

atom	x	y	z
C1	3.72527	2.72980	-0.67594
C2	-2.12489	0.00438	-0.87428
C3	-1.65082	-3.96518	-2.25563
C4	1.81232	0.04768	-1.41165
C5	-4.84296	2.41312	-0.19120
C6	2.88230	2.81045	-3.62045
C7	0.31000	-0.42182	2.23730
C8	-2.30476	-1.33908	-0.62632
C9	4.42965	-2.00201	-1.29132
C10	0.95297	0.85187	1.95088
C11	2.00893	1.71887	4.72479
C12	1.22648	3.86096	2.69936
C13	-2.04390	1.12221	0.05396
C14	3.01842	-3.03020	-3.83787
C15	2.27051	-4.14515	-1.09467
C16	-0.70729	-4.49108	1.69281
C17	1.40779	-4.02982	3.84719
C18	-1.35412	-2.66377	4.04573
C19	-4.49825	-3.30223	-1.37227
C20	-0.94665	2.14234	4.03741
C21	-3.11942	-1.64785	-3.58485
C22	1.31173	4.42066	-1.56043
C23	1.52418	-1.19338	-1.93651
C24	-2.45160	4.17587	0.49961
C25	1.11378	1.31416	-1.57233
C26	0.75111	-1.70647	2.00528
C27	-2.72396	2.99183	-2.32712
Li1	-0.01114	-1.60256	-0.21079
Si1	2.23818	2.79858	-1.84130
Si2	0.80428	2.12910	3.32446

Table 35, continued.

atom	x	y	z
Si3	-2.98974	2.65662	-0.48559
Si4	0.02174	-3.19975	2.86946
Si5	2.78531	-2.57588	-2.01981
Si6	-2.86491	-2.54652	-1.94428
Zn1	0.00993	1.42899	0.18796

Table 36. Atomic coordinates for optimized structure of $[Li(C_2H_4)]^+$; (PBE1PBE/Li: cc-pCVTZ; C,H: aug-cc-pVTZ).

atom	x	y	z
C1	-0.00552	-0.31886	0.68074
C2	-0.00643	-0.37164	-0.65342
H1	0.91780	-0.45250	-1.21951
H2	0.91949	-0.35479	1.25020
H3	-0.93291	-0.42046	-1.21951
H4	-0.93122	-0.32275	1.25020
Li1	0.03285	1.89784	-0.07511

Table 37. Atomic coordinates for optimized structure of $[Na(C_2H_4)]^+$; (PBE1PBE/Na: cc-pCVTZ; C,H: aug-cc-pVTZ).

atom	x	y	z
C1	-0.01793	-1.03568	0.70800
C2	-0.01884	-1.08838	-0.62394
H1	0.90441	-1.16953	-1.19016
H2	0.90610	-1.07190	1.27760
H3	-0.94434	-1.13753	-1.19016
H4	-0.94265	-1.03990	1.27760
Na1	0.02701	1.56029	-0.06175

Table 38. Atomic coordinates for optimized structure of $[K(C_2H_4)]^+$; (PBE1PBE/K: Feller Misc. CVTZ; C,H: aug-cc-pVTZ).

atom	x	y	z
C1	-0.02872	-1.65878	0.73080
C2	-0.02963	-1.71133	-0.59743
H1	0.89306	-1.78751	-1.16426
H2	0.89474	-1.69000	1.30062
H3	-0.95439	-1.75553	-1.16426
H4	-0.95270	-1.65801	1.30062
K1	0.02470	1.42693	-0.05647

Table 39. Atomic coordinates for optimized structure of $[Li(C_2H_4)_2]^+$; (PBE1PBE/Li: cc-pCVTZ; C,H: aug-cc-pVTZ).

atom	x	y	z
C1	-0.02756	-2.28413	-0.64114
C2	0.70326	2.26691	-0.06515
C3	-0.04917	-2.27071	0.69225
C4	-0.62794	2.28793	0.01268
H1	1.21693	2.28479	-1.02225
H2	-0.94385	-2.31099	-1.22414
H3	0.86562	-2.32135	1.27602
H4	-0.98389	-2.28615	1.24567
H5	-1.14046	2.34756	0.96869
H6	-1.24882	2.32370	-0.87807
H7	0.90565	-2.34619	-1.19382
H8	1.32530	2.30866	0.82452
Li1	0.00390	-0.00003	0.00374

Table 40. Atomic coordinates for optimized structure of $[Na(C_2H_4)_2]^+$; (PBE1PBE/Na: cc-pCVTZ; C,H: aug-cc-pVTZ).

atom	x	y	z
C1	-0.40456	2.69582	-0.27991
C2	-0.52077	-2.65260	0.44943
C3	0.68833	2.60937	0.47626
C4	0.23699	-2.65260	-0.64577
H1	-1.60468	-2.63188	0.39053
H2	-0.34292	2.77199	-1.36118
H3	0.63090	2.61177	1.56044
H4	1.68267	2.61177	0.04032
H5	1.31670	-2.75187	-0.58978
H6	-0.20022	-2.63188	-1.63933
H7	-1.39469	2.77199	0.15894
H8	-0.08776	-2.75187	1.44008
Na1	0.00000	0.00000	0.00000

Table 41. Atomic coordinates for optimized structure of $[K(C_2H_4)_2]^+$; (PBE1PBE/K: Feller Misc. CVTZ; C,H: aug-cc-pVTZ).

atom	x	y	z
C1	-0.37671	3.19278	-0.26065
C2	-0.54649	-3.14966	0.42977
C3	0.71367	3.10654	0.49379
C4	0.20954	-3.14966	-0.66291
H1	-1.63012	-3.12580	0.37159
H2	-0.31584	3.26580	-1.34193
H3	0.65666	3.10573	1.57774
H4	1.70794	3.10573	0.05832
H5	1.28931	-3.24573	-0.60740
H6	-0.22691	-3.12580	-1.65647
H7	-1.36713	3.26580	0.17749
H8	-0.11391	-3.24573	1.42066
K1	0.00000	0.00000	0.00000

Table 42. Atomic coordinates for optimized structure of $[Li(C_2H_4)_3]^+$; (PBE1PBE/Li: cc-pCVTZ; C,H: aug-cc-pVTZ).

atom	x	y	z
C1	-0.47251	2.18508	-0.96398
C2	-0.64537	-1.11315	2.06675
C3	1.90841	-1.12783	-1.00641
C4	0.01754	-0.01852	2.43442
C5	-1.65358	1.58721	-0.82082
C6	0.84552	-1.51279	-1.70994
H1	-2.25209	1.71800	0.07538
H2	1.08806	-0.03573	2.61566
H3	-0.49598	0.91670	2.63484
H4	-1.72524	-1.11278	1.95252
H5	-0.14137	-2.06551	1.93445
H6	0.29155	-2.41202	-1.45764
H7	-0.06186	2.82619	-0.18970
H8	0.53287	-0.98218	-2.60393
H9	2.50339	-0.26793	-1.29920
H10	2.26276	-1.69842	-0.15356
H11	0.09382	2.11140	-1.88720
H12	-2.09589	1.00231	-1.62170
Li1	-0.00003	-0.00002	0.00001

Table 43. Atomic coordinates for optimized structure of $[Na(C_2H_4)_3]^+$; (PBE1PBE/Na: cc-pCVTZ; C,H: aug-cc-pVTZ).

atom	x	y	z
C1	-0.63904	2.47699	-1.11258
C2	-0.68619	-1.20622	2.41990
C3	2.12261	-1.34243	-1.21397
C4	-0.04015	-0.10295	2.78741
C5	-1.82053	1.88706	-0.95223
C6	1.06331	-1.71243	-1.92853
H1	-2.40789	2.02658	-0.05009
H2	1.02944	-0.10521	2.97313
H3	-0.56695	0.82554	2.98411
H4	-1.76535	-1.22125	2.30289
H5	-0.16883	-2.15175	2.29090
H6	0.50055	-2.60932	-1.68894
H7	-0.21645	3.12128	-0.34785
H8	0.76207	-1.17181	-2.82033
H9	2.72742	-0.48586	-1.49504
H10	2.46527	-1.92276	-0.36301
H11	-0.08364	2.39422	-2.04156
H12	-2.27560	1.30036	-1.74419
Na1	-0.00001	-0.00001	0.00000

Table 44. Atomic coordinates for optimized structure of $[K(C_2H_4)_3]^+$; (PBE1PBE/K: Feller Misc. CVTZ; C,H: aug-cc-pVTZ).

atom	x	y	z
C1	-0.85441	2.85267	-1.30665
C2	-0.73648	-1.32719	2.87598
C3	2.39848	-1.62166	-1.48075
C4	-0.11702	-0.21119	3.24300
C5	-2.03578	2.27537	-1.11965
C6	1.34523	-1.96801	-2.21191
H1	-2.60500	2.42660	-0.20816
H2	0.95142	-0.18914	3.43204
H3	-0.66355	0.70715	3.43182
H4	-1.81379	-1.36525	2.75059
H5	-0.19874	-2.26139	2.75022
H6	0.76638	-2.85875	-1.98990
H7	-0.41146	3.49879	-0.55557
H8	1.06033	-1.41114	-3.09871
H9	3.01626	-0.76824	-1.74118
H10	2.72198	-2.21550	-0.63199
H11	-0.31496	2.75431	-2.24314
H12	-2.50880	1.68258	-1.89595
K1	-0.00001	0.00000	-0.00001

Table 45. Atomic coordinates for optimized structure of $[Li(C_6H_6)]^+$; (PBE1PBE/Li: cc-pCVTZ; C,H: aug-cc-pVTZ).

atom	x	y	z
C1	0.00000	0.12027	-1.39581
C2	-1.20881	0.12027	-0.69791
C3	-1.20881	0.12027	0.69791
C4	0.00000	0.12027	1.39581
C5	1.20881	0.12027	0.69791
C6	1.20881	0.12027	-0.69791
H1	0.00000	0.12411	2.47880
H2	-2.14671	0.12411	-1.23940
H3	-2.14671	0.12411	1.23940
H4	2.14671	0.12412	1.23940
H5	2.14671	0.12412	-1.23940
H6	0.00000	0.12412	-2.47880
Li1	0.00000	-1.69150	0.00000

Table 46. Atomic coordinates for optimized structure of $[Na(C_6H_6)]^+$; (PBE1PBE/Na: cc-pCVTZ; C,H: aug-cc-pVTZ).

atom	x	y	z
C1	0.00000	0.48851	-1.39391
C2	-1.20716	0.48851	-0.69696
C3	-1.20716	0.48851	0.69696
C4	0.00000	0.48851	1.39391
C5	1.20716	0.48851	0.69696
C6	1.20716	0.48851	-0.69696
H1	0.00000	0.51581	2.47696
H2	-2.14511	0.51581	-1.23848
H3	-2.14511	0.51581	1.23848
H4	2.14511	0.51581	1.23848
H5	2.14511	0.51581	-1.23848
H6	0.00000	0.51581	-2.47696
Na1	0.00000	-1.88011	0.00000

Table 47. Atomic coordinates for optimized structure of $[K(C_6H_6)]^+$; (PBE1PBE/K: Feller Misc. CVTZ; C,H: aug-cc-pVTZ).

atom	x	y	z
C1	0.00000	0.87883	-1.39208
C2	-1.20558	0.87883	-0.69604
C3	-1.20558	0.87883	0.69604
C4	0.00000	0.87883	1.39208
C5	1.20558	0.87883	0.69604
C6	1.20558	0.87883	-0.69604
H1	0.00000	0.90975	2.47521
H2	-2.14360	0.90975	-1.23761
H3	-2.14360	0.90975	1.23761
H4	2.14360	0.90975	1.23761
H5	2.14360	0.90975	-1.23761
H6	0.00000	0.90975	-2.47521
K1	0.00000	-1.95244	0.00000

Table 48. Atomic coordinates for optimized structure of $(C_3H_5)_3Ga$; (B3PW91/cc-pVDZ).

atom	x	y	z
C1	0.36124	1.63209	-0.93434
C2	1.42710	2.34637	-0.18077
C3	1.25052	3.37344	0.66073
C4	-3.66517	0.25633	0.45183
C5	-1.84499	-1.00345	-0.77443
C6	1.07131	-1.09788	1.13417
C7	1.75845	-2.14413	0.32291
C8	2.95854	-2.03372	-0.26915
C9	-2.79275	-0.75898	0.35083
Ga1	-0.12051	-0.16160	-0.17717
H1	2.44786	1.96588	-0.32030
H2	0.47509	-1.53943	1.94737
H3	1.77832	-0.36938	1.55858
H4	2.09195	3.82251	1.19356
H5	3.57940	-1.14021	-0.14592
H6	1.19451	-3.07334	0.16245
H7	3.36647	-2.84294	-0.87909
H8	-2.17895	-0.51998	-1.70530
H9	0.25947	3.80198	0.84348
H10	-3.78934	0.98913	-0.35234
H11	-2.72528	-1.45977	1.19425
H12	-0.57617	2.21333	-0.97128
H13	0.66301	1.44410	-1.98077
H14	-4.29528	0.37659	1.33598
H15	-1.70058	-2.07931	-0.95914

Table 49. Atomic coordinates for optimized structure of [1,3-$(SiH_3)_2C_3H_3]_3Ga$; (B3PW91/cc-pVDZ).

atom	x	y	z
C1	-2.21818	2.62037	1.17922
C2	2.92091	-2.33994	0.88017
C3	-0.98940	-0.37395	-2.71398
C4	-1.23226	-1.55152	-3.32577
C5	2.11115	0.06359	0.73743
C6	-1.45979	0.22342	0.82092
C7	-1.51264	1.52904	1.54656
C8	0.31248	0.08434	-2.15133
C9	2.22098	-1.28980	1.36172
Ga1	0.30109	0.14166	-0.14002
H1	1.11921	-0.63423	-2.39166
H2	-1.82399	0.33567	-2.61104
H3	-0.39742	-2.25888	-3.43355
H4	3.48487	-2.19825	-0.05324
H5	2.12563	2.21418	-2.19397
H6	3.90085	1.48027	2.37204
H7	2.14797	2.80146	1.31289
H8	4.42117	-4.35108	2.09903
H9	2.17053	-3.97096	2.97189
H10	-3.62197	4.55986	2.61020
H11	-1.34075	4.08293	3.34511
H12	-1.75194	5.36865	1.30919
H13	-2.84431	-2.29009	-5.48269
H14	-3.41525	-3.29293	-3.35853
H15	-3.88168	-0.92663	-3.74151
H16	1.09149	1.67971	-4.33652
H17	-0.20298	2.79648	-2.60033
H18	1.61107	1.32550	3.17749
H19	-0.87528	-1.22763	3.13526

Table 49, continued.

atom	x	y	z
H20	-3.20519	-1.26713	2.43719
H21	-1.54086	-2.54824	1.19806
H22	2.50422	-5.09869	0.83045
H23	-2.21403	0.20259	0.01438
H24	-0.90626	1.58920	2.46225
H25	-2.82889	2.55578	0.26713
H26	2.82493	0.15378	-0.10085
H27	1.66169	-1.42771	2.29894
Si1	-2.23413	4.22136	2.14926
Si2	-1.78762	-1.27202	1.94614
Si3	3.00786	-4.00618	1.72904
Si4	0.85607	1.76656	-2.85804
Si5	-2.90725	-2.03625	-4.00446
Si6	2.46033	1.48093	1.95187

Table 50. Atomic coordinates for optimized structure of [1,3-$(SiMe_3)_2C_3H_3]_3Ga$; (B3PW91/cc-pVDZ).

atom	x	y	z
C1	-3.61341	3.42650	4.54138
C2	0.85112	1.09601	-1.51715
C3	1.08723	0.51685	-2.87244
C4	0.58290	0.96363	-4.04443
C5	3.90064	0.54573	-0.98840
C6	2.20912	1.99802	1.14710
C7	2.89843	3.40866	-1.51716
C8	1.65875	1.64578	-6.83797
C9	2.19458	-1.15711	-5.63635
C10	2.81486	-3.65537	4.89844
C11	-0.65467	-0.36184	-6.54813
C12	-1.91259	0.30842	0.43481
C13	0.78160	-1.97617	1.71110
C14	1.88261	-1.97533	2.49469
C15	-1.75883	-3.84611	0.17781
C16	1.08703	-4.99969	0.00743
C17	-0.05888	-3.45596	-2.38975
C18	2.79805	-0.58485	5.09690
C19	0.11876	-2.13849	5.03495
C20	0.73963	-1.93817	0.21623
C21	-1.79536	1.52028	1.30181
C22	-2.04599	1.60284	2.62676
C23	-3.04259	-0.61855	-2.36110
C24	-3.25109	2.33555	-1.55381
C25	-4.95168	0.22375	-0.08191
C26	-1.56996	4.66855	2.57916
C27	-0.59950	2.98528	4.98656
Ga1	-0.12144	-0.20126	-0.32669
H1	2.60950	2.02431	-6.42886

Table 50, continued.

atom	x	y	z
H2	1.84723	1.28770	-7.86382
H3	1.80157	-1.99330	-5.03584
H4	2.42093	-1.54775	-6.64215
H5	3.14425	-0.82683	-5.18504
H6	-1.40915	0.44038	-6.60102
H7	-0.47356	-0.72001	-7.57535
H8	-1.08808	-1.19332	-5.96902
H9	-0.07941	1.84300	-3.99520
H10	1.77190	-1.89987	-0.18019
H11	-0.19924	-2.01866	2.20729
H12	2.85746	-1.93686	1.98283
H13	-1.74843	-3.96780	1.27300
H14	-2.44894	-3.02276	-0.06466
H15	-2.17675	-4.77035	-0.25451
H16	1.18118	-5.06152	1.10319
H17	0.66909	-5.95342	-0.35548
H18	0.95484	-3.30761	-2.79644
H19	-0.45009	-4.39804	-2.80861
H20	-0.69532	-2.63685	-2.76025
H21	2.87136	-0.65990	6.19472
H22	3.82272	-0.51034	4.69682
H23	2.27189	0.35218	4.85378
H24	0.12378	-2.19397	6.13593
H25	-0.44522	-1.23651	4.74732
H26	-0.42700	-3.01932	4.65935
H27	2.87725	-3.72931	5.99702
H28	2.30633	-4.55869	4.52429
H29	3.84396	-3.66129	4.50284
H30	-2.23448	-0.55215	1.05027
H31	-1.49047	2.43970	0.78035

Table 50, continued.

atom	x	y	z
H32	-2.35711	0.67493	3.13278
H33	-2.10179	-0.41062	-2.89911
H34	-3.03983	-1.67526	-2.04914
H35	-3.86621	-0.49155	-3.08345
H36	2.10124	-4.89469	-0.41160
H37	-2.27946	2.59647	-2.00339
H38	-4.02035	2.45345	-2.33491
H39	-3.46791	3.06478	-0.75742
H40	-5.08444	0.85622	0.81070
H41	-5.78073	0.43542	-0.77728
H42	-5.03678	-0.82905	0.23351
H43	-2.34695	4.81814	1.81207
H44	-1.52746	5.58180	3.19540
H45	-0.59871	4.56947	2.06789
H46	-0.55064	3.87939	5.63041
H47	-0.79136	2.11445	5.63475
H48	0.38922	2.84670	4.52026
H49	-4.42898	3.55777	3.81182
H50	-3.86612	2.56161	5.17677
H51	-3.58523	4.32018	5.18678
H52	0.18229	1.97260	-1.60496
H53	1.75566	-0.35637	-2.90137
H54	3.69475	-0.44990	-0.56446
H55	4.12460	0.42313	-2.05994
H56	4.81058	0.93245	-0.50006
H57	2.03955	1.04051	1.66906
H58	3.09933	2.46571	1.59954
H59	1.34696	2.65279	1.35366
H60	3.85331	3.79936	-1.12800
H61	2.99452	3.29873	-2.60944

Table 50, continued.

atom	x	y	z
H62	2.11975	4.16377	-1.32074
H63	0.95953	2.49587	-6.90301
Si1	-0.01469	-3.54525	-0.49830
Si2	1.89156	-2.08408	4.37244
Si3	-3.27503	0.56014	-0.89490
Si4	-1.95059	3.16504	3.66777
Si5	2.46532	1.74973	-0.71326
Si6	0.94840	0.26376	-5.75029

Table 51. Atomic coordinates for optimized structure of $(C_5H_4F)_2Fe$; (B3PW91/Fe: cc-pwCVTZ; C,H,F: cc-pVTZ).

atom	x	y	z
C1	-0.44421	-1.06001	-1.70757
C2	1.18187	1.56289	0.59752
C3	0.26120	1.99310	-0.39472
C4	0.44421	1.06001	1.70757
C5	-0.26120	-1.99310	0.39472
C6	-1.05940	1.76262	0.08706
C7	1.05940	-1.76262	-0.08706
C8	-0.92364	1.20326	1.37871
C9	-1.18187	-1.56289	-0.59752
C10	0.92364	-1.20326	-1.37871
F1	-1.94094	0.86952	2.17793
F2	1.94094	-0.86952	-2.17793
Fe1	0.00000	0.00000	0.00000
H1	-0.83597	-0.64688	-2.62258
H2	0.51652	2.40072	-1.35994
H3	2.25690	1.58748	0.51575
H4	-2.25690	-1.58748	-0.51575
H5	1.98784	-1.96638	0.42076
H6	-0.51652	-2.40072	1.35994
H7	0.83597	0.64688	2.62258
H8	-1.98784	1.96638	-0.42076

Table 52. Atomic coordinates for optimized structure of $(C_5F_5)_2Fe$; (BP86/DGDZVP2).

atom	x	y	z
C1	0.91848	1.23057	1.32701
C2	-0.98947	-1.77135	-0.00446
C3	0.34658	-1.94234	0.47398
C4	1.24221	-1.50708	-0.55151
C5	0.45955	-1.06748	-1.66379
C6	-1.24205	1.50724	0.54982
C7	-0.34498	1.94253	-0.47437
C8	-0.46117	1.06744	1.66328
C9	0.99042	1.77132	0.00589
C10	-0.91965	-1.23087	-1.32582
F1	-2.56894	1.56618	0.50196
F2	0.69572	-2.47840	1.63897
F3	-2.09935	-2.11870	0.63892
F4	-1.95313	-0.98807	-2.12545
F5	0.93213	-0.64626	-2.83250
F6	2.56907	-1.56535	-0.50555
F7	-0.93518	0.64623	2.83132
F8	1.95103	0.98750	2.12789
F9	2.10128	2.11810	-0.63583
F10	-0.69228	2.47880	-1.63981
Fe1	-0.00010	-0.00001	0.00002

REFERENCES

(1) Pauson, P. L.; Kealy, T. J. *Nature* **1951**, *168*, 1039.

(2) Wilkinson, G.; Rosenblum, M.; Whiting, M. C.; Woodward, R. B. *J. Am. Chem. Soc.* **1952**, *74*, 2125.

(3) Wilke, G.; Bogdanovic, B. *Angew. Chem.* **1961**, *73*, 756.

(4) Wilke, G.; Bogdanovic, B.; Hardt, P.; Heimbach, P.; Keim, W.; Kroner, M.; Oberkirch, W.; Tanaka, K.; Walter, D.; Zimmermann, H. *Angew. Chem., Int. Ed. Engl.* **1966**, *5*, 151.

(5) Karol, F. J.; Johnson, R. N. *J. Polym. Sci., Polym. Chem. Ed.* **1975**, *13*, 1607.

(6) Novakov, P. P.; Kuckling, D.; Fedorova, L.; Adler, H. J. P. *Macromol. Symp.* **1998**, 195.

(7) Chance, J. M.; Linebarrier, D. L.; Nile, T. A. *Transition Met. Chem. (Dordrecht, Netherlands)* **1987**, *12*, 276.

(8) Alonso, B.; Cuadrado, I.; Moran, M.; Losada, J. *J. Am. Chem. Soc., Chem. Comm.* **1994**, 2575.

(9) Franks, R. J.; Nicholas, K. M. *Organometallics* **2000**, *19*, 1458.

(10) Hirashita, T.; Hayashi, Y.; Mitsui, K.; Araki, S. *J. Org. Chem.* **2003**, *68*, 1309.

(11) Barreca, D.; Buchberger, A.; Daolio, S.; Depero, L. E.; Fabrizio, M.; Morandini, F.; Rizzi, G. A.; Sangaletti, L.; Tondello, E. *Langmuir* **1999**, *15*, 4537.

(12) Hierso, J. C.; Serp, P.; Feurer, R.; Kalck, P. *Coord. Chem. Rev.* **1998**, *12*, 161.

(13) Betz, P.; Jolly, P. W.; Krueger, C.; Zakrzewski, U. *Organometallics* **1991**, *10*, 3520-5.

(14) Gabor, B.; Holle, S.; Jolly, P. W.; Mynott, R. *Journal of Organometallic Chemistry* **1994**, *466*, 201-9.

(15) Grosselin, J. M.; Dixneuf, P. H. *J. Organomet. Chem.* **1986**, *314*, C76.

(16) Fraenkel, G.; Chow, A.; Winchester, W. R. *Journal of the American Chemical Society* **1990**, *112*, 1382-6.

(17) Harvey, M. J.; Hanusa, T. P.; Young, V. G., Jr. *Angew. Chem. Int. Ed.* **1999**, *38*, 217-9.

(18) Quisenberry, K. T. Ph.D. Dissertation, Vanderbilt University, 2005.

(19) Gren, C. K.; Hanusa, T. P.; Brennessel, W. W. *Polyhedron* **2006**, *25*, 286-92.

(20) Boche, G.; Fraenkel, G.; Cabral, J.; Harms, K.; Van Eikema Hommes, N. J. R.; Lohrenz, J.; Marsch, M.; Schleyer, P. v. R. *J. Am. Chem. Soc.* **1992**, *114*, 1562-5.

(21) Smith, J. D.; Hanusa, T. P.; Young, V. G., Jr. *J. Am. Chem. Soc.* **2001**, *123*, 6455-6.

(22) Carlson, C. N. Ph.D. Dissertation, Vanderbilt University, 2004.

(23) Smith, J. D.; Quisenberry, K. T.; Hanusa, T. P.; Brennessel, W. W. *Acta Crystallographica, Section C: Crystal Structure Communications* **2004**, *C60*, m507-m8.

(24) Layfield, R. A.; Humphrey, S. M. *Angew. Chem.* **2004**, *43*, 3067-9.

(25) Quisenberry, K. T.; Smith, J. D.; Voehler, M.; Stec, D. F.; Hanusa, T. P.; Brennessel, W. W. *J. Am. Chem. Soc.* **2005**, *127*, 4376-87.

(26) Schormann, M.; Garratt, S.; Bochmann, M. *Organometallics* **2005**, *24*, 1718-24.

(27) Carlson, C. N.; Smith, J. D.; Hanusa, T. P.; Brennessel, W. W.; Young, V. G. *J. Organomet. Chem.* **2003**, *683*, 191-9.

(28) Ihara, E.; Koyama, K.; Yasuda, H.; Kanehisa, N.; Kai, Y. *J. Organomet. Chem.* **1999**, *574*, 40-9.

(29) Woodman, T. J.; Schormann, M.; Bochmann, M. *Isr. J. Chem.* **2002**, *42*, 283-93.

(30) Kuehl, C. J.; Simpson, C. K.; John, K. D.; Sattelberger, A. P.; Carlson, C. N.; Hanusa, T. P. *J. Organomet. Chem.* **2003**, *683*, 149-54.

(31) Carlson, C. N.; Hanusa, T. P.; Brennessel, W. W. *Journal of the American Chemical Society* **2004**, *126*, 10550-1.

(32) Woodman, T. J.; Schormann, M.; Hughes, D. L.; Bochmann, M. *Organometallics* **2004**, *23*, 2972-9.

(33) Simpson, C. K.; White, R. E.; Carlson, C. N.; Wrobleski, D. A.; Kuehl, C. J.; Croce, T. A.; Steele, I. M.; Scott, B. L.; Young, V. G.; Hanusa, T. P.; Sattelberger, A. P.; John, K. D. *Organometallics* **2005**, *24*, 3685-91.

(34) Elschenbroich, C. *Organometallics*; VCH Publishers: Weinheim, 2006.

(35) Hitchcock, P. B.; Lappert, M. F.; Leung, W.-P.; Liu, D.-S.; Mak, T. C. W.; Wang, Z.-X. *J. Chem. Soc., Dalton Trans.* **1999**, 1257-62.

(36) Hitchcock, P. B.; Lappert, M. F.; Wang, Z.-X. *Chem. Commun.* **1996**, 1647-8.

(37) Praesang, C.; Sahin, Y.; Hofmann, M.; Geiseler, G.; Massa, W.; Berndt, A. *Eur. J. Inorg. Chem.* **2004**, 3063-73.

(38) Marr, F.; Fröhlich, R.; Hoppe, D. *Tetrahedron: Asymmetry* **2002**, *13*, 2587-92.

(39) Wilkes, J. B. *J. Org. Chem.* **1967**, *32*, 3231-3.

(40) Woodman, T. J.; Schormann, M.; Hughes, D. L.; Bochmann, M. *Organometallics* **2003**, *22*, 3028-30.

(41) Quisenberry, K. T.; Gren, C. K.; White, R. E.; Hanusa, T. P.; Brennessel, W. W. *Organometallics* **2007**, *26*, 4354-6.

(42) Gren, C. K.; Hanusa, T. P.; Rheingold, A. L. *Organometallics* **2007**, *26*, 1643–9.

(43) Cheon, J.; Dubois, L. H.; Girolami, G. S. *Chem. Mater.* **1994**, *6*, 2279-87.

(44) Solomon, S. A.; Muryn, C. A.; Layfield, R. A. *Chem. Commun.* **2008**, 3142-4.

(45) Chmely, S. C. *Unpublished work* **2009**.

(46) Halstead, G. W.; Baker, E. C.; Raymond, K. N. *J. Am. Chem. Soc.* **1975**, *97*, 3049-52.

(47) Marks, T. J.; Wachter, W. A. *J. Am. Chem. Soc.* **1976**, *98*, 703-10.

(48) Chmely, S. C.; Carlson, C. N.; Hanusa, T. P.; Rheingold, A. L. *J. Am. Chem. Soc.* **2009**, *131*, 6344-5.

(49) Reddy, A. S.; Sastry, G. N. *J. Phys. Chem. A* **2005**, *109*, 8893-903.

(50) Cheng, J.; Zhu, W.; Tang, Y.; Xu, Y.; Li, Z.; Chen, K.; Jiang, H. *Chem. Phys. Lett.* **2006**, *422*, 455-60.

(51) Reddy, A. S.; Zipse, H.; Sastry, G. N. *J. Phys. Chem. B* **2007**, *111*, 11546-53.

(52) Hommes, N. v. E.; Bühl, M.; Schleyer, P. v. R.; Wu, Y.-D. *J. Organomet. Chem.* **1991**, *409*, 307-20.

(53) Merino, P.; Mannucci, V.; Tejero, T. *Tetrahedron* **2005**, *61*, 3335-47.

(54) Ma, J. C.; Dougherty, D. A. *Chem. Rev.* **1997**, *97*, 1303-24.

(55) Meyer, E. A.; Castellano, R. K.; Diederich, F. *Angew. Chem., Int. Ed.* **2003**, *42*, 1210-50.

(56) Kim, D.; Hu, S.; Tarakeshwar, P.; Kim, K. S.; Lisy, J. M. *J. Phys. Chem. A* **2003**, *107*, 1228-38.

(57) Gokel, G. W.; De Wall, S. L.; Meadows, E. S. *Eur. J. Org. Chem.* **2000**, 2967-78.

(58) Krossing, I.; Reisinger, A. *Angew. Chem. Int. Ed.* **2003**, *42*, 5725-8.

(59) Saarenketo, P.; Suontamo, R.; Jödicke, T.; Rissanen, K. *Organometallics* **2000**, *19*, 2346-53.

(60) Amicangelo, J. C.; Armentrout, P. B. *J. Phys. Chem. A* **2000**, *104*, 11420-32.

(61) Sunner, J.; Nishizawa, K.; Kebarle, P. *J. Phys. Chem.* **1981**, *85*, 1814-20.

(62) Bartoli, S.; Roelens, S. *J. Am. Chem. Soc.* **2002**, *124*, 8307-15.

(63) Sarri, P.; Venturi, F.; Cuda, F.; Roelens, S. *J. Org. Chem.* **2004**, *69*, 3654-61.

(64) Araki, K.; Shimizu, H.; Shinkai, S. *Chem. Lett.* **1993**, *2*, 205-8.

(65) Arduini, A.; Pochini, A.; Secchi, A. *Eur. J. Org. Chem.* **2000**, 2325-34.

(66) Matthews, S. E.; Schmitt, P.; Felix, V.; Drew, M. G. B.; Beer, P. D. *J. Am. Chem. Soc.* **2002**, *124*, 1341-53.

(67) Matthews, S. E.; Rees, N. H.; Felix, V.; Drew, M. G. B.; Beer, P. D. *Inorg. Chem.* **2003**, *42*, 729-34.

(68) Choi, H. S.; Suh, S. B.; Cho, S. J.; Kim, K. S. *Proc. Nat. Acad. Sci. U.S.A.* **1998**, *95*, 12094-9.

(69) Clegg, W.; Dale, S. H.; Hevia, E.; Hogg, L. M.; Honeyman, G. W.; Mulvey, R. E.; O'Hara, C. T. *Angew. Chem., Int. Ed.* **2006**, *45*, 6548-50.

(70) Dougherty, D. A. *Science (Washington, D. C.)* **1996**, *271*, 163-8.

(71) Nakamura, R. L.; Anderson, J. A.; Gaber, R. F. *J. Biol. Chem.* **1997**, *272*, 1011-8.

(72) Dougherty, D. A.; Lester, H. A. *Angew. Chem., Int. Ed.* **1998**, *37*, 2329-31.

(73) De Wall, S. L.; Meadows, E. S.; Barbour, L. J.; Gokel, G. W. *Proc. Nat. Acad. Sci., U.S.A.* **2000**, *97*, 6271-6.

(74) Macias, A. T.; Norton, J. E.; Evanseck, J. D. *J. Am. Chem. Soc.* **2003**, *125*, 2351-60.

(75) Bubnov, Y. N.; Gurskii, M. E.; Gridnev, I. D.; Ignatenko, A. V.; Ustynyuk, Y. A.; Mstislavskii, V. I. *J. Organomet. Chem.* **1992**, *424*, 127-32.

(76) Hanusa, T. P.; Carlson, C. N. In *Encyclopedia of Inorg. Chem.-II*; King, R. B., Ed.; Wiley: 2005; Vol. 9, p 5690–5.

(77) Restorp, P.; Fischer, A.; Somfai, P. *Journal of the American Chemical Society* **2006**, *128*, 12646-7.

(78) Te Velde, G.; Bickelhaupt, F. M.; Baerends, E. J.; Fonseca Guerra, C.; Van Gisbergen, S. J. A.; Snijders, J. G.; Ziegler, T. *Journal of Computational Chemistry* **2001**, *22*, 931-67.

(79) Guerra, C. F.; Snijders, J. G.; Te Velde, G.; Baerends, E. J. *Theoretical Chemistry Accounts* **1998**, *99*, 391-403.

(80) ADF2008.01; SCM; Theoretical Chemistry; Vrije Universiteit; Amsterdam; The Netherlands; (http://www.scm.com).

(81) Perdew, J. P.; Burke, K.; Ernzerhof, M. *Phys. Rev. Lett.* **1996**, *77*, 3865-8.

(82) Grimme, S. *Journal of Computational Chemistry* **2006**, *27*, 1787-99.

(83) Fraenkel, G.; Chow, A.; Fleischer, R.; Liu, H. *J. Am. Chem. Soc.* **2004**, *126*, 3983-95.

(84) Weiss, E.; Lambertsen, T.; Schubert, B.; Cockeroft, J. K.; Wiedenmann, A. *Chem. Ber.* **1990**, *123*, 79-81.

(85) Greenwood, N. N.; Earnshaw, A. *Chemistry of the Elements*; 2nd ed.; Butterworth-Heinemann: Oxford, 1997.

(86) Shannon, R. D. *Acta Crystallogr., Sect A.* **1976**, *32*, 751-67.

(87) Corbelin, S.; Kopf, J.; Lorenzen, N. P.; Weiss, E. *Angewandte Chemie International Edition in English* **1991**, *30*, 825-7.

(88) Bock, H.; Ruppert, K.; Havlas, Z.; Fenske, D. *Angew. Chem. Int. Ed. Engl.* **1990**, *29*, 1042-4.

(89) Dinnebier, R. E.; Behrens, U.; Olbrich, F. *Organometallics* **1997**, *16*, 3855-8.

(90) Aoyagi, T.; Shearer, H. M. M.; Wade, K.; Whitehead, G. *J. Organomet. Chem.* **1979**, *175*, 21-31.

(91) Edelman, M. A.; Hitchcock, P. B.; Lappert, M. F.; Liu, D.-S.; Shun, T. *Journal of Organometallic Chemistry* **1998**, *550*, 397-408.

(92) Harvey, M. J.; Hanusa, T. P.; Pink, M. *J. Chem. Soc., Dalton Trans.* **2001**, 1128-30.

(93) Pratt, L. M.; Khan, I. M. *Journal of Computational Chemistry* **1995**, *16*, 1067-80.

(94) Chung, L. W.; Chan, T. H.; Wu, Y.-D. *Organometallics* **2005**, *24*, 1598-607.

(95) *Lithium Chemistry: A Theoretical and Experimental Overview*; Sapse, A.-M.; Schleyer, P. v. R., Eds.; Wiley: New York, 1995.

(96) Winchester, W. R.; Bauer, W.; Schleyer, P. v. R. *Chem. Commun.* **1987**, 177-9.

(97) Boche, G.; Etzrodt, H.; Marsch, M.; Massa, W.; Baum, G.; Dietrich, H.; Mahdi, W. *Angew. Chem. Int. Ed.* **1986**, *25*, 104-5.

(98) Werner, B.; Krauter, T.; Neumuller, B. *Organometallics* **1996**, *15*, 3746-51.

(99) Kralik, M. S.; Stahl, L.; Arif, A. M.; Strouse, C. E.; Ernst, R. D. *Organometallics* **1992**, *11*, 3617-21.

(100) Hu, J.; Barbour, L. J.; Gokel, G. W. *Chem. Commun.* **2001**, 1858-9.

(101) Feller, D. *Chem. Phys. Lett.* **2000**, *322*, 543-8.

(102) Choi, H. S.; Kim, D.; Tarakeshwar, P.; Suh, S. B.; Kim, K. S. *J. Org. Chem.* **2002**, *67*, 1848-51.

(103) King, R. B.; Bisnette, M. B. *Journal of Organometallic Chemistry* **1967**, *7*, 311-19.

(104) Mueller, H. J.; Nagel, U.; Beck, W. *Organometallics* **1987**, *6*, 193-4.

(105) Beck, W.; Niemer, B.; Wieser, M. *Angewandte Chemie* **1993**, *105*, 969-96 (See also Angew Chem , Int Ed Engl , 1993, 32(7), 923-49).

(106) Hueffer, S.; Wieser, M.; Polborn, K.; Beck, W. *Journal of Organometallic Chemistry* **1994**, *481*, 45-55.

(107) Gunnoe, T. B.; White, P. S.; Templeton, J. L. *Organometallics* **1997**, *16*, 3794-9.

(108) Gaussian **2003**, Gaussian 03, Revision B.1, M. J. Frisch, G. W. Trucks, H. B. Schlegel, G. E. Scuseria, M. A. Robb, J. R. Cheeseman, J. A. Montgomery, Jr., T. Vreven, K. N. Kudin, J. C. Burant, J. M. Millam, S. S. Iyengar, J. Tomasi, V. Barone, B. Mennucci, M. Cossi, G. Scalmani, N. Rega, G. A. Petersson, H. Nakatsuji, M. Hada, M. Ehara, K. Toyota, R. Fukuda, J. Hasegawa, M. Ishida, T. Nakajima, Y. Honda, O. Kitao, H. Nakai, M. Klene, X. Li, J. E. Knox, H. P. Hratchian, J. B. Cross, C. Adamo, J. Jaramillo, R. Gomperts, R. E. Stratmann, O. Yazyev, A. J. Austin, R. Cammi, C. Pomelli, J. W. Ochterski, P. Y. Ayala, K. Morokuma, G. A. Voth, P. Salvador, J. J. Dannenberg, V. G. Zakrzewski, S. Dapprich, A. D. Daniels, M. C. Strain, O. Farkas, D. K. Malick, A. D. Rabuck, K. Raghavachari, J. B. Foresman, J. V. Ortiz, Q. Cui, A. G. Baboul, S. Clifford, J. Cioslowski, B. B. Stefanov, G. Liu, A. Liashenko, P. Piskorz, I. Komaromi, R. L. Martin, D. J. Fox, T. Keith, M. A. Al-Laham, C. Y. Peng, A. Nanayakkara, M. Challacombe, P. M. W. Gill, B. Johnson, W. Chen, M. W. Wong, C. Gonzalez, and J. A. Pople, Gaussian, Inc., Pittsburgh PA, 2003.

(109) Becke, A. D. *J. Chem. Phys.* **1993**, *98*, 5648-52.

(110) Perdew, J. P.; Wang, Y. *Phys. Rev. B* **1992**, *45*, 13244-9.

(111) Smith, J. D.; Hanusa, T. P. *Organometallics* **2001**, *20*, 3056-62.

(112) Ziegler, T. *Chem. Rev.* **1991**, *91*, 651-67.

(113) White, R. E.; Hanusa, T. P. *Organometallics* **2006**, *25*, 5621–30.

(114) Godbout, N.; Salahub, D. R.; Andzelm, J.; Wimmers, E. *Can. J. Chem.* **1992**, *50*, 560-71.

(115) Feller, D.; Glendening, E. D.; Woon, D. E.; Feyereisen, M. W. *J. Chem. Phys.* **1995**, *103*, 3526-42.

(116) Schaefer, A.; Horn, H.; Ahlrichs, R. *J. Chem. Phys.* **1992**, *97*, 2571-7.

(117) Csaszar, P.; Pulay, P. *J. Molec. Struct.* **1984**, *114*, 31-4.

(118) Farkas, O.; Schlegel, H. B. *J. Chem. Phys.* **1999**, *111*, 10806-14.

(119) SHELXTL; 6.1 ed.; Bruker Analytical X-Ray Systems, Madison, WI.: 2000.

(120) Scherr, P. A.; Hogan, R. J.; Oliver, J. P. *J. Am. Chem. Soc.* **1974**, *96*, 6055-9.

(121) Fernández, I.; Martinez-Viviente, E.; Breher, F.; Pregosin, P. S. *Chem–Eur. J.* **2005**, *11*, 1495-506.

(122) Erlich, R. H.; Popov, A. I. *J. Am. Chem. Soc.* **1971**, *93*, 5620-3.

(123) Westerhausen, M.; Rademacher, B.; Schwarz, W. *Z. Anorg. Allg. Chem.* **1993**, *619*, 675-89.

(124) Clegg, W.; Forbes, G. C.; Kennedy, A. R.; Mulvey, R. E.; Liddle, S. T. *Chem. Commun.* **2003**, 406-7.

(125) Forbes, G. C.; Kennedy, A. R.; Mulvey, R. E.; Roberts, B. A.; Rowlings, R. B. *Organometallics* **2002**, 5115-21.

(126) Mulvey, R. E. *Organometallics* **2006**, *25*, 1060-75.

(127) Bock, H.; Ruppert, K.; Fenske, D. *Angew. Chem., Int. Ed. Engl.* **1989**, *28*, 1685-7.

(128) Dietrich, H. *J. Organomet. Chem.* **1981**, *205*, 291-9.

(129) Armstrong, D. R.; Mulvey, R. E.; Walker, G. T.; Barr, D.; Snaith, R.; Clegg, W.; Reed, D. *J. Chem. Soc., Dalton Trans.* **1988**, 617-28.

(130) Veith, M.; Koban, A.; Fries, K.; Spaniol, P.; Elsaesser, R.; Rammo, A.; Huch, V.; Kleinsteuber, U. *Organometallics* **1998**, *17*, 2612-8.

(131) Amicangelo, J. C.; Armentrout, P. B. *Int. J. Mass Spec.* **2001**, *212*, 301-25.

(132) Feller, D.; Dixon, D. A.; Nicholas, J. B. *J. Phys. Chem. A* **2000**, *104*, 11414-9.

(133) Quinonero, D.; Garau, C.; Frontera, A.; Ballester, P.; Costa, A.; Deya, P. M. *J. Phys. Chem. A* **2005**, *109*, 4632-7.

(134) Lau, J. K.-C.; Wong, C. H. S.; Ng, P. S.; Siu, F. M.; Ma, N. L.; Tsang, C. W. *Chem–Eur. J.* **2003**, *9*, 3383-96.

(135) Nicholas, J. B.; Hay, B. P.; Dixon, D. A. *J. Phys. Chem. A* **1999**, *103*, 1394-400.

(136) Kristyán, S.; Pulay, P. *Chem. Phys. Lett.* **1994**, *229*, 175-80.

(137) Koch, W.; Holthausen, M. C. *A Chemist's Guide to Density Functional Theory*; 2nd ed.; John Wiley: New York, 2001.

(138) Johnson, E. R.; Wolkow, R. A.; DiLabio, G. A. *Chem. Phys. Lett.* **2004**, *394*, 334-8.

(139) Zierkiewicz, W.; Michalska, D.; Cerny, J.; Hobza, P. *Mol. Phys.* **2006**, *104*, 2317-25.

(140) Chmely, S. C.; Meier, R. M.; Hanusa, T. P. *Manuscript in preparation.* **2009**.

(141) Mohajeri, A.; Karimi, E. *Journal of Molecular Structure: THEOCHEM* **2006**, *774*, 71-6.

(142) Hoyau, S.; Norrman, K.; McMahon, T. B.; Ohanessian, G. *J. Am. Chem. Soc.* **1999**, *121*, 8864-75.

(143) Sugimura, H.; Watanabe, T. *Synlett* **1994**, 175-7.

(144) Wallbridge, M. G. H.; Fishwick, M. *J. Chem. Soc. [Section] A: Inorganic, Physical, Theoretical* **1971**, 57-63.

(145) Meijboom, R.; Moss, J. R.; Hutton, A. T.; Makaluza, T.-A.; Mapolie, S. F.; Waggie, F.; Domingo, M. R. *J. Organomet. Chem.* **2004**, *689*, 1876-81.

(146) Fernandes, R. A.; Yamamoto, Y. *J. Org. Chem.* **2004**, *69*, 735-8.

(147) Braddock, D. C.; Matsuno, A. *Synlett* **2004**, 2521-4.

(148) Meijboom, R.; Hutton, A. T.; Moss, J. R. *Organometallics* **2003**, *22*, 1811-5.

(149) Gozzi, M. F.; Goncalves, M. D. C.; Yoshida, I. V. P. *Journal of Materials Science* **1999**, *34*, 155-9.

(150) Van der Made, A. W.; Van Leeuwen, P. W. N. M. *J. Chem. Soc., Chem. Commun.* **1992**, 1400-01.

(151) Nakanishi, K.; Mizuno, K.; Otsuji, Y. *J. Chem. Soc., Chem. Commun.* **1991**, 90-2.

(152) Dejean, V.; Gornitzka, H.; Oba, G.; Koenig, M.; Manuel, G. *Organometallics* **2000**, *19*, 711-3.

(153) Akiyama, T.; Iwai, J.; Sugano, M. *Tetrahedron* **1999**, *55*, 7499-508.

(154) Cerveau, G.; Chuit, C.; Corriu, R. J. P.; Reye, C. *Organometallics* **1991**, *10*, 1510-15.

(155) Mazerolles, P.; Gregoire, F.; Morancho, R.; Reynes, A.; Sefiani, N. *J. Organomet. Chem.* **1987**, *328*, 49-59.

(156) Rogers, P. J.; Selco, J. I.; Rowland, F. S. *Chemical Physics Letters* **1983**, *97*, 313-16.

(157) Wagner, C. E.; Shea, K. J. *Organic Letters* **2004**, *6*, 313-6.

(158) Pastukhov, F. V.; Yampolsky, I. V.; Bubnov, Y. N. *J. Organomet. Chem.* **2002**, *657*, 123-8.

(159) Bubnov, Y. N.; Zhun, I. V.; Klimkina, E. V.; Ignatenko, A. V.; Starikova, Z. A. *European J. Org. Chem.* **2000**, 3323-7.

(160) Wrackmeyer, B.; Tok, O. L.; Klimkina, E.; Bubnov, Y. N. *Inorg. Chim. Acta* **2000**, *300-302*, 169-74.

(161) Wrackmeyer, B.; Tok, O. L.; Bubnov, Y. N. *Angewandte Chemie, International Edition* **1999**, *38*, 124-6.

(162) Brown, H. C.; Racherla, U. S.; Pellechia, P. J. *J. Org. Chem.* **1990**, *55*, 1868-74.

(163) Brown, H. C.; Racherla, U. S. *Tetrahedron Lett.* **1985**, *26*, 4311-14.

(164) Mikhailov, B. M. *Pure and Applied Chemistry* **1974**, *39*, 505-23.

(165) Yanagisawa, A.; Nakamura, Y.; Arai, T. *Tetrahedron: Asymmetry* **2004**, *15*, 1909-13.

(166) Yadav, J. S.; Reddy, B. V. S.; Swamy, T. *Tetrahedron Lett.* **2003**, *44*, 4861-4.

(167) Kii, S.; Maruoka, K. *Chirality* **2003**, *15*, 68-70.

(168) Jin, Y. Z.; Yasuda, N.; Furuno, H.; Inanaga, J. *Tetrahedron Lett.* **2003**, *44*, 8765-8.

(169) Waltz, K. M.; Gavenonis, J.; Walsh, P. J. *Angewandte Chemie, International Edition* **2002**, *41*, 3697-9.

(170) Gordon, C. M.; Ritchie, C. *Green Chemistry* **2002**, *4*, 124-8.

(171) Cunningham, A.; Woodward, S. *Synlett* **2002**, 43-4.

(172) McCluskey, A.; Garner, J.; Young, D. J.; Caballero, S. *Tetrahedron Lett.* **2000**, *41*, 8147-51.

(173) Cokley, T. M.; Harvey, P. J.; Marshall, R. L.; McCluskey, A.; Young, D. J. *J. Org. Chem.* **1997**, *62*, 1961-4.

(174) Shi, M.; Nicholas, K. M. *J. Am. Chem. Soc.* **1997**, *119*, 5057-8.

(175) Yanagisawa, A.; Inoue, H.; Morodome, M.; Yamamoto, H. *J. Am. Chem. Soc.* **1993**, *115*, 10356-7.

(176) Fishwick, M.; Wallbridge, M. G. H. *J. Organomet. Chem.* **1970**, *25*, 69-79.

(177) Araki, S.; Horie, T.; Kato, M.; Hirashita, T.; Yamamura, H.; Kawai, M. *Tetrahedron Lett.* **1999**, *40*, 2331-4.

(178) Hirashita, T.; Akutagawa, K.; Kamei, T.; Araki, S. *Chem. Commun. (Cambridge, U. K.)* **2006**, 2598-600.

(179) Hirashita, T.; Daikoku, Y.; Osaki, H.; Ogura, M.; Araki, S. *Tetrahedron Letters* **2008**, *49*, 5411-3.

(180) Metza, J. T.; Terzian, R. A.; Minehan, T. *Tetrahedron Letters* **2006**, *47*, 8905-10.

(181) Shen, K.-H.; Kuo, C.-W.; Yao, C.-F. *Tetrahedron Letters* **2007**, *48*, 6348-51.

(182) Zhou, H.; Liu, G.; Zeng, C. *Journal of Organometallic Chemistry* **2008**, *693*, 787-91.

(183) Blessing, R. H. *Acta Crystallogr.* **1995**, *A51*, 33-8.

(184) Woon, D. E.; Dunning, T. H., Jr. *J. Chem. Phys.* **1993**, *98*, 1358-71.

(185) Mitzel, N. W.; Lustig, C.; Berger, R. J. F.; Runeberg, N. *Angewandte Chemie, International Edition* **2002**, *41*, 2519-22.

(186) Beachley, O. T., Jr.; Churchill, M. R.; Pazik, J. C.; Ziller, J. W. *Organometallics* **1986**, *6*, 1814-7.

(187) Beachley, O. T., Jr.; Getman, T. D.; Kirss, R. U.; Hallock, R. B.; Hunter, W. E.; Atwood, J. L. *Organometallics* **1985**, *4*, 751-4.

(188) Buehl, M.; Schleyer, P. v. R.; Ibrahim, M. A.; Clark, T. *J. Am. Chem. Soc.* **1991**, *113*, 2466-71.

(189) Resa, I.; Carmona, E.; Gutierrez-Puebla, E.; Monge, A. *Science* **2004**, *305*, 1136.

(190) Harvey, M. J.; Hanusa, T. P. *Organometallics* **2000**, *19*, 1556-66.

(191) Hedberg, F. L.; Rosenberg, H. *J. Organometal. Chem.* **1971**, *28*, C14-C6.

(192) Kovar, R. F.; Rausch, M. D.; Rosenberg, H. *Organometallics in Chemical Synthesis* **1971**, *1*, 173-81.

(193) Paprott, G.; Lehmann, S.; Seppelt, K. *Chem. Ber.* **1988**, *121*, 727-33.

(194) Hedberg, F. L.; Rosenberg, H. *J. Amer. Chem. Soc.* **1973**, *95*, 870-5.

(195) Winter, C. H. *Synthesis and properties of perfluoroferrocene and perfluororuthenocene. A potential class of high temperature materials*, Dept. Chem., Wayne State Univ., Detroit, MI, USA., 1995.

(196) Curnow, O. J.; Hughes, R. P. *J. Am. Chem. Soc.* **1992**, *114*, 5895-7.

(197) Hughes, R. P.; Zheng, X.; Ostrander, R. L.; Rheingold, A. L. *Organometallics* **1994**, *13*, 1567-8.

(198) Bishop, J. J.; Davison, A.; Katcher, M. L.; Lichtenberg, D. W.; Merrill, R. E.; Smart, J. C. *Journal of Organometallic Chemistry* **1971**, *27*, 241-9.

(199) Shafir, A.; Power, M. P.; Whitener, G. D.; Arnold, J. *Organometallics* **2000**, *19*, 3978-82.

(200) Shechter, H.; Helling, J. F. *Journal of Organic Chemistry* **1961**, *26*, 1034-7.

(201) Bennett, B. K.; Harrison, R. G.; Richmond, T. G. *Journal of the American Chemical Society* **1994**, *116*, 11165-6.

(202) Jutzi, P.; Sauer, R. *Journal of Organometallic Chemistry* **1973**, *50*, C29-C30.

(203) Yoshida, Y.; Kimura, Y. *J. Fluorine Chem.* **1989**, *44*, 291-8.

(204) Sun, H.; DiMagno, S. G. *Journal of the American Chemical Society* **2005**, *127*, 2050-1.

(205) Stavber, G.; Zupan, M.; Stavber, S. *Tetrahedron Letters* **2007**, *48*, 2671-3.

(206) Laali, K. K.; Borodkin, G. I. *J. Chem. Soc., Perkin Trans. 2* **2002**, 953-7.

(207) Banks, R. E.; Mohialdin-Khaffaf, S. N.; Lal, G. S.; Sharif, I.; Syvret, R. G. *Journal of the Chemical Society, Chemical Communications* **1992**, 595-6.

(208) Burkey, D. J.; Hays, M. L.; Duderstadt, R. E.; Hanusa, T. P. *Organometallics* **1997**, *16*, 1465-75.

(209) Krishnaswami, S. Ph.D. Dissertation, Vanderbilt University, 1997.